

## Reply to reviewer #3

We thank anonymous **reviewer #3** very much for his/her detailed and constructive review that would improve the contents of our paper. The review comments by anonymous **reviewer #3** are numbered and repeated below as *in italic letters*, followed by our answers. In the new draft with track changes (supplement file), **red** corrections are the revisions suggested by **reviewer #3**.

### **General**

*(1) In response to the three reviews, the authors have substantially changed and improved their manuscript. I think that the discussion has improved in many parts of the paper and also the description of the FTIR data is better in the revised version. I think that in particularly adding information on HOCl to the manuscript constitutes a significant improvement of the paper.*

Thank you for your comment.

*(2) However, there are still some issues where I think the paper needs improvement. In my first review I had the point that “the initial Cly correlation needs to be adjusted to 2007 and 2011 – or the adjustment made should be described”. I think this aspect is not completely resolved (see below). Further I stated that “the model behaviour (‘HCl discrepancy’) reported by Grooß et al. (2018) should be discussed in terms of MIROC3.2”. Here there still seems to be discrepancy in opinion, which will require some further discussion (see below). I would be optimistic, however, that this problem can be resolved. Finally, I think the model issue of the transport barrier at the vortex edge needs some attention.*

We will try to answer your questions in the following answers.

*(3) Overall, clearly, the new FTIR measurements presented here are of great scientific interest and are combined in a meaningful way with satellite measurements and model (MIROC3.2) results. In spite of the fact that I recommend a further revision of the paper; I would be optimistic that such a revised version would be further improved and would be close to being accepted by ACP.*

Thank you for your comments.

### **Comments in Detail**

#### **(5) Year-to-year variability and temporal trend of Cly**

*As stated in the first review, the main driver for Antarctic ozone loss is the available Cly. The authors now*

*discuss the year-to-year variability in this quantity (Strahan et al., 2014), which is good. However, I think the point of the applicability of the employed empirical relation for  $Cl_y$  (Eq. 2) to the years discussed here (2007, 2011) needs to be addressed in the paper better than in the present draft (see also details below).*

*There is a statement in the paper that observed  $Cl_y$  in 2011 (2.53 ppbv) was about -5.2% less than the projected  $Cl_y$  from Newman et al. (2007) (2.76 ppbv for 2007 and 2.67 ppbv for 2011). It is not clear to me that the projected values by Newman et al. (2007) were indeed used in the analysis here. Moreover, there is also an alternative projection of  $Cl_y$  values (Engel et al., 2018; WMO, 2019).*

We agree to the reviewer that the year-to-year variability and temporal trend of  $Cl_y$  and  $N_2O$  should not be ignored to derive the empirical correlation between  $N_2O$  and  $Cl_y^*$  using Equation (2). Therefore, we now consider the value for  $Cl_y$  and  $N_2O$  in each year (1997, 2007, and 2011) to derive  $Cl_y$  via Eq. (2). The Newman's calculated  $Cl_y$  values for 1997, 2007, 2011 are; 2.90, 2.76, and 2.67 ppbv, respectively by Strahan et al. (2014), and measured  $N_2O$  values for those years are; 313, 321, and 324 ppbv, respectively by WMO (2011); WMO (2014). We have now considered these differences to derive  $Cl_y^*$  from MLS  $N_2O$  values using Eq. (2). The results of  $Cl_y^*$ , chlorine related ratios are all changed, and Figures 4, 5, 6, 7, 8, 9, 11, and 12 are modified.

#### ***(6) HCl remains in the core of the polar vortex in austral winter***

*In my first review it was stated: "The authors find here for the MIROC3.2 CCM that some HCl remains in winter in the core of the polar vortex in darkness. Such a model behaviour is expected as there is not enough  $ClONO_2$  and no light in the core of the vortex. This model behaviour was reported by Grooß et al. (2018) for three models. Further they showed that this model feature is not found in observations of HCl. I suggest stating that the MIROC3.2 CCM shows the same issue – provided that the authors agree."*

*In their reply, the authors state that they "do not agree with the reviewer's opinion that MIROC3.2 CCM shows the same issue". They have added information and discussion on the role of HOCl, which I consider an important improvement. However, if I look at the HCl values at 87.9 in figure 15, I see that HCl remains constant (and above 0.5 ppb) for days 140-160 (this airmass is in darkness as can be seen from  $Cl_2$ , panel c). Isn't this the issue discussed by Grooß et al. (2018)? HCl is only close to zero at day ~200 (I would argue due to HOx production in sunlight); after this day HOCl starts increasing (see also below).*

We agree with the reviewer that HCl remains constant for days 140-160 in our MIROC3.2 CCM, which might be the same phenomena as shown for three models in Grooß et al. (2018). However, HCl starts to decrease from day 160, and reached almost zero around day 210 (29 July) at 87.9°S in Figure 15. At this point, sun light is not yet available at 87.9°S, and HOCl has not yet started increasing. This is the main difference of our MIROC3.2 CCM result with other three models in Grooß et al. (2018).

*If the authors really do not agree that they see the "HCl discrepancy", this is only possible if they have a*

*process in the model which removes the remaining HCl in darkness. Which process could there be in the model? Does the model contain some process producing NOx in polar night? The latter point would be very interesting. Another possibility would be that MIROC3.2 does not see this issue because of a too coarse spatial resolution, but this would be a model artefact.*

Our MIROC3.2 CCT doesn't have a process which removes the remaining HCl in darkness, as is now shown by the list of chemical reactions in Appendix Table A2. As is described in the revised text, attached Figure R5 in this reply, and reply to the reviewer for the point "(8) Continuous loss of HCl in the core of the polar vortex", we consider the continuous loss of HCl occurs by the mixing of ClONO<sub>2</sub> rich airmass with remaining HCl by the heterogeneous reaction (R1) and with HOCl by reaction (R4).

#### ***(7) Overestimated transport across the vortex edge in models***

*The paper originally stated that transport across the vortex edge might be overestimated in the MIROC3.2 model results. This is perhaps no surprise given the relatively coarse (T42) horizontal spatial resolution. In the reply, the authors now state that they "looked at the differences between observed and modeled N<sub>2</sub>O gradients at the vortex edge, but could not find apparent differences between them". Thus they do not seem to find the same result as Hoppe et al. (2014) who found that models might overestimate mixing across the vortex edge.*

*Such a point should not be covered only in passing in the reply. I suggest to include the relevant plots in the reply (which will remain accessible at ACP) or, even better, include this information as an appendix to the paper.*

We now prepared the comparison plots for N<sub>2</sub>O field between MLS measurements and MIROC3.2 CCM outputs, which are attached at the end of this reply as Figures R1, R2, R3, and R4. For those Figures, upper panels show southern polar plots of temperature and N<sub>2</sub>O field by MLS measurements at 490 K (~56 hPa), while lower panels show N<sub>2</sub>O field by MIROC3.2 CCM output at 50 hPa, for June 24 (Fig. R1), June 29 (Fig. R2), July 4 (Fig. R3), and July 9 (Fig. R4). The color scale are chosen to be similar values between MLS and MIROC3.2 CCM. The most apparent difference is that the low N<sub>2</sub>O values seen in MLS measurements at the vortex core were not reproduced by MIROC3.2 CCM. For the N<sub>2</sub>O gradients around the vortex edge, it is rather difficult to tell the difference between MLS measurements and MIROC3.2 CCM outputs. However, if you see the difference in N<sub>2</sub>O values between the core of polar vortex and vortex edge on July 4 in Fig. R3, it was about 100 ppbv (100 and 200 ppbv for core and edge, respectively) for MLS measurement. On the other hand, the difference in N<sub>2</sub>O values between the core of the polar vortex and vortex edge for MIROC3.2 CCM was about 80 ppbv (150 and 230 ppbv). Therefore, it is supposed that there may exist more mixing of airmass by MIROC3.2 CCM compared with MLS measurements, due to coarse resolution of the model calculation.

#### ***(8) Continuous loss of HCl in the core of the polar vortex***

*In response to the review comments, the authors have substantially revised the discussion on continuous loss of HCl in the core of the polar vortex. Nonetheless, I would like to come back on a few points of which I think that they could be better represented in the manuscript.*

*Note that the HCl loss processes described by Grooß et al. (2018) and Solomon et al. (2015) are very different: Grooß et al. (2018) describe a polar night process, whereas Solomon et al. (2015) describe a dynamical process (acting later in the course of the existence of the polar vortex). The dynamical process suggested by Solomon et al. (2015) requires light as formation of ClONO<sub>2</sub> is involved. This is also true for the explanation for the continuing decline of HCl under sunlit conditions through the formation of HOCl (Grooß et al., 2011; Müller et al., 2018).*

*Finally, ClONO<sub>2</sub> is not enhanced at the vortex edge in June or May (see Figs. 13 and 14). Also transport of ClONO<sub>2</sub> from the vortex edge to the vortex core does not occur in isolation but in mid-winter likely mixes in air with enhanced HCl and ozone (see below and first review). A very different issue again is the mixing of 'out-of-vortex' air; first, this is less likely and, second, it would certainly bring in non-activated air with substantial concentrations of HCl.*

We agree to reviewer that Solomon et al. (2015) and Jaeglé et al. (1997) are describing rather different dynamical process on mixing of airmass after August (day 210-), which is different from the continuous loss of HCl at the core of the polar vortex in June and July (day 160-210). Therefore, we deleted the citation of Solomon et al. (2015) and Jaeglé et al. (1997) here. Nevertheless, we believe that the continuous loss of HCl in June and July occurs due to the mixing of ClONO<sub>2</sub> containing air with remaining HCl at the vortex core. In order to show our idea of mixing of ClONO<sub>2</sub> rich air with remaining HCl at the core of the polar vortex during the polar night time (June to July), we now created a Figure R5 (attached at the end of this reply) which shows equivalent-latitude-mean distribution of HCl and ClONO<sub>2</sub> from MIROC3.2 CCM at 50 hPa from early June to late July in 2007. At the beginning of June (Fig. R5(a)), the shape of distributions of HCl and ClONO<sub>2</sub> were quite similar. Gradually, the amount of HCl and ClONO<sub>2</sub> in the polar vortex decreased in mid-June, (Fig. R5(b)), then the amount of ClONO<sub>2</sub> at the vortex edge (equivalent latitude of ~60°S) showed an increase while HCl continued to decrease there (Fig. R5(c)). Afterwards, there existed an apparent difference in the distribution of ClONO<sub>2</sub> and HCl at the vortex boundary region (equivalent latitude of 62-70°S; Figs. R5(d)-(f)). ClONO<sub>2</sub> existed about 5-8 degrees toward poleward compared with HCl throughout this period. Consequently, HCl near the vortex edge reacted with the ClONO<sub>2</sub> due to the mixing of airmass by heterogeneous reaction (R1) until HCl was totally depleted (See HCl values at ~65°S equivalent latitude on June 29 and July 9 in Figure R5 (d) and (e)). Such reaction continues toward poleward during the polar night period between June and July, and gradually HCl value in the polar vortex decreased as is shown in Figure R5 (f). Such differences in distribution of HCl and ClONO<sub>2</sub> can be also seen if you look at the distribution of these species carefully at the edge of polar vortex on June 24, 2007 in Figure 13.

## **(9) Model description**

*In response to my first review, the authors have substantially extended the model description. However, the detailed description of the heterogeneous reactions is in Japanese and the paper still does not contain a list of reactions (e.g. add a list of reactions as an electronic appendix). Perhaps a bit more could be done regarding model description. As discussed below, some model behaviour raises the questions, exactly which reactions are taken into account in the model formulation.*

In response to the reviewer's comment, we now added a new appendix Table A2 which shows all the 42 photolysis reactions, 140 gas phase reactions, and 13 heterogeneous reactions with their reaction coefficients.

#### **(10) Data Availability**

*A data availability statement has now been added to this paper. I think in particular making the FTIR data available is very helpful. You might want to add statements regarding MLS, MIPAS and MIROC3.2.*

The data availability for MIROC3.2 CCM outputs were already stated in the previous manuscript. Now, we added data availability statement for MLS, MIPAS, and CALIOP satellite data at the same place.

#### **Some details regarding the revised version**

*(11) p 1, l 21: ClONO<sub>2</sub> was almost depleted; but what about HCl?*

HCl was also almost depleted in our observations. We now modified the text to: “**both HCl** and ClONO<sub>2</sub> were almost depleted ...”.

*(12) p 1, l 25 “comprehensive behaviour” is unclear, what is meant here?*

We reworded to: “... to see the behavior of **whole** chlorine and related species ...”.

*(13) p. 3, l 6: perhaps you want to add a reference here for R 12 also? Santee et al. (2008) would be a possibility.*

We added **Santee et al. (2008)** for the reference here.

*(14) p. 3, l 22: replace 'formation' by 'existence'*

It was replaced as suggested.

*(15) p. 8, l 31: This relation (Eq. 2) is only true for conditions of 1997. Assuming that N<sub>2</sub>O is constant, the Cly calculated from this equation is only valid for 1997. Correct? So one needs to take into account the temporal trend of Cly between 1997 and 2007 or 2011. In reality there are also temporal changes of N<sub>2</sub>O that should be*

taken into account. Only thereafter the adjustments suggested by Strahan et al. (2014) should be taken into account.

Thank you for your comment. We now considered the temporal trends of Cl<sub>y</sub> and N<sub>2</sub>O values, and calculated Cl<sub>y</sub>\* values by considering the change of Cl<sub>y</sub> and N<sub>2</sub>O trends. Accordingly, plot values of Cl<sub>y</sub>\* and ratios to Cl<sub>y</sub>\* in Figs. 4-9, 11, and 12 are also modified.

(16) p 9, l 5: state here to which figure the 'light shaded region' etc belongs.

It was for Figures 4-7. It is now stated in the text.

(17) p 9, l 16: "was occurred" ---> "occurred"

It was modified as suggested.

(18) p 10, l 20: 'ratio of HCl' etc – this is unclear. I think you mean mixing ratio here? Or HCl/Cl<sub>y</sub> ratio? This should be clarified. (similar in l. 29).

In this section, we meant "ratio of HCl" to "HCl/Cl<sub>y</sub>\* ratio". However, it might be a bit unclear for readers. Instead, we now reworded to use the term "HCl/Cl<sub>y</sub>\*" etc. throughout this section.

(19) p. 11, l 32: taken up by PSCs (or similar)

It was modified as suggested.

(20) p 12, l 2 (R18): there is also the reaction  $HNO_3 + OH \rightarrow NO_3 + H_2O$

We now added the suggested new reaction (R19) here.

(21) p 12, l. 27: this is indeed not unlikely, however the change of stratospheric Cl<sub>y</sub> between 1997 and 2007 as well as between 1997 and 2011 can be quantified and should not be ignored.

We agree. We deleted this explanation here. Also, the change of stratospheric Cl<sub>y</sub> among 1997, 2007, and 2011 is now considered in the draft.

(22) 13, l 8: note that enhanced ClONO<sub>2</sub> is not seen in June!

As stated in the response (8), there is a ClONO<sub>2</sub> enhanced area at equivalent latitude 62-70°S in June and July where the HCl is very low (see attached Figure R5).

(23) p 13, l 11: *not only CLaMS but also SD-WACCM and TOMCAT/SLIMCAT*

Now, all three models are stated in the draft.

(24) p 14, l 21: *“the decrease of HCl stopped . . . ” – I think the authors have an important point here. But is this not the model behaviour reported by Grooß et al. (2018)? And a model behaviour which is not in agreement with HCl observations. I suggest more discussion here.*

I think at this point, HCl sudden decrease stopped because the counter-part of reaction (R1); ClONO<sub>2</sub> was gone at this moment. This is the same as the model behavior reported by Grooß et al. (2018). However, the decrease of HCl continued from mid-June to late July (days 160-210) in the core of the vortex (87.9°S), which is the different feature as Grooß et al. (2018). This point is now discussed in Section 4.6 in more detail.

(25) p. 15, l 2: *note that there is also HOCl production in the gas-phase (ClO + HO<sub>2</sub>; the details might depend on the HO<sub>2</sub> production in the photolysis of CH<sub>2</sub>O, see e.g. Müller et al. (2018). I would be interesting to analyse here in detail the assumptions in the MIROC3.2 model.*

We checked the list of all the reactions in MIROC3.2 CCM in new Table A2 and confirmed that all the reactions which consist of C1, C2, C3, and C4 in Müller et al. (2018) was included in our model calculation. Therefore, the formation of HOCl at the vortex core was suggested to be due to chemical cycles C1, C2, C3, or C4 if the airmass was travelled at the sunlit area a few days earlier due to the distortion of the polar vortex in this period. Such a discussion is now added in the new draft.

(26) p. 15., l 7: *I think cycles C3 and C4 are not defined in the manuscript. I suggest to include a brief explanation here not just a reference.*

The explanation of cycles C1, C2, C3, and C4 are now added in Appendix C, including all related reactions.

(27) p. 15, l 19: *For this interpretation, it is important to take into account that the poleward transport of ClONO<sub>2</sub> by mixing (this is the point here if I understand the text correctly) does not occur in isolation. The impact of such mixing depends on the time period considered. In deep winter mixing would not transport only ClONO<sub>2</sub>, but also HCl and ozone. On the other hand, in June (Fig. 13) there is no enhancement of ClONO<sub>2</sub> at the vortex edge, so what could be the effect of mixing of vortex edge air in June?*

As is now explicitly shown in attached Figure R5, there is an airmass at equivalent latitude of ~62-70°S where there was substantial amount of ClONO<sub>2</sub>, but almost no HCl between the middle of June and the end of July. If such an airmass mixes with more poleward airmass, it can destroy the remaining HCl at the vortex core without sunlight. If you carefully look at the ClONO<sub>2</sub> distribution on June 24, 2007 in Figure 13, you can

see some enhancement of ClONO<sub>2</sub> around the polar vortex edge where there is no HCl there.

*(28) p 16, l 10: PSCs do not form at NAT saturation temperature as stated in this sentence. In general; I suggest using the same wording throughout the paper for this issue. Be clear if you mean onset of heterogeneous chemistry, PSC formation/existence etc. For example it is NAT saturation temperature, not NAT PSC saturation temperature.*

Thank you for your comments. We checked the PSC-related description throughout the draft, and tried to more clearly define the PSC formation/existence etc. Now, it was stated “When the stratospheric temperature over Syowa Station fell ~4K below NAT saturation temperature, PSCs started to form ...”.

*(29) p 16, l 15: ‘comprehensive behaviour’?*

It was reworded as: “To see the behavior of **whole** chlorine and related species ...”.

*(30) Fig 13: It is difficult to see two white circles here – I can see only one.*

There is only one circle in each panel, because only one of outer or inner edges were defined for these days (please see Figures A1 and A2). In order to more clearly state this, the term “**(outer)** edge” was added in the caption.

*(31) Fig 14: It is difficult to see two white circles here for August and October – I can see only one. The last sentence of the caption is difficult to understand. The dotted line for 5 July 2011 is confusing – is it correct? It looks rather different than the various chemical species. Is the point here that on 5 July 2011 only an inner vortex edge is defined but no actual vortex edge?*

We are sorry for the confusion. In all these four days, only either outer edge (Aug. 19, 21, Oct. 9) or inner edge (July 5) was defined at 450 K (see Figure A2 (a)). Since the locations of inner and outer edge were different, we plotted the inner edge with different dotted circle. We modified the captions to more clearly show the feature of defined vortex edges in Figures 13 and 14.

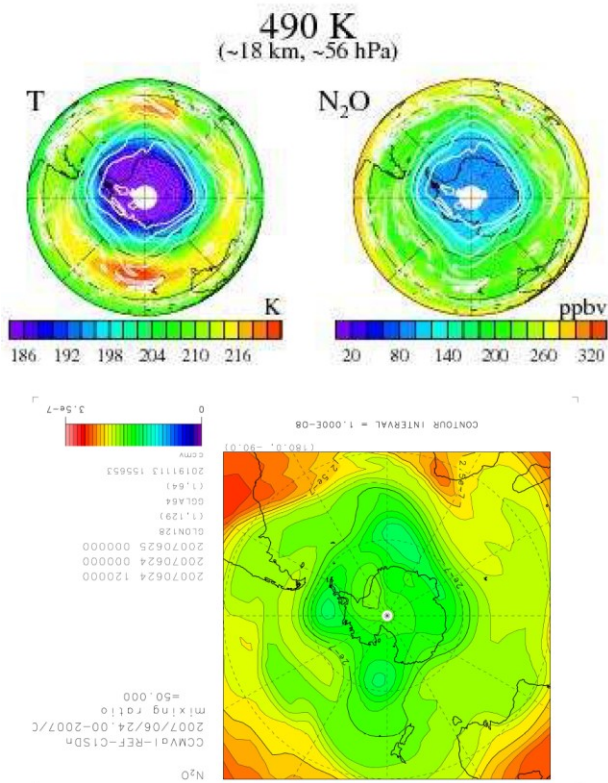


Fig. R1. SH N<sub>2</sub>O field on 2007/06/24 (175 days)

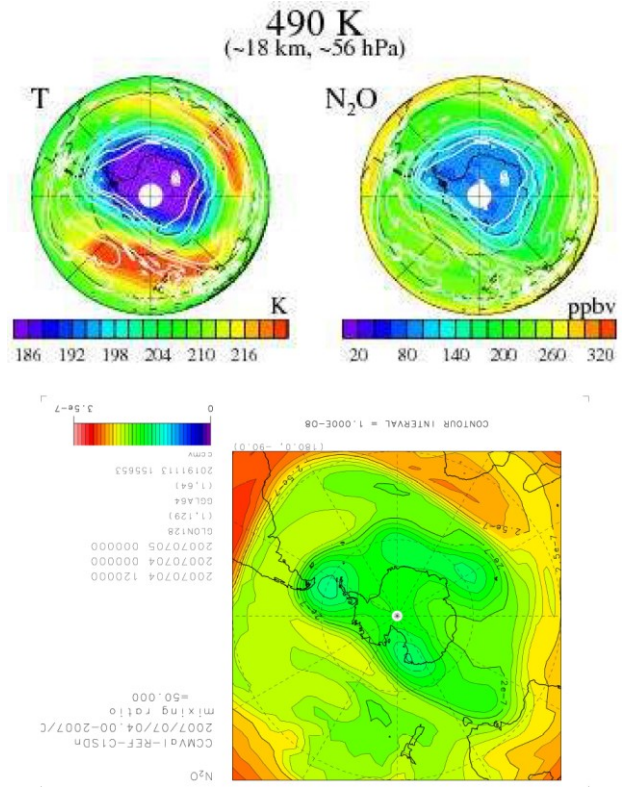


Fig. R3. SH N<sub>2</sub>O field on 2007/07/04 (185 days)

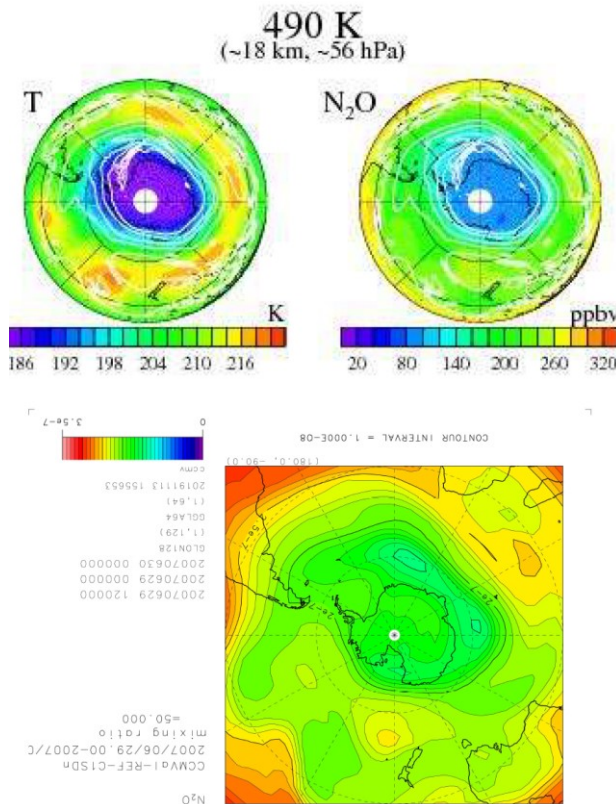


Fig. R2. SH N<sub>2</sub>O field on 2007/06/29 (180 days)

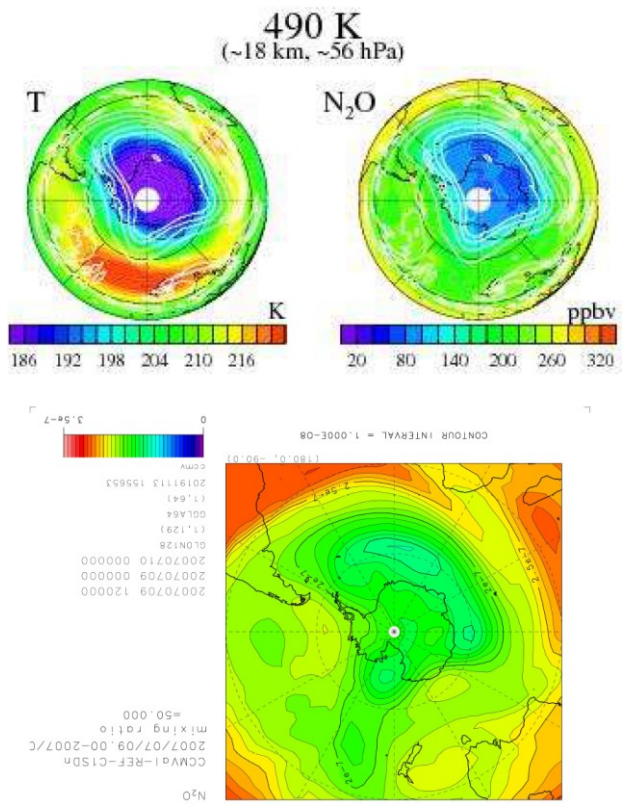
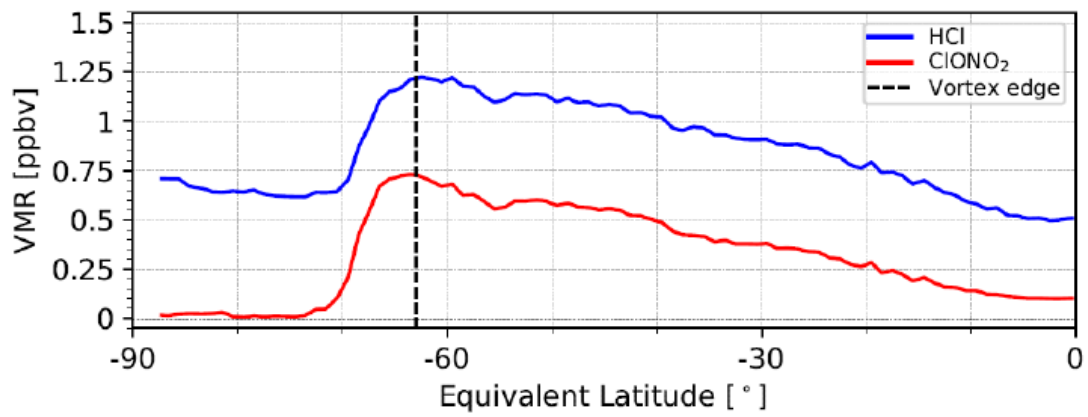


Fig. R4. SH N<sub>2</sub>O field on 2007/07/09 (190 days)

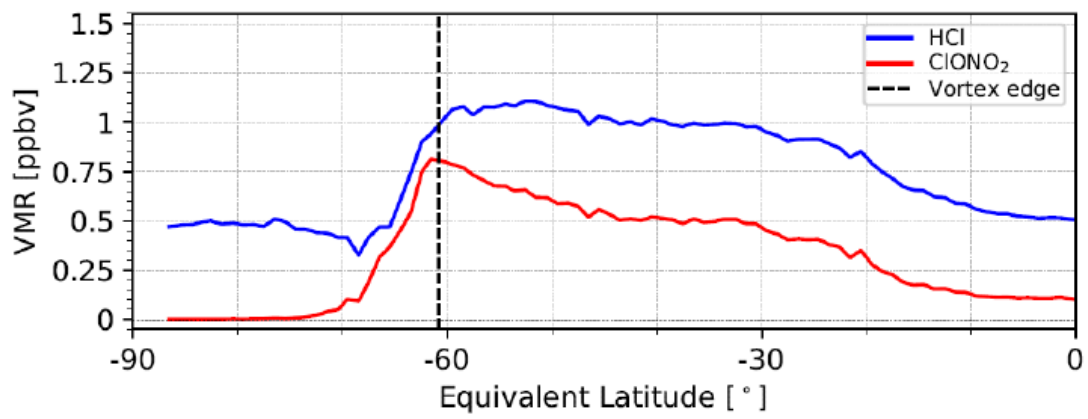
(a)

VMR vs. Equiv. Lat. - 2007-06-01



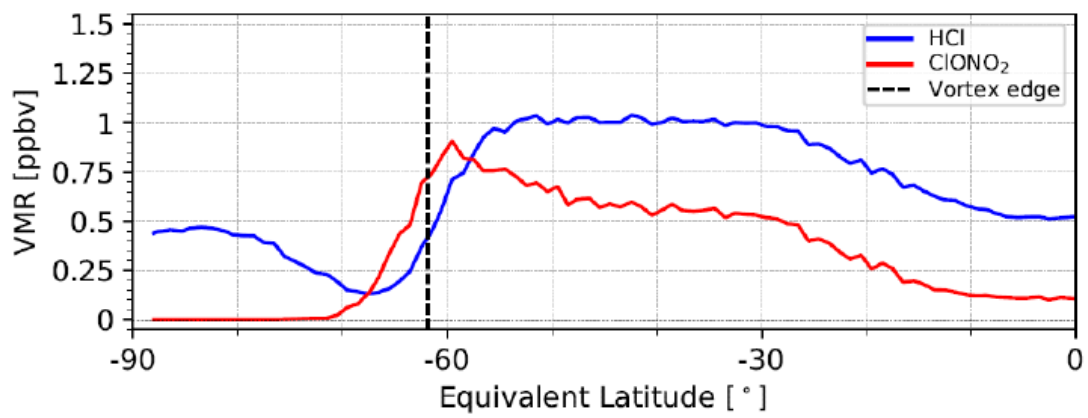
(b)

VMR vs. Equiv. Lat. - 2007-06-11



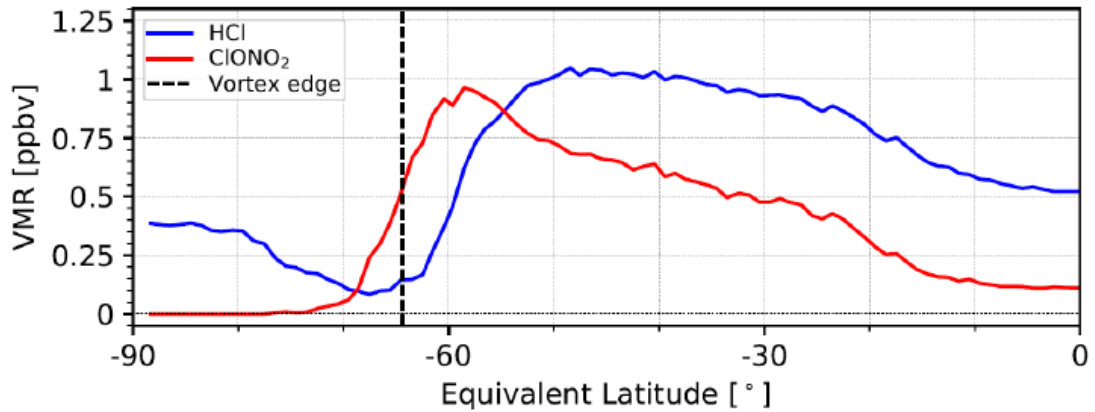
(c)

VMR vs. Equiv. Lat. - 2007-06-21



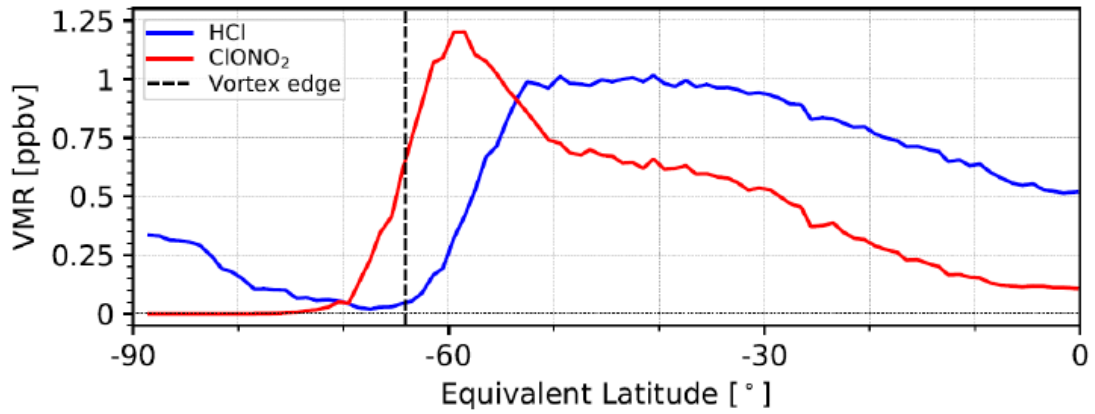
(d)

VMR vs. Equiv. Lat. - 2007-06-29



(e)

VMR vs. Equiv. Lat. - 2007-07-09



(f)

VMR vs. Equiv. Lat. - 2007-07-19

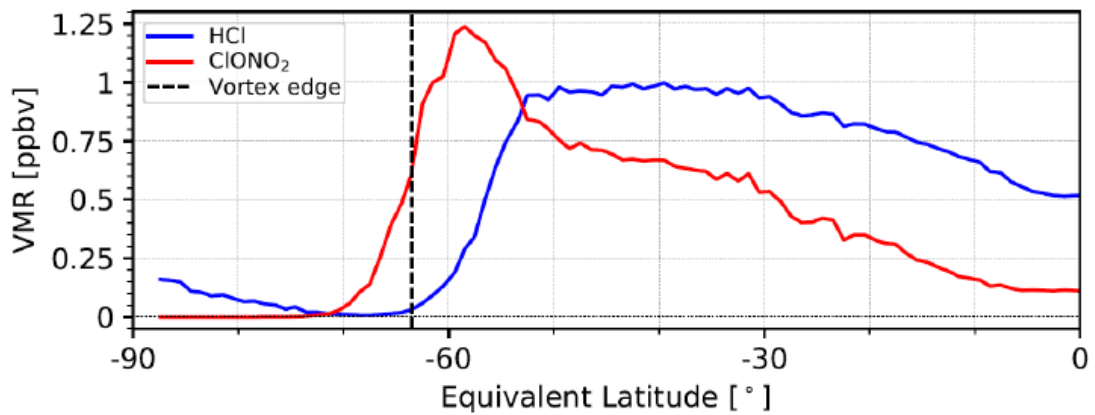


Figure R5. Equivalent-latitude-mean distribution of HCl and ClONO<sub>2</sub> from MIROC3.2 CCM at 50 hPa on (a) June 1 (day 152), (b) June 11 (day 162), (c) June 21 (day 172), (d) June 29 (day 180), (e) July 9 (day 190), and (f) July 19 (day 200), 2007. Dotted line shows the defined (outer) polar vortex edge at 450 K.

# Chlorine partitioning near the polar vortex edge observed with ground-based FTIR and satellites at Syowa Station, Antarctica in 2007 and 2011

5 Hideaki Nakajima<sup>1,2</sup>, Isao Murata<sup>2</sup>, Yoshihiro Nagahama<sup>1</sup>, Hideharu Akiyoshi<sup>1</sup>, Kosuke Saeki<sup>2,3</sup>, Takeshi Kinase<sup>4</sup>, Masanori Takeda<sup>2</sup>, Yoshihiro Tomikawa<sup>5,6</sup>, Eric Dupuy<sup>1</sup>, and Nicholas B. Jones<sup>7</sup>

<sup>1</sup>National Institute for Environmental Studies, Tsukuba, Ibaraki, 305-8506, Japan

<sup>2</sup>Graduate School of Environmental Studies, Tohoku University, Sendai, Miyagi, 980-8572, Japan

<sup>3</sup>now at Weathernews Inc., Chiba, 261-0023, Japan

<sup>4</sup>Meteorological Research Institute, Tsukuba, Ibaraki, 305-0052, Japan

10 <sup>5</sup>National Institute of Polar Research, Tachikawa, Tokyo, 190-8518, Japan

<sup>6</sup>The Graduate University for Advanced Studies, Tachikawa, Tokyo, 190-8518, Japan

<sup>7</sup>University of Wollongong, Wollongong, New South Wales, 2522, Australia

*Correspondence to:* Hideaki Nakajima (nakajima@nies.go.jp)

## Abstract.

15 We retrieved lower stratospheric vertical profiles of O<sub>3</sub>, HNO<sub>3</sub>, and HCl from solar spectra taken with a ground-based Fourier-Transform infrared spectrometer (FTIR) installed at Syowa Station, Antarctica (69.0°S, 39.6°E) from March to December 2007 and September to November 2011. This was the first continuous measurements of chlorine species throughout the ozone hole period from the ground in Antarctica. We analyzed temporal variation of these species combined with ClO, HCl, and HNO<sub>3</sub> data taken with the Aura/MLS (Microwave Limb Sounder) satellite sensor, and ClONO<sub>2</sub> data taken with the  
20 Envisat/MIPAS (The Michelson Interferometer for Passive Atmospheric Sounding) satellite sensor at 18 and 22 km over Syowa Station. HCl and ClONO<sub>2</sub> decrease occurred at both 18 and 22 km, and soon both HCl and ClONO<sub>2</sub> were almost depleted in early winter. When the sun returned to Antarctica in spring, enhancement of ClO and gradual O<sub>3</sub> destruction were observed. During the ClO enhanced period, negative correlation between ClO and ClONO<sub>2</sub> was observed in the time-series of the data at Syowa Station. This negative correlation was associated with the relative distance between Syowa Station and  
25 the edge of the polar vortex. We used MIROC3.2 Chemistry-Climate Model (CCM) results to see the comprehensive-behavior of whole chlorine and related species inside the polar vortex and the boundary region in more detail. From CCM model results, rapid conversion of chlorine reservoir species (HCl and ClONO<sub>2</sub>) into Cl<sub>2</sub>, gradual conversion of Cl<sub>2</sub> into Cl<sub>2</sub>O<sub>2</sub>, increase of HOCl in winter period, increase of ClO when sunlight became available, and conversion of ClO into HCl, was successfully reproduced. HCl decrease in the winter polar vortex core continued to occur due to both~~either the~~ transport of ClONO<sub>2</sub> from  
30 the subpolar region to higher latitudes, providing a flux of ClONO<sub>2</sub> from more sunlit latitudes into the polar vortex, and~~er~~ the heterogeneous reaction with HOCl. Temporal variation of chlorine species over Syowa Station was affected by both heterogeneous chemistry~~chemistries~~ related to Polar Stratospheric Cloud (PSC) occurrence inside the polar vortex, and transport of ~~a~~ NO<sub>x</sub>-rich air mass from the polar vortex boundary region which can produce additional ClONO<sub>2</sub> by reaction of

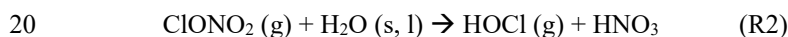
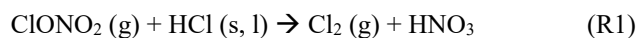
ClO with NO<sub>2</sub>. The deactivation pathways from active chlorine into reservoir species (HCl and/or ClONO<sub>2</sub>) were confirmed to be highly dependent on the availability of ambient O<sub>3</sub>. At an altitude where most ozone was depleted in Antarctica (18 km), most ClO was converted to HCl. However, at an altitude where there were some O<sub>3</sub> available (22 km), additional increase of ClONO<sub>2</sub> from pre-winter value can occur, similar to the case as in the Arctic.

5

## 1. Introduction

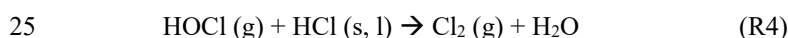
Discussion of the detection of “recovery” of the Antarctic ozone hole as the result of chlorofluorocarbon (CFC) regulations has been attracting attention. The occurrence of the Antarctic ozone hole is considered to continue at least until the middle of this century. The world’s leading Chemistry-Climate Models (CCMs) indicate that the multi-model mean time series of the springtime Antarctic total column ozone will return to 1980 levels shortly after mid-century (about 2060) (WMO, 2019). In fact, the recovery time predicted by CCMs has large uncertainty, and the observed ozone hole magnitude also shows year-to-year variability (e.g., see Figure 4-6 in WMO (2019)). Although Solomon et al. (2016) and de Laat et al. (2017) reported signs of healing in the Antarctic ozone layer only in September, there is no statistically conclusive report on the Antarctic ozone hole recovery (Yang et al., 2008; Kuttippurath et al, 2010; WMO, 2019).

To understand ozone depletion processes in polar regions, understanding of the behavior and partitioning of active chlorines (ClO<sub>x</sub>=Cl+Cl<sub>2</sub>+ClO+ClOO+Cl<sub>2</sub>O<sub>2</sub>) and chlorine reservoirs (HCl and ClONO<sub>2</sub>) are crucial. Recently, the importance of ClONO<sub>2</sub> was reviewed by von Clarmann and Johansson (2018). Chlorine reservoir is converted to active chlorine that destroys ozone on polar stratospheric clouds (PSCs) and/or cold binary sulphate through heterogeneous reactions:



where g, s, and l represent the gas, solid, and liquid phases, respectively (Solomon et al., 1986; Solomon, 1999; Drdla and Müller, 2012; Wegner et al., 2012; Nakajima et al., 2016).

Heterogeneous reactions:



are responsible for additional chlorine activation. When solar illumination is available, Cl<sub>2</sub>, HOCl, and ClNO<sub>2</sub> are photolyzed to produce chlorine atoms by reactions:

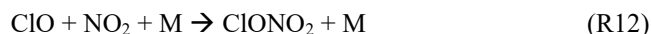


The yielded chlorine atoms then start to destroy ozone catalytically through reactions (Canty et al., 2016):





5 There are three types of PSCs, i.e., nitric acid trihydrate (NAT), supercooled ternary solution (STS), and ice PSCs. When the stratospheric temperatures get warmer than NAT ~~PSC~~-saturation temperature (about 195 K at 50 hPa) and no PSCs are present, deactivation of chlorine starts to occur. Re-formation of ClONO<sub>2</sub> and HCl mainly occurs through reactions ([Santee et al., 2008](#); Grooß et al., 2011; Müller et al., 2018):



The re-formation of ClONO<sub>2</sub> by reaction (R12) from active chlorine is much faster than that of HCl by reactions (R13) and (R14), if enough NO<sub>x</sub> are available (Mellqvist et al., 2002; Dufour et al., 2006). But the formation rates of ClONO<sub>2</sub> and HCl are also related to ozone concentration. Grooß et al. (1997) showed that HCl increases more rapidly in the Antarctic polar vortex than in the Arctic polar vortex due to lower ozone concentrations in the Antarctic polar vortex. Low ozone reduces the rate of reaction (R8), and then Cl/ClO ratio becomes high. Low ozone also reduces the rate of the following reaction:



This makes NO/NO<sub>2</sub> ratio high and increases Cl/ClO ratio by the following reaction:



High Cl/ClO ratio leads to rapid HCl formation by reactions (R13) and (R14), and reduces the formation ratio of ClONO<sub>2</sub> by reaction (R12) (Grooß et al., 2011; Müller et al., 2018).

The processes of deactivation of active chlorine are different between typical conditions in the Antarctic and those in the Arctic. In the Antarctic, the temperature cools below the NAT PSC ~~existence~~~~formation~~ threshold (about 195 K at 50 hPa) in the whole area of the polar vortex in all years, and almost complete denitrification and chlorine activation occur (WMO, 2007), followed by severe ozone depletion in spring. In the chlorine reservoir recovery phase, HCl is mainly formed by reaction (R13) due to the lack of ozone (typically less than 0.5 ppmv) by the mechanism described in the previous paragraph (Grooß et al., 2011).

On the other hand, in the Arctic, typically less PSC formation occurs in the polar vortex due to generally higher stratospheric temperatures (~10-15K in average) compared with that of Antarctica. Then only partial denitrification and chlorine activation occur in some years (Manney et al., 2011; WMO, 2014). In this case, some ozone and NO<sub>2</sub> are available in the chlorine reservoir recovery phase. Therefore, the ClONO<sub>2</sub> amount becomes higher than that of HCl after PSCs have disappeared due to the rapid reaction (R12) (Michelsen et al., 1999; Santee et al., 2003), which results in additional increase of ClONO<sub>2</sub> than pre-winter value at the time of chlorine deactivation in spring (von Clarmann et al., 1993; Müller et al., 1994; Oelhaf et al., 1994). In this way, the partitioning of the chlorine reservoir in springtime is related to temperature, PSC amounts, ozone, and NO<sub>2</sub> concentrations (Santee et al., 2008; Solomon et al., 2015).

In the polar regions, the ozone and related atmospheric trace gas species have been intensively monitored by several measurement techniques since the discovery of the ozone hole. These measurements consist of direct observations by high-altitude aircrafts (e.g., Anderson et al., 1989; Ko et al., 1989; Tuck et al., 1995; Jaeglé et al., 1997; Bonne et al., 2000), remote sensing observations by satellites (e.g., Müller et al., 1996; Michelsen et al., 1999; Höpfner et al., 2004; Dufour et al., 2006; Hayashida et al., 2007), remote sensing observations of OClO using UV-visible spectrometer from the ground (Solomon et al., 1987; Kreher et al., 1996), and remote sensing observations of ClO by a microwave spectrometer from the ground (de Zafra et al., 1989). Within these observations, ground-based measurements have the characteristic of high temporal resolution. In addition, the Fourier-Transform infrared spectrometer (FTIR) has the capability of measuring several trace gas species at the same time or in a short time interval (Rinsland et al., 1988). In this paper, we show the results of ground-based FTIR observations of O<sub>3</sub> and other trace gas species at Syowa Station in the Antarctic in 2007 and 2011, combined with ~~the~~ satellite measurements of trace gas species from theby Microwave Limb Sounder onboard the Aura satellite (Aura/MLS) and Michelson Interferometer for Passive Atmospheric Sounding onboard the European Environmental Satellite (Envisat/MIPAS), to show the temporal variation and partitioning of active chlorine (ClO<sub>x</sub>) and chlorine reservoirs (HCl, ClONO<sub>2</sub>) from fall to spring during the ozone hole formation and dissipation period. In order to monitor the appearance of PSCs over Syowa Station, we used the Cloud-Aerosol Lidar with Orthogonal Polarization (CALIOP) data onboard the Cloud-Aerosol Lidar and Infrared Pathfinder Satellite Observations (CALIPSO) satellite. The methods of FTIR and satellite measurements are described in Section 2. The validation of FTIR measurements is described in Section 3. The results of FTIR and satellite measurements and discussion on the behavior of active and inert chlorine species using the MIROC3.2 chemistry-climate model are described in Section 4.

20

## 2. Measurements

### 2.1 FTIR measurements

The Japanese Antarctic Syowa Station (69.0°S, 39.6°E) was established in January 1957. Since then, several scientific observations related to meteorology, upper atmospheric physics, glaciology, biology, geology, seismology, etc. have been performed. The ozone hole was first detected by Dobson spectrometer and ozonesonde measurements from Syowa Station in 1982 (Chubachi, 1984) and by Dobson spectrometer measurement at Halley Bay (Farman et al., 1985). We installed a Bruker IFS-120M high-resolution Fourier-Transform infrared spectrometer (FTIR) in the Observation Hut at Syowa Station in March 2007. This was the third high-resolution FTIR site in Antarctica in operation after U.S.A.'s South Pole Station (90.0°S) (Goldman et al., 1983; Goldman et al., 1987; Murcray et al., 1987), U.S.A.'s McMurdo Station and New Zealand's Arrival Heights facility at Scott Station (77.8°S, 166.7°E) (Farmer et al., 1987; Murcray et al., 1989; Kreher et al., 1996; Wood et al., 2002; Wood et al., 2004). The IFS-120M FTIR has a wavenumber resolution of 0.0035 cm<sup>-1</sup>, with two liquid nitrogen cooled detectors (InSb and HgCdTe covering the frequency ranges 2000-5000 and 700-1300 cm<sup>-1</sup>, respectively) with six optical filters,

and fed by an external solar tracking system. One measurement takes about 10 minutes. At least six spectra were taken per day covering each filter region. Since Syowa Station is located at a relatively low latitude (69.0°S) compared with McMurdo or Scott Stations (77.8°S), there is an advantage of the short (about one month) polar night period, when we cannot measure atmospheric species using the sun as a light source. Since FTIR measurements at Syowa Station are possible from early spring (late July), FTIR can measure chemical species during ozone hole development. On the other hand, FTIR observations become possible only after September at McMurdo and Scott Stations. Another advantage of Syowa Station is that it is sometimes located at vortex boundary as well as inside and outside of the polar vortex and this enables us to measure chemical species at the different regions of polar chemistry related to the ozone hole. From March to December 2007, we made in total 78 days of FTIR measurements on sunny days. Another 19 days of FTIR measurements were performed from September to November 2011. After a few more measurements were performed in 2016, the FTIR was brought back to Japan in 2017. In Appendix, Table A1 shows the days when FTIR measurements were made at Syowa Station with the information inside/boundary/outside of the polar vortex defined by the method described in Appendix BA2 using ERA-Interim reanalysis data. Strahan et al. (2014) showed the year-to-year variation of Cl<sub>y</sub> observed in the lower stratosphere of the Antarctic polar vortex. The Cl<sub>y</sub> observed in 2007 (2.88 ppbv) was about +4.3% more, and that observed in 2011 (2.53 ppbv) was about -5.2% less, than the projected Cl<sub>y</sub> from Newman et al. (2007) (2.76 ppbv for 2007 and 2.67 ppbv for 2011).

The retrieval of the FTIR spectra was done with the SFIT2 Version 3.92 program (Rinsland et al., 1998; Hase et al., 2004). SFIT2 retrieves a vertical profile of trace gases using an optimal estimation formulation of Rodgers (2000), implemented with a semi-empirical method which was originally developed for microwave measurements (Parrish et al., 1992; Connor et al., 1995). The SFIT2 forward model fully describes the FTIR instrument response, with absorption coefficients calculated using the algorithm of Norton and Rinsland (1991). The atmosphere is constructed with 47 layers from the ground to 100 km, using the FSCATM (Gallery et al., 1983) program for atmospheric ray-tracing to account for refractive bending. The retrieval parameters for each gas, typical vertical resolution, and typical degrees of freedoms for signal (DOFS) are shown in Table 1. Temperature and pressure profiles between 0 and 30 km are taken by the Rawin sonde observations flown from Syowa Station on the same day by the Japanese Meteorological Agency (JMA), while values between 30 and 100 km are taken from the COSPAR International Reference Atmosphere 1986 (CIRA-86) standard atmosphere profile (Rees et al., 1990).

We retrieved vertical profiles of O<sub>3</sub>, HCl, and HNO<sub>3</sub> from the solar spectra. We used monthly averaged ozonesondes profiles (0-30 km) and Improve Limb Atmospheric Spectrometer-II (ILAS-II) (Nakajima, 2006; Nakajima et al., 2006; Sugita et al., 2006) profiles (30-100 km) for the a priori of O<sub>3</sub>, monthly averaged profiles from ILAS-II for HNO<sub>3</sub> and monthly averaged profiles from HALOE (Anderson et al., 2000) for HCl. We focus on the altitude range of 15-25 km in this study. Typical averaging kernels of the SFIT2 retrievals for O<sub>3</sub>, HNO<sub>3</sub>, and HCl are shown in Figures 1(a), (b), and (c), respectively.

## 2.2 Satellite measurements

The Earth Observing System (EOS) MLS onboard the Aura satellite was launched on 15 July 2004, to monitor several atmospheric chemical species in the upper troposphere to mesosphere (Waters et al., 2006). The Aura orbit is sun-synchronous

at 705 km altitude with an inclination of 98°, 13:45 ascending (north-going) equator-crossing time, and 98.8-min period. Vertical profiles are measured every ~165 km along the suborbital track, horizontal resolution is ~200-600 km along-track, ~3-10 km across-track, and vertical resolution is ~3-4 km in the lower to middle stratosphere (Froidevaux et al., 2006). ClO, HCl, and HNO<sub>3</sub> profiles used in this study were taken from Aura/MLS version 4.2 data (Liversey et al., 2006; Santee et al., 2011; Ziemke et al., 2011; Liversey et al., 2018). Only daytime ClO data was used for the analysis. ~~The MLS data were taken from the following site: <http://avdc.gsfc.nasa.gov/index.php?site=2045907950>.~~ The daily MLS data within 320 km distance between the measurement location and Syowa Station were selected.

MIPAS is a Fourier transform spectrometer sounding the thermal emission of the earth's atmosphere between 685 and 2410 cm<sup>-1</sup> (14.6-4.15 μm) in limb geometry (Fischer and Oelhaf, 1996; Fischer et al., 2008). The maximum optical path difference of MIPAS is 20 cm. The field-of-view of the instrument at the tangent points is about 3 km in the vertical and 30 km in the horizontal. In the standard observation mode in one limb-scan, 17 tangent points are observed with nominal altitudes 6, 9, 12, 15, 18, 21, 24, 27, 30, 33, 36, 39, 42, 47, 52, 60, and 68 km. In this mode, about 73 limb scans are recorded per orbit. The measurements of each orbit cover nearly the complete latitude range from about 87°S to 89°N. MIPAS was ~~placed~~ on board ~~the~~ Envisat, which was launched on 1 March 2002, and was put into a polar sun-synchronous orbit at an altitude of about 800 km with an inclination of 98.55° (von Clarmann et al., 2003). On its descending node, the satellite crosses the equator at 10:00 local time. Envisat performs 14.3 orbits per day, which results in a good global coverage. ClONO<sub>2</sub> profiles which we used in this study were taken from Envisat/MIPAS IMK/IAA version V5R\_CLONO2\_220 and V5R\_CLONO2\_222 (Höpfner et al., 2007). ~~The MIPAS data were taken from the following site: [http://share.lsd.f.kit.edu/imk/asf/sat/mipas-export/Data\\_by\\_Target/](http://share.lsd.f.kit.edu/imk/asf/sat/mipas-export/Data_by_Target/).~~ The daily MIPAS data within 320 km distance between the measurement location and Syowa Station were selected.

The CALIPSO satellite was launched on 28 April 2006. On ~~the~~ CALIPSO satellite, ~~the~~ CALIOP instrument was on board, to monitor aerosols, clouds, and PSCs (Pitts et al., 2007). CALIOP is a two-wavelength, polarization sensitive lidar that provides high vertical resolution profiles of backscatter coefficient at 532 and 1064 nm, as well as two orthogonal (parallel and perpendicular) polarization components at 532 nm (Winker et al., 2007). ~~The CALIOP data were taken from the following site: [https://www.calipso.larc.nasa.gov/resources/calipso\\_users\\_guide/data\\_summaries/psc/index.php](https://www.calipso.larc.nasa.gov/resources/calipso_users_guide/data_summaries/psc/index.php).~~ In order to monitor the appearance of PSCs over Syowa Station, the daily CALIOP PSC data (Pitts et al., 2007; 2009; 2011) within 320 km distance between the measurement location and Syowa Station were selected.

### 3. Validation of retrieved profiles from FTIR spectra with other measurements

We validated retrieved FTIR profiles of O<sub>3</sub> with ozonesondes and Aura/MLS version 3.3 data (Liversey et al., 2013) for 2007 measurements. Also, retrieved FTIR profiles of HNO<sub>3</sub> and HCl were validated with Aura/MLS data. We identified the nearest Aura/MLS data from the distance between the Aura/MLS tangent point at 20 km altitude and the point at 20 km altitude for

the direction of the sun from Syowa Station at the time of the FTIR measurement. The spatial and temporal collocation criteria used was within 300 km radius and  $\pm 6$  hours. The ozonesonde and Aura/MLS profiles were interpolated onto a 1 km-grid, then smoothed using a 5 km-wide running mean.

Figures 2(a)-(b) show absolute and relative differences of O<sub>3</sub> profiles retrieved from FTIR measurements and those from model 1Z ECC-type ozonesonde measurements, respectively, calculated from 14 coincident measurements from September 5 to December 17, 2007. Typical precision and accuracy of the ECC-type ozone sondes are considered to be  $\pm(3-5)\%$  and  $\pm(4-5)\%$ , respectively (Komhyr, 1986). We define the relative percentage difference D as:

$$D (\%) = 100 * (FTIR-sonde) / ((FTIR+sonde)/2). \quad (1)$$

The mean absolute difference between 15 and 25 km was within -0.02 to 0.40 ppmv. The mean relative difference D between 15 and 25 km was within -10.4 to +24.4%. The average of the mean relative differences D of O<sub>3</sub> for the altitude of interest in this study (18-22 km) was +6.1%, with the minimum of -10.4% and the maximum of +19.2%. FTIR data agree with validation data within root mean squares of typical errors in FTIR and validation data at the altitude of interest. Note that relatively large D values between 16 and 18 km are due to small ozone amount in the ozone hole. Our validation results are quite comparable with ~~o~~the validation study at Izaña Observatory by Schneider et al. (2008).

Figures 2(c)-(d) show absolute and relative differences of O<sub>3</sub> profiles retrieved from FTIR measurements and those from Aura/MLS measurements, respectively, calculated from 33 coincident measurements from April 1 to December 20, 2007. The accuracy of MLS O<sub>3</sub> data are reported to be 5-8% between 0.5 and 46 hPa (Livesey et al., 2013). The mean absolute difference between 15 and 25 km was within -0.13 to +0.16 ppmv. The mean relative difference D between 15 and 25 km was within -16.2 to +5.2%. The average of the mean relative differences D for O<sub>3</sub> for the altitude of interest in this study (18-22 km) was -5.5%, with the minimum of -16.3% and the maximum of +4.5%. Froidevoux et al. (2008) showed that Aura/MLS is +8% higher than ACE-FTS at 70°S, which may explain the negative bias of FTIR data compared with MLS data.

Figures 2(e)-(f) show absolute and relative differences of HNO<sub>3</sub> profiles retrieved by FTIR measurements and those from Aura/MLS measurements, respectively, calculated from 47 coincident measurements from March 25 to December 20, 2007. The mean absolute difference between 15 and 25 km was within -0.56 to +0.57 ppbv. The mean relative difference D between 15 and 25 km was within -25.5 to +21.9%. The average of the mean relative differences D for HNO<sub>3</sub> for the altitude of interest in this study (18-22 km) was +13.2%, with the minimum of +0.2% and the maximum of +21.9%. This positive bias of FTIR data is still within the error bars of FTIR measurements. Livesey et al. (2013) showed that Aura/MLS version 3.3 data has no bias within errors ( $\sim 0.6-0.7$  ppbv (10-12%) at pressure level of 100-3.2 hPa) compared with other measurements. Livesey et al. (2018) showed no major differences between Aura/MLS version 3.3 and version 4.2 data for HNO<sub>3</sub>.

Figures 2(g)-(h) show absolute and relative differences of HCl profiles retrieved by FTIR measurements and those from Aura/MLS measurements, respectively, calculated from 50 coincident measurements from March 25 to December 20, 2007. The mean absolute difference between 15 and 25 km was within -0.20 to -0.09 ppbv. The mean relative difference D between 15 and 25 km was within -34.1 to -3.0%. The average of mean relative differences D for HCl for the altitude of interest in this study (18-22 km) is -9.7%, with a minimum of -14.6% and a maximum of -3.0%. This negative bias of FTIR data is still

within the error bars of FTIR measurements. Moreover, Livesey et al. (2013) showed that Aura/MLS version 3.3 values are systematically greater than HALOE values by 10-15% with a precision of 0.2-0.6 ppbv (10-30%) in the stratosphere, which may partly explain the negative bias of FTIR data compared with MLS data. Livesey et al. (2018) showed no major differences between Aura/MLS version 3.3 and version 4.2 data for HCl.

5 Table 2 summarizes validation results of FTIR profiles compared with ozonesonde or Aura/MLS measurements, and possible Aura/MLS biases from literature.

## 4. Results and discussion

### 4.1 Time series of observed species

10 Figure 3(a) shows daytime hours at Syowa Station. Polar night ends at Syowa Station on July 14 (day 195). Figures 3(b)-(e) show the time series of temperatures at 18 and 22 km over Syowa Station using ERA-Interim data (Dee et al., 2011) for 2007 and 2011. Approximate saturation temperatures for NAT PSC ( $T_{\text{NAT}}$ ) and ice PSC ( $T_{\text{ICE}}$ ) calculated by assuming 6 ppbv  $\text{HNO}_3$  and 4.5 ppmv  $\text{H}_2\text{O}$  are also shown in the figures. The dates when PSCs were observed at Syowa Station identified by the nearest CALIOP data of that day were indicated by asterisks at the bottom of the figures. Over Syowa Station, PSCs were  
15 observed when temperature fell  $\sim 4\text{K}$  below  $T_{\text{NAT}}$ . PSCs were often observed at 15-25 km from the beginning of July (day 183) to late August (day 241) in 2007, and from late June (day 175) to early September (day 251) in 2011.

PSCs were observed only at 18 km after August, due to the sedimentation of PSCs and downwelling of vortex air in late winter as is seen in Figure 3. Although temperatures above Syowa Station were sometimes below  $T_{\text{NAT}} - 4\text{K}$  in June and in late  
20 September, no PSC was observed during those periods. This may be due to other reasons, such as a different time history of temperature for PSC formation, and/or low  $\text{HNO}_3$  (denitrification) and/or  $\text{H}_2\text{O}$  concentration (dehydration) which are needed for PSC formation in late winter season (Saitoh et al., 2006).

Figures 4-7 show time series of HCl, ClONO<sub>2</sub>, ClO, Cl<sub>y</sub>\*, O<sub>3</sub>, and HNO<sub>3</sub> over Syowa Station in 2007 and 2011 at altitudes of 18 and 22 km for all ground-based and satellite-based observations used in this study, respectively. O<sub>3</sub> (sonde) is observed with the KC96 ozonesonde for 2007, which is different from the ones that were used for the validation in Section 3, and the  
25 ECC-1Z ozonesonde for 2011 by JMA (Smit and Straeter, 2004). HCl and HNO<sub>3</sub> observed by Aura/MLS and FTIR are plotted by different symbols. Total inorganic chlorine Cl<sub>y</sub>\* corresponds to the sum of HCl, ClONO<sub>2</sub>, and Cl<sub>x</sub>, where active chlorine species Cl<sub>x</sub> is defined as the sum of ClO, Cl, and 2\*Cl<sub>2</sub>O<sub>2</sub> (Bonne et al., 2000). It is known that total inorganic chlorine Cl<sub>y</sub>\* has a compact relationship with N<sub>2</sub>O (Bonne et al., 2000; Schauffler et al., 2003; Strahan et al., 2014). Inferred total inorganic chlorine Cl<sub>y</sub>\* is calculated from the N<sub>2</sub>O value (in ppbv) measured by MLS and by using the empirical polynomial equation  
30 derived from the correlation analysis of Cl<sub>y</sub> and N<sub>2</sub>O from the Photochemistry of Ozone Loss in the Arctic Region in Summer (POLARIS) mission which took place from April to September 1997 (Bonne et al., 2000). In order to compensate for the temporal trends of Cl<sub>y</sub> and N<sub>2</sub>O values (2.09, 2.76, and 2.67 ppbv for Cl<sub>y</sub> (Strahan et al., 2014), and 313, 321, and 324 ppbv

for N<sub>2</sub>O (WMO, 2007; 2011; 2014) for the years 1997, 2007, and 2011, respectively), we used values 8 and 11 for constant A, and 140 and 230 for constant B for years 2007 and 2011 in the following equation, respectively:

$$Cl_y^*(pptv) = 4.7070 \cdot 10^{-7} (N_2O - A)^4 - 3.2708 \cdot 10^{-4} (N_2O - A)^3 + 4.0818 \cdot 10^{-2} (N_2O - A)^2 - 4.6856 (N_2O - A) + 3225 - B. \quad (2)$$

If we consider the change of the Cl<sub>y</sub>, the estimated Cl<sub>y</sub>\* in 2007 might be 0.7% less than this value, while that in 2011 might be 12.8% less than this value (Strahan et al., 2014).

A transport barrier of minor constituents at the edge of polar vortex was reported by Lee et al. (2001) and Tilmes et al. (2006). The distribution of minor constituents is quite different among the inside, the boundary region, and outside the polar vortex. In Figures 4-7, the dark shaded area, the light shaded area, and the white area indicate the days when Syowa Station was located outside, in the boundary region, and inside the polar vortex, respectively. In the Antarctic winter, there are often double peaks in the isentropic potential vorticity gradient with respect to equivalent latitude at the 450-600 K level (Tomikawa et al., 2015). The method to determine the three polar regions, i.e., inside the polar vortex, the boundary region, and outside the polar vortex is described in Appendix B. Note that the Syowa Station is often located near the vortex edge and the temporal variations of chemical species observed over Syowa Station reflect the spatial distributions as well as local chemical evolution. When Syowa Station was located at the boundary region or outside the polar vortex (e.g., day 310-316 in Figure 4, day 192-195 in Figure 5, day 309-316 in Figure 6, day 276-282 in Figure 7), chemical species showed different values compared with the ones inside the polar vortex. The lack of data for ClO and HCl (MLS) from day 195 to day 219, 2007 and ClONO<sub>2</sub> from day 170 to day 216, 2007 (Figures 4(a) and 6(a)) is due to unrealistic large error values in Aura/MLS or Envisat/MIPAS data products during these periods.

The altitude of 18 km was selected because it was one of the altitudes where nearly complete ozone loss was occurred. The altitude of 22 km, where only about half of the ozone was depleted, was selected to show the difference in the behavior of chemical species from that at 18 km.

The general features of the chemical species observed inside the polar vortex at 18 and 22 km in 2007 and 2011 are summarized as follows: HCl and ClONO<sub>2</sub> decreased first, then ClO started to increase in winter, while HCl increases and ClO decreases were synchronized in spring. HCl was almost zero from late June to early September and the day-to-day variations were small over this period. HCl over Syowa Station indicates relatively larger values when it was located outside the polar vortex: For example, early August and the beginning of September at 22 km, 2007 in Figure 6. HNO<sub>3</sub> showed large decreases from June to July, and then gradually increased in summer. Day-to-day variations of HNO<sub>3</sub> from June to August were large. O<sub>3</sub> decreased from July to late September when ClO concentration was increased. ClO was enhanced in August and September and the day-to-day variations were large over this period. Cl<sub>y</sub>\* gradually increased in the polar vortex from late autumn to spring. The Cl<sub>y</sub>\* value became larger compared with its mixing ratio outside of the polar vortex in spring.

The following characteristics are evident at 18 km (Figures 4 and 5). O<sub>3</sub> gradually decreased from values of 2.5-3 ppmv before winter to values less than one fifth, 0.3-0.5 ppmv, in October. The values of HCl from late June to early September were as small as 0-0.3 ppbv. The recovered values of HCl inside the vortex in spring (October-December) were larger than

those before winter and those outside the polar vortex during the same period. ClONO<sub>2</sub> inside the vortex kept near zero even after ClO disappeared and did not recover to the level before winter until spring.

At 22 km (Figures 6 and 7), O<sub>3</sub> gradually decreased from winter to spring, but the magnitude of the decrease was much smaller than that at 18 km. The values of HCl from late June to early September were 0-1 ppbv, larger than those at 18 km. The recovered values of HCl in spring were nearly the same as those before winter (around 2.2 ppbv). ClONO<sub>2</sub> recovered to larger values than those before winter after ClO disappeared.

As for the temporal increase of ClONO<sub>2</sub> in spring during the ClO decreasing phase, we can see a peak of 1.5 ppbv at 18 km in 2011, and at 22 km in both 2007 and 2011 around September 27 (day 270), but we see no temporal increase of ClONO<sub>2</sub> at 18 km in 2007.

Figure 7 shows that temporal ClO enhancement and decrease of O<sub>3</sub>, ClONO<sub>2</sub>, and HNO<sub>3</sub> occurred in early winter (May 30-June 19; day 150-170) at 22 km in 2011. This small ozone depletion event before winter may be due to an air mass movement from the polar night area to a sunlit area at lower latitudes.

#### 4.2 Time series of ratios of chlorine species

In order to discuss the temporal variations of the chlorine partitioning, the ratios of observed HCl, ClONO<sub>2</sub>, and ClO with respect to Cl<sub>y</sub>\* were calculated. Hereafter, we will discuss the ratios of chlorine species only for the cases when Syowa Station was located inside the polar vortex.

Figures 8 and 9 show the time series of the ratios of each chlorine species with respect to Cl<sub>y</sub>\* in 2007 (a) and in 2011 (b) at 18 km and 22 km, respectively. In these plots, HCl data from Aura/MLS were used. Note that light blue in these figures shows either ClONO<sub>2</sub> or ClO data was missing on that day, while dark blue shows all three data were available on that day. For both in 2007 and 2011 at 18 km (Figure 8), the ratio of HCl/Cl<sub>y</sub>\* was 0.6-0.8 and the ratio of ClONO<sub>2</sub>/Cl<sub>y</sub>\* was 0.2-0.3 before winter (May 10-20; day 130-140). The ratio of HCl to Cl<sub>y</sub>\* was three times larger than that of ClONO<sub>2</sub> at that time. The ratio of ClO/Cl<sub>y</sub>\* increased to ~0.5 during the ClO enhanced period (the period when ClO values were more than 80 % of its maximum value: August 18-September 17; day 230-260). The ratio of HCl/Cl<sub>y</sub>\* was 0-0.2 and the ratio of ClONO<sub>2</sub>/Cl<sub>y</sub>\* was 0-0.6 during this same period. ClONO<sub>2</sub> shows negative correlation with ClO, while HCl kept low even when ClO was low during this period. This negative correlation is shown in Figure 10. When ClO was enhanced, the O<sub>3</sub> amount gradually decreased, and finally reached <0.5 ppmv (>80% destruction) in October (October 7; day 280) (See Figures 4 and 5). The ratios to Cl<sub>y</sub>\* became 0.9-1.0 for HCl and 0-0.1 for ClONO<sub>2</sub> after the recovery in spring (after October 17; day 290), indicating that almost all chlorine reservoir species became HCl via reactions (R13) and/or (R14), due to the lack of O<sub>3</sub> and NO<sub>2</sub> during this period. The sum ratios of (HCl + ClONO<sub>2</sub> + ClO)/Cl<sub>y</sub>\* were around 0.5-0.8 at the time of ClO enhanced period. The remaining chlorine is thought to be either Cl<sub>2</sub>O<sub>2</sub> or HOCl, which will be shown in model simulation result in Section 4.6. The sum ratio of (HCl + ClONO<sub>2</sub>)/Cl<sub>y</sub>\* became close to 1 after the recovery period (after October 7; day 280).

For both in 2007 and 2011 at 22 km (Figure 9), the ratio of HCl/Cl<sub>y</sub>\* was 0.8-0.9 and the ratio of ClONO<sub>2</sub>/Cl<sub>y</sub>\* was 0.2-0.3 before winter (April 20-May 20; day 110-140). The ratio of HCl to Cl<sub>y</sub>\* was three to four times larger than that of ClONO<sub>2</sub>.

The ratio of  $\text{ClO}/\text{Cl}_y^*$  increased to 0.5-0.7 during the ClO enhanced period (August 8-28; day 220-240 in 2007, August 18-September 7; day 230-250 in 2011). The ratio of  $\text{HCl}/\text{Cl}_y^*$  was 0-0.2 and the ratio of  $\text{ClONO}_2/\text{Cl}_y^*$  was 0-0.6 during this period.  $\text{ClONO}_2$  shows negative correlation with ClO, while HCl kept low even when ClO was low during this period as in the case at 18 km. The  $\text{O}_3$  amount gradually decreased during the ClO enhanced period but kept the concentration at more than 1.5 ppmv (less than half destruction) at this altitude (See Figures 6 and 7). When the ClO enhancement ended, increase of both  $\text{ClONO}_2$  and HCl occurred simultaneously in early spring (September 17-October 7; day 260-280). Then, the reservoir ratios to  $\text{Cl}_y^*$  became 0.6-0.7 for HCl and 0.3-0.4 for  $\text{ClONO}_2$  in spring (after October 7; day 280). This phenomenon shows that more chlorine deactivation via reaction (R12) occurred towards  $\text{ClONO}_2$  at 22 km rather than at 18 km. This is attributed to the existence of  $\text{O}_3$  and  $\text{NO}_2$  during this period at 22 km, which was different from the case at 18 km. The sum ratios of  $(\text{HCl} + \text{ClONO}_2 + \text{ClO})/\text{Cl}_y^*$  were around 0.7-1.2 at the time of ClO enhanced period. The remaining chlorine is thought to be either  $\text{Cl}_2\text{O}_2$  or  $\text{HOCl}$ . The sum ratio of  $(\text{HCl} + \text{ClONO}_2 + \text{ClO})/\text{Cl}_y^*$  became around 1.2 after the recovery period (after September 27; day 270). The reason why the observed sum ratio exceed the calculated  $\text{Cl}_y^*$  value might be because the  $\text{N}_2\text{O}-\text{Cl}_y$  correlation from the one in the equation (2) is not applicable at this altitude.

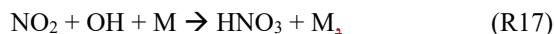
In 2011 at 18 km (Figure 8), another temporal increase of  $\text{ClONO}_2$  up to a ratio of 0.4 occurred in early spring (around October 2-12; day 275-285) in accordance with HCl increase, then the  $\text{ClONO}_2$  amount gradually decreased to nearly zero after late October (after October 27; day 300). This temporal increase in  $\text{ClONO}_2$  could be attributed to the temporal change of the location of Syowa Station with respect to the polar vortex. Although Syowa Station was judged to be inside the polar vortex during July 14-December 16 (day 195-350) by our analysis, the difference between the equivalent latitude over Syowa Station and that at the inner edge became less than 10 degrees at around October 7 (day 280), while it was typically between 15 and 20 degrees on other days.  $\text{O}_3$  and  $\text{HNO}_3$  showed higher values around October 7 (day 280) (see Figure 5), indicating that Syowa Station was located close to the boundary region during this period (See Figure A2). Therefore, the temporal increase of  $\text{ClONO}_2$  in 2011 at 18 km was attributed to spatial variation, not to chemical evolution.

### 4.3 Correlation between ClO and $\text{ClONO}_2$

Figure 10 shows the correlation between ClO and  $\text{ClONO}_2$  during the ClO enhanced period (August 8-September 17; day 220-260) at 18 km in 2007 (a) and 2011 (b), and at 22 km in 2007 (c) and 2011 (d). In this plot, the location of Syowa Station with respect to the polar vortex (inside, the boundary region, and outside the polar vortex) is indicated by different symbols. Note that MLS ClO and MIPAS  $\text{ClONO}_2$  data were sampled on the same day at the nearest orbit to Syowa Station for both satellites. The maximum differences between these two satellites' observational times and locations are 9.0 hours in time and 587 km in distance. Mean differences are 6.8 hours in time and 270 km in distance, respectively. Solid lines show regression lines obtained by Reduced Major Axis (RMA) regression. Negative correlations of slope about -1.0 between ClO and  $\text{ClONO}_2$  are seen in all figures.

The negative correlation between ClO and  $\text{ClONO}_2$  at Syowa Station is explained by the difference in the concentration of ClO,  $\text{NO}_2$ ,  $\text{ClONO}_2$ , and  $\text{HNO}_3$  inside, outside, and at the boundary region of the polar vortex around the station. Outside of

the polar vortex, ClO concentration is lower and NO<sub>2</sub> concentration is higher than those inside the polar vortex. Inside of the polar vortex, HNO<sub>3</sub> is taken up by into PSCs and removed by the sedimentation of PSCs from the lower stratosphere (denitrification process). The NO<sub>x</sub> concentration is low because HNO<sub>3</sub> is a reservoir of NO<sub>x</sub> through the reactions;



5 and



and



The NO<sub>2</sub> concentration is low and ClONO<sub>2</sub> concentration is also low due to the consumption of ClONO<sub>2</sub> by heterogeneous reaction (R2) inside the polar vortex. In spring, the ClO amount gets high due to the activation of chlorine species by reactions (R1~R8) inside the polar vortex. At the boundary region, ClO and NO<sub>2</sub> concentrations indicate the value between inside and outside of the polar vortex, that is, the ClO concentration is much higher than that outside of the polar vortex and NO<sub>2</sub> concentration is much higher than that inside of the polar vortex. Thus, the ClONO<sub>2</sub> concentration there is elevated in August-September due to the reaction (R12). This causes the negative correlation between ClO and ClONO<sub>2</sub> due to the relative distance between Syowa Station and the edge of the polar vortex. When Syowa Station was located deep inside the polar vortex, there was more ClO and less ClONO<sub>2</sub>. On the contrary when Syowa Station was located near the vortex edge, there was less ClO and more ClONO<sub>2</sub>. The equivalent latitude (EL) over Syowa Station was calculated as described in Appendix B for each correlation point. The EL at each correlation point is now shown by the color code in Figure 10. It generally shows the tendency, that warm coloured higher equivalent latitude points are located more towards the bottom right-hand side. This is further confirmed by 3-dimensional model simulation as shown later.

#### 4.4 Comparison with model results

Figures 11 and 12 show comparisons of daily time series of simulated mixing ratios of ClO, HCl, ClONO<sub>2</sub>, Cl<sub>y</sub>, and O<sub>3</sub> by the MIROC3.2 Chemistry-Climate Model (CCM) (Akiyoshi et al., 2016) with FTIR, Aura/MLS, and Envisat/MIPAS measurements at 18 km and 22 km, respectively. For a description of the MIROC3.2 CCM, please see Appendix A for detail. In these figures, Cl<sub>y</sub> for Aura/MLS in the panels (d) and (i) actually represents the Cl<sub>y</sub>\* value calculated by equation (2) using the N<sub>2</sub>O value measured by Aura/MLS. Cl<sub>y</sub> from the MIROC3.2 CCM is the sum of total reactive chlorines, i.e., Cl<sub>y</sub> = Cl + 2\*Cl<sub>2</sub> + ClO + 2\*Cl<sub>2</sub>O<sub>2</sub> + OCIO + HCl + HOCl + ClONO<sub>2</sub> + ClNO<sub>2</sub> + BrCl. Note that we plotted modeled values at 12h UTC (~15h local time of Syowa Station) calculated by the MIROC3.2 CCM in order to compare the daytime measurements of FTIR and satellites. In Figures 11(b), (d), (g), and (i), modeled HCl and Cl<sub>y</sub> are systematically smaller by 20-40% compared with FTIR or MLS measurements. The cause of this discrepancy may be partly due to either smaller downward advection and/or faster horizontal mixing of air mass across the subtropical barrier in MIROC3.2 CCM (Akiyoshi et al., 2016). Another possibility of the discrepancy is the difference of Cl<sub>y</sub>\*-N<sub>2</sub>O correlation used to calculate the Cl<sub>y</sub>\* value by equation (2), since this correlation comes from the aircraft measurement in summer in 1997 (Bonne et al., 2000), and our observations are in

winter in 2007 and 2011, when projected  $Cl_y$  was -0.7% and -12.8% smaller than in 1997, respectively (Strahan et al., 2014). Nevertheless, evolutions of measured ClO and ClONO<sub>2</sub> for the period are well simulated by the MIROC3.2 CCM. Modeled O<sub>3</sub> were in very good agreement with FTIR and/or MLS measurements throughout the year in both altitudes for both years. Hereafter, the result of MIROC3.2 CCM at 50 hPa (~18 km) is discussed.

5

#### 4.5 Polar distribution of minor species

Figure 13 shows distributions of temperature from the model nudged toward the ERA-Interim data, and simulated mixing ratios of O<sub>3</sub>, NO<sub>2</sub>, HNO<sub>3</sub>, ClO, HCl, and ClONO<sub>2</sub> by the MIROC3.2 CCM at 50 hPa for June 24 (day 175), September 2 (day 245), September 6 (day 249), and October 6 (day 279) in 2007. Polar vortex edges defined by the method described in Appendix B were plotted with white circles. The location of Syowa Station is shown by a white star in each panel. On June 24 (day 175), stratospheric temperatures over Antarctica were already low enough for the onset of heterogeneous chemistry. Consequently, NO<sub>2</sub> was converted into HNO<sub>3</sub> via reaction (R17), and HNO<sub>3</sub> in the polar vortex was condensed onto PSCs. Note that the depleted area of NO<sub>2</sub> was greater than that of HNO<sub>3</sub>. This is due to the occurrence of reaction (R12) that converts ClO and NO<sub>2</sub> into ClONO<sub>2</sub> at the edge of the polar vortex, which is shown by the enhanced ClONO<sub>2</sub> area at the vortex edge in Figure 13. Also, HCl and ClONO<sub>2</sub> are depleted in the polar vortex due to the heterogeneous reactions (R1), (R2), (R3), and (R4) on the surface of PSCs and aerosols. Some HCl remains near the core of the polar vortex, because the initial amount of the counter-part of heterogeneous reaction (R1) (ClONO<sub>2</sub>) was less than that of HCl, as was also shown by CLaMS, SD-WACCM, and TOMCAT/SLIMCAT model simulations by Grooß et al. (2018). The O<sub>3</sub> amount was only slightly depleted within the polar vortex on this day.

On September 2 (day 245), amounts of NO<sub>2</sub>, HNO<sub>3</sub>, HCl, and ClONO<sub>2</sub> all show very depleted values in the polar vortex. The amount of ClO shows some enhanced values inside the polar vortex. Development of ozone depletion was seen in the polar vortex. Note that ClONO<sub>2</sub> shows enhanced values around the boundary region of the polar vortex. This might be due to ~~the~~ reaction (R12) at this location. On this day (day 245), Syowa Station was located inside the polar vortex close to the vortex edge, where ClO was smaller and ClONO<sub>2</sub> was greater than the values deep inside the polar vortex as observed and indicated by upper left circle with cross in Figure 10 (a).

On September 6 (day 249), most features were the same as on September 2, but the shape of the polar vortex was different. Consequently, Syowa Station was located deep inside the polar vortex, where ClO was greater and ClONO<sub>2</sub> was smaller than the values around the boundary region of the polar vortex as observed and indicated by lower right circle with cross in Figure 10 (a). Hence, the negative correlation between ClO and ClONO<sub>2</sub> seen in Figure 10 was due to variation of the relative distance between Syowa Station and the edge of the polar vortex.

As for HCl, it kept nearly zero ~~value~~ not only on this day (September 6) but also on September 2 when Syowa Station was located inside the polar vortex close to the vortex edge. Therefore, observed day-to-day variations of HCl were small and did not show any correlation with ClO (see Figures 4-7). A possible explanation to keep a near zero HCl ~~low-value~~ close to near

the vortex edge is due to a so-called “HCl-null cycles” which was started with fast reaction (R13) proposed by Müller et al. (2018). This cycle is discussed later.

On October 6 (day 279), ClO enhancement has almost disappeared. Inside the polar vortex, O<sub>3</sub>, NO<sub>2</sub>, HNO<sub>3</sub>, and ClONO<sub>2</sub> showed very low values. Ozone was almost fully destroyed at this altitude in the polar vortex. However, the amount of HCl increased deep inside the polar vortex. This might be due to the recovery of HCl by reactions (R13) and/or (R14) deep inside the polar vortex, where there was no O<sub>3</sub> or NO<sub>2</sub> left and reactions (R13) and/or (R14) were favoured compared with reaction (R12). Syowa Station was located deep inside the polar vortex and the simulated and observed amounts of HCl were both more than ten times greater than those of ClONO<sub>2</sub> on this day (see Figure 4).

Figure 14 shows distributions of temperature from the model nudged toward the ERA-Interim data, and simulated mixing ratios of O<sub>3</sub>, NO<sub>2</sub>, HNO<sub>3</sub>, ClO, HCl, and ClONO<sub>2</sub> by the MIROC3.2 CCM at 50 hPa for July 5 (day 186), August 19 (day 231), August 21 (day 233), and October 9 (day 282) in 2011. Polar vortex edges and location of Syowa Station were also plotted. On July 5 (day 186), the situation was similar to that of June 24 (day 175) in 2007. Note that inner edge of the polar vortex was defined on this day. Syowa Station was located deeper inside the polar vortex on July 5 in 2011 than on June 24 in 2007 and remaining HCl was observed by MLS (see Figure 5).

On August 19 (day 231) and August 21 (day 233), the situations were similar to those of September 2 (day 245) and September 6 (day 249) in 2007, respectively. ClO and ClONO<sub>2</sub> correlations on these days are also indicated by circles with crosses in Figure 10 (b).

On October 9 (day 282), the situation was similar to that of October 6 (day 279) in 2007, but Syowa Station was located inside the polar vortex closer to the inner vortex edge than in 2007. The recovery of ClONO<sub>2</sub> by reaction (R12) was simulated and observed at Syowa Station besides the recovery of HCl by reaction (R13) (see Figure 8 (b)), because there were some O<sub>3</sub> and NO<sub>2</sub> near the inner vortex edge (see Figure 5). This shows the phenomena described on the last paragraph in Section 4.2.

#### 4.6 Time evolution of chlorine species from CCM and discussion

Three-hourly time series of zonal-mean active chlorine species, Cl<sub>2</sub>O<sub>2</sub> (b), Cl<sub>2</sub> (c), ClO (d), and their sum (ClO+2\*Cl<sub>2</sub>O<sub>2</sub>+2\*Cl<sub>2</sub>) (a), HOCl (e), and chlorine reservoir species HCl (f) and ClONO<sub>2</sub> (g) modeled by MIROC3.2 CCM at 68.4°S, 71.2°S, 76.7°S, and 87.9°S in 2007 are plotted in Figure 15. The dates on which the distribution of each species is shown in Figure 13 are indicated by vertical dotted lines. In Figure 15, it is shown that HCl and ClONO<sub>2</sub> rapidly decreased at around May 10 (day 130) at 87.9°S due to heterogeneous reaction (R1), when PSCs started to form in the Antarctic polar vortex (Figures 15(f) and 15(g)). Consequently, Cl<sub>2</sub> was formed (Figure 15(c)). Similar chlorine activation was seen at 76.7°S about 5-10 days later than at 87.9°S. The decrease of HCl stopped when the counter-part of the heterogeneous reaction (R1) (ClONO<sub>2</sub>) was missing at around May 20 (day 140). Continuous loss of HCl occurred from June to July (day 160-200). The possible cause of this loss will be discussed later. ~~Consequently, Cl<sub>2</sub> was formed (Figure 15(c)). Similar chlorine activation was seen at 76.7°S about 5-10 days later than at 87.9°S.~~ Gradual conversion from Cl<sub>2</sub> into Cl<sub>2</sub>O<sub>2</sub> (ClO-dimer) was seen at all latitudes at around May 30-June 9 (day 150-160) (Figures 15(b) and 15(c)) through reactions (R5), (R8), and (R9).

At 87.9°S, conversion from Cl<sub>2</sub> to Cl<sub>2</sub>O<sub>2</sub> was slow, due to lack of sunlight which is needed for reaction (R5). Increase of ClO occurred much later in winter (July 9; day 190 or later), because sun light is needed to form ClO by reactions (R5) and (R8) in the polar vortex (Figure 15(d)). Nevertheless, there were some enhancements of ClO in early winter, June 24 (day 175), simulated at the edge of the polar vortex (Figure 13) where there was some sunlight available due to the distortion of the shape of the polar vortex. Increase of ClO occurred from lower latitude (68.4°S) at around July 14 (day 195), towards higher latitude (87.9°S) at around September 12 (day 255) (Figure 15(d)). Diurnal variation of ClO was also seen at latitudes between 68.4°S and 76.7°S. When the stratospheric temperature increased above NATPSC saturation temperature at around September 27 (day 270) (Figure 3(b)), chlorine activation ended, and ClO was mainly converted into HCl at all latitudes inside the polar vortex (Figures 15(d) and 15(f)). This is because reactions (R13) and/or (R14) occur more frequently than reaction (R12) inside the polar vortex due to the depleted O<sub>3</sub> amount there, as was described in Section 1 (Douglass et al., 1995). Increase of HOCl due to heterogeneous reaction (R2) on the surface of PSCs occurred gradually from June at lower latitudes (68.4°S and 71.2°S) (Figure 15(e)). It also occurred at 76.7°S from July, and at 87.9°S from August. The cause of HOCl increase at 87.9°S from August is not clear at the moment. In Figure 15, the species which decreased at 87.9°S from August was Cl<sub>2</sub> (Figure 15 (c)). If sunlight was available, Cl<sub>2</sub> was converted into HOCl through reactions (R5), (R8), and the following reaction



Here, HO<sub>2</sub> was needed to yield HOCl. One possibility to yield HO<sub>2</sub> in August is either one of “HCl null cycles” C1 or C2 (see Appendix C), or “HCl destruction chemical cycles” C3 or C4 (see Appendix C) which was described in Müller et al. (2018). If the airmass at 87.9°S was located equatorward due to the obliqueness of the polar vortex a few days earlier, then sunlight may have been available and such reactions could yield HOCl at 87.9°S.

Continuous loss of HCl was seen at 87.9°S between June 9 (day 160) and July 19 (day 200) even after the disappearance of the counterpart of heterogeneous reaction (R1) (Figure 15(f)). The cause of this continuous loss was unknown until recently, where a hypothesis was proposed that includes the effect of decomposition of particulate HNO<sub>3</sub> by some processes like ionisation of air molecules caused by galactic cosmic rays during the winter polar vortex or photolysis of dissolved HNO<sub>3</sub> in PSC particles (Groß et al., 2018). However, they concluded that these processes could not explain the HCl discrepancy between their models and observations. Solomon et al. (2015) proposed a transport mechanism on this issue: Continuous transport of ClONO<sub>2</sub> from the sun-rich subpolar regions near 55–65°S to higher latitudes near 65–75°S provides a flux of NO<sub>x</sub> from more sunlit latitudes into the polar vortex. Jaeglé et al. (1997) also described similar mechanism for HCl loss near the vortex edge with ER-2 Observations. They explained We consider that the continuous loss of HCl was caused by the mixing of ClONO<sub>2</sub>-containing air with the air at the core of polar vortex, due to the excursions of air parcels in and out of sunlight during the winter caused by the distortion of polar vortex, which photochemically resupply ClONO<sub>2</sub> and HOCl. Our result is partly consistent with the mechanism proposed by Solomon et al. (2015), which was indicated by some sporadic increase in ClONO<sub>2</sub> at around June 7 (day 158), June 28 (day 179), and July 8 (day 189) at 76.7°S as shown in Figure 15(g). We confirmed that the shapes of polar vortex were rather distorted on these days. Subsequently, HCl losses were observed at

76.7°S and 87.9°S during these episodes in Figure 15(f). Thus, the continuous loss of HCl at the most polar latitude (87.9°S) could be due to the gradual mixing of air within the polar vortex during the winter period, when polar vortex was still strong.

The ClONO<sub>2</sub> distribution on June 24, 2007 in Figure 13 shows a peak at around the polar vortex outer edge (equivalent latitude of ~62°S) where there was no HCl. We confirmed that such a peak continued to exist from the middle of June to the end of July, when sunlight was not available in geographical latitude higher than 70°S due to polar night. However, substantial amount of ClONO<sub>2</sub> exists between equivalent latitude of 62°S (polar vortex outer edge) and 70°S, mainly due to the distortion of the polar vortex and availability of O<sub>3</sub>. At 62°S equivalent latitude, the amount of ClONO<sub>2</sub> has a peak around these days, while HCl amounts were low. Around 65-70°S, HCl was almost fully depleted. Therefore, if the air mass which contains some ClONO<sub>2</sub> travelled toward poleward due to mixing, it can react with HCl by reaction (R1) and continuously destroy HCl in the core of the polar vortex during polar night in June and July. However, we are not sure if such transport really occurs and affect the HCl loss at the core of the polar vortex. Another explanation of the loss of HCl is by heterogeneous reaction (R4) on the surface of PSCs with HOCl. Spiky increases of HOCl at 76.7°S and 87.9°S, and simultaneous decrease of HCl was occurred at around July 7 (day 188) and July 20 (day 201) in Figures 15(e) and 15(f). Continuous loss of HCl at the core of the polar vortex in August and September was recently proposed by Müller et al. (2018), that “HCl destruction chemical cycles” C3 and C4 (See Appendix C) are responsible for the decline of HCl in the vortex core. However, these chemical cycles also require sun light to occur, which may not be available in June and July at the vortex core. Therefore, the distortion of the polar vortex is also important for that reaction to occur as well. We consider that the reactions of HCl with both ClONO<sub>2</sub> and HOCl contribute the continuous loss of HCl during winter in the vortex core.

Recently, Müller et al. (2018) discussed on “race” between chlorine activation and deactivation to maintain enhanced levels of active chlorine during the time period (September and early October) when rapid ozone loss occurs. They proposed a so-called “HCl null-cycles” to keep enhanced chlorine levels. They proposed a mechanism that the formation HCl (R13) is followed by immediate reactivation of HCl by null-cycles C1 and C2 (Müller et al., 2018). Our MIROC3.2 CCM model results support the mechanism by high ClO and HOCl levels in September as shown in Figures 15(d) and 15(e).

## 5. Conclusions

Lower stratospheric vertical profiles of O<sub>3</sub>, HNO<sub>3</sub>, and HCl were retrieved using SFIT2 from solar spectra taken with a ground-based FTIR installed at Syowa Station, Antarctica from March to December 2007 and September to November 2011. This was the first continuous measurements of chlorine species throughout the ozone hole period from the ground in Antarctica. Retrieved profiles were validated with Aura/MLS and ozonesonde data. The absolute differences between FTIR and Aura/MLS or ozonesonde measurements were within measurement error bars at the altitudes of interest.

To study the temporal variation of chlorine partitioning and ozone destruction from fall to spring in the Antarctic polar vortex, we analyzed temporal variations of measured minor species by FTIR over Syowa Station combined with satellite measurements of ClO, HCl, ClONO<sub>2</sub> and HNO<sub>3</sub>. When the stratospheric temperature over Syowa Station fell ~4K below NAT ~~PSC~~-saturation temperature, PSCs started to form and heterogeneous reaction between HCl and ClONO<sub>2</sub> occurred and both HCl and ClONO<sub>2</sub> ~~were~~ almost completely depleted at both 18 km and 22 km in early winter. When the sun came back to the Antarctic in spring, enhancement of ClO and gradual O<sub>3</sub> destruction were observed. During the ClO enhanced period, negative correlation between ClO and ClONO<sub>2</sub> was observed in the time-series of the data at Syowa Station. This negative correlation is associated with the relative distance between Syowa Station and the edge of the polar vortex.

To see the ~~comprehensive~~-behavior of whole chlorine and related species inside the polar vortex and the boundary region in more detail, results of MIROC3.2 CCM simulation were analyzed. Direct comparison between CCM results and observations show good day-to-day agreement in general, although some species show systematic differences especially at 18 km. The modeled O<sub>3</sub> is in good agreement with FTIR and satellite observations. Rapid conversion of chlorine reservoir species (HCl and ClONO<sub>2</sub>) into Cl<sub>2</sub>, gradual conversion of Cl<sub>2</sub> into Cl<sub>2</sub>O<sub>2</sub>, increase of HOCl in winter period, increase of ClO when sunlight became available, and conversion of ClO into HCl were successfully reproduced by the CCM. HCl decrease in the winter polar vortex core continued to occur due to ~~both~~either the transport of ClONO<sub>2</sub> from the polar vortex boundary~~subpolar~~ region to higher latitudes, providing a flux of ClONO<sub>2</sub> from more sunlit latitudes into the polar vortex, ~~and~~or the heterogeneous reaction with HOCl. Temporal variation of chlorine species over Syowa Station was affected both by heterogeneous chemist~~ri~~es related to PSC occurrence inside the polar vortex, and transport of NO<sub>x</sub>-rich air mass from the polar vortex boundary region, which can produce additional ClONO<sub>2</sub> by reaction (R12).

The deactivation pathways from active ClO into reservoir species (HCl and/or ClONO<sub>2</sub>) were confirmed to be very dependent on the availability of ambient O<sub>3</sub>. At an altitude (18 km) where most ozone was depleted in the Antarctic, most ClO was converted to HCl. However, at an altitude (22 km) when there was some O<sub>3</sub> available, additional increase of ClONO<sub>2</sub> than pre-winter value can occur, as in the case in the Arctic, through reactions (R15) and (R12) (Douglass et al., 1995; Groöb et al., 1997).

*Data availability:* The FTIR data presented here can be obtained in electronic form (hdf files) from the following DOIs:

doi:10.17595/20190911.001 (FTIR data for 2007),

doi:10.17595/20190911.002 (FTIR data for 2011).

The MIROC3.2 CCM outputs are from the REF-C1SD simulation data from the CCMI, which are stored at the CCMI site of BADC at:

<http://badc.nerc.ac.uk/browse/badc/wcrp-ccmi/data/CCMI-1/output/NIES>.

The MLS data were taken from the following site: <http://avdc.gsfc.nasa.gov/index.php?site=2045907950>.

-The MIPAS data were taken from the following site: <http://share.lsd.fkit.edu/imk/asf/sat/mipas-export/Data> by Target/.

-The CALIOP data were taken from the following site: [https://www-calipso.larc.nasa.gov/resources/calipso\\_users\\_guide/data\\_summaries/psc/index.php](https://www-calipso.larc.nasa.gov/resources/calipso_users_guide/data_summaries/psc/index.php).

*Author contributions.* HN, IM, YN, and MT conceived and worked on the current research project. HN, KS, and TK made FTIR observations at Syowa Station in 2007 and 2011. HN, YN, KS, and NBJ conducted the SFIT2 retrievals. HA conducted MIROC3.2 CCM simulations and ED analysed them. YT performed polar vortex categorization calculation. HN, IM, YN, HA, YT, and NBJ contributed to the interpretation of the results and wrote the paper.

*Competing interests.* The authors declare that they have no competing financial interests.

## 10 **Appendix A: MIROC3.2 nudged chemistry–climate model**

The chemistry–climate model (CCM) used in this study was MIROC3.2 CCM, which was developed on the basis of version 3.2 of the Model for Interdisciplinary Research on Climate (MIROC3.2) general circulation model (GCM). The MIROC3.2 CCM introduces the stratospheric chemistry module of the old version of the CCM that was used for simulations proposed by the chemistry–climate model validation (CCMVal) and the second round of CCMVal (CCMVal2) (WMO, 2007, 2011; SPARC CCMVal, 2010; Akiyoshi et al., 2009, 2010). The MIROC3.2 CCM is a spectral model with a T42 horizontal resolution ( $2.8^\circ \times 2.8^\circ$ ) and 34 vertical atmospheric layers above the surface. The top layer is located at approximately 80 km (0.01 hPa). Hybrid sigma–pressure coordinates are used for the vertical coordinate. The horizontal wind velocity and temperature in the CCM were nudged toward the ERA–Interim data (Dee et al., 2011) to simulate global distributions of ozone and other chemical constituents on a daily basis. The transport is calculated by a semi–Lagrangian scheme (Lin and Rood, 1996). The chemical constituents included in this model are  $O_x$ ,  $HO_x$ ,  $NO_x$ ,  $ClO_x$ ,  $BrO_x$ , hydrocarbons for methane oxidation, heterogeneous reactions on the surface for sulfuric-acid aerosols, supercooled ternary solutions, nitric-acid trihydrate, and ice particles. The CCM contains 13 heterogeneous reactions on multiple aerosol types (Akiyoshi, 2007) as well as gas-phase chemical reactions and photolysis reactions. The surface of the particles for the heterogeneous reactions are calculated from the volume of condensation, assuming number density of the particles and the size distributions. Sedimentation of the particles is considered. The reaction-rate and absorption coefficients are based on JPL–2010 (Sander et al., 2011). Family method is used to calculate gas phase chemical reactions. The time integrations for the families and heterogeneous reactions are performed explicitly. The time step for the chemistry scheme is 6 minutes. A scheme of spherical geometry for radiation transfer was developed (Kurokawa et al., 2005) and used for radiation transfer calculation in the CCM. The photolysis rates of chemical constituents are calculated online, using the radiation flux in the CCM with 32 spectral bins. [All the 42 photolysis reactions, 140 gas phase reactions, and 13 heterogeneous reactions are summarized in Table A2.](#) See Akiyoshi et al. (2016) and Supplement of Morgenstern et al. (2017) for more details.

## Appendix B: Determined polar vortex edges

Inner and outer edges of the polar vortex were determined as follows:

1) Equivalent latitudes (EL) (McIntyre and Palmer, 1984; Butchart and Remsberg, 1986) were computed based on isentropic potential vorticity at 450 K and 560 K isentropic surfaces for 18 km and 22 km using the ERA-Interim reanalysis data (Dee et al., 2011), respectively.

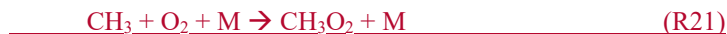
2) Inner and outer edges (at least 5° apart from each other) of the polar vortex were defined by local maxima of the isentropic potential vorticity gradient with respect to equivalent latitude only when a tangential wind speed (i.e., mean horizontal wind speed along the isentropic potential vorticity contour; see Eq. (1) of Tomikawa and Sato (2003)) near the vortex edge exceeds a threshold value (i.e., 20 m s<sup>-1</sup>, see Nash et al. (1996) and Tomikawa et al. (2015)).

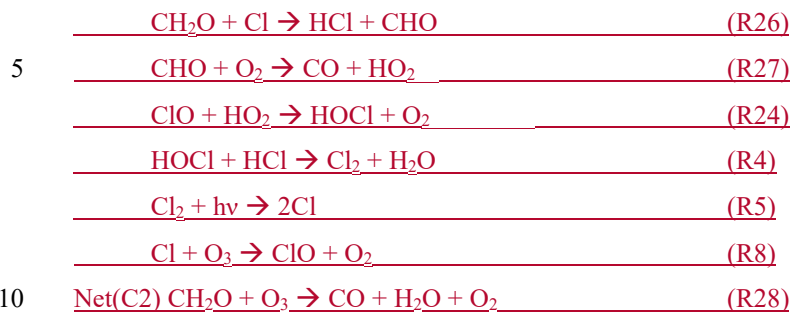
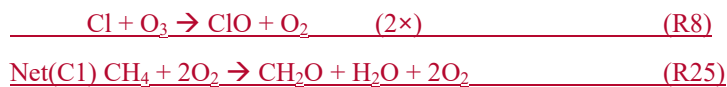
3) Then, the polar region was divided into three regions; i.e., inside the polar vortex (inside of inner edge), the boundary region (between inner and outer edges), and outside the polar vortex (outside of outer edge) when there were two polar vortex edges. When there was only one edge, the polar region was divided into two regions; i.e., inside the polar vortex and outside the polar vortex.

Figures A1 and A2 show time-equivalent latitude sections of modified potential vorticity (MPV) and its gradient with respect to EL at 450 and 560 K isentropic potential temperature (PT) surfaces in 2007 and 2011, respectively. MPV is a scaled PV to remove its exponential increase with height (cf., Lait, 1994). The inner and outer edge(s) are plotted by black dots, while the ELs of Syowa Station on those days are plotted by red dots. It can be seen that inner edges were first formed at around EL of 70 degrees in April, and outer edges started to form at around EL of 55 degrees in July-August, emerging the boundary region. Then, those two edges converge into one edge at around EL of 60 degrees in November. Finally, the polar vortex edge disappeared in December. Syowa Station was mostly located inside the polar vortex, but sometimes located at the boundary region or outside the polar vortex, depending on different PT levels.

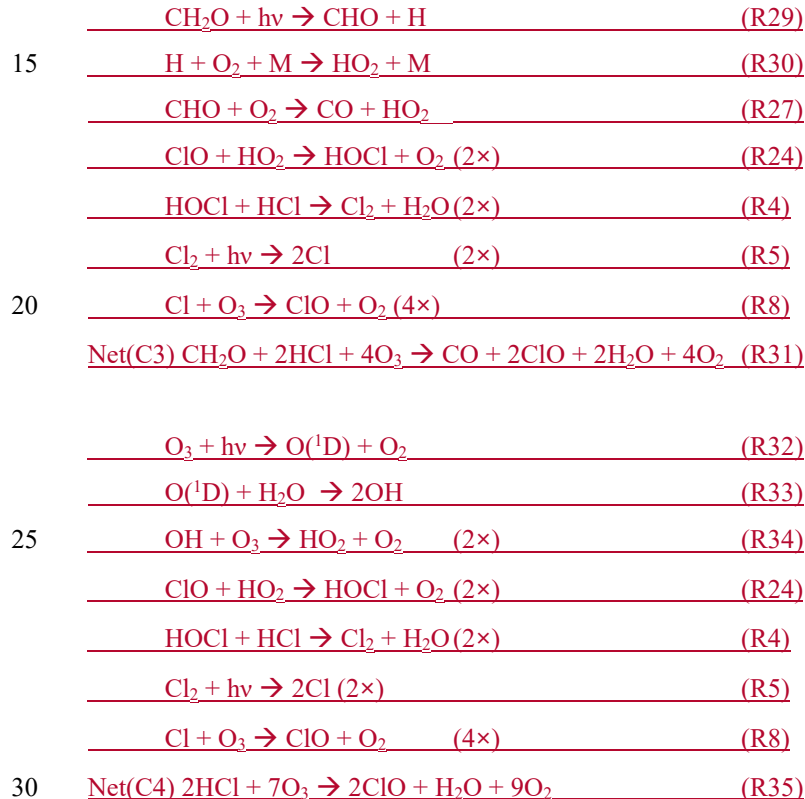
## Appendix C: “HCl null cycles” C1, C2 and “HCl destruction cycles” C3, C4

In Müller et al. (2018), new chemical cycles C1 and C2 were proposed to maintain high levels of active chlorine in Antarctic spring, referred to as “HCl null cycles”, as follows:





Also, other chemical cycles which are responsible for the decline of HCl during Antarctic August and September, referred to “HCl destruction cycles”, are also proposed by Müller et al. (2018) as follows:



## Acknowledgments

We acknowledge all the members of the 48<sup>th</sup> Japanese Antarctic Research Expedition (JARE-48), JARE-52 for their support in making the FTIR observation at Syowa Station. Data provision of Aura/MLS and Envisat/MIPAS are much appreciated. We thank Japan Meteorological Agency for providing the ozonesonde and Rawin sonde data at Syowa Station. Thanks are  
5 due to Dr. Yosuke Yamashita for performing the CCM run. The model computations were performed on NEC-SX9/A(ECO) and NEC SX-ACE computers at the CGER, NIES, supported by the Environment Research and Technology Development Funds of the Ministry of the Environment (2-1303) and Environment Restoration and Conservation Agency (2-1709). We thank Dr. Takafumi Sugita for useful discussion and comments.

## 10 References

- Akiyoshi, H.: Modeling of the heterogeneous reaction processes on the polar stratospheric clouds in chemical transport models and the effects on the Arctic ozone layer through bromine species, *Eurozoru Kenkyu*, 22, 196-203, 2007 (in Japanese).
- Akiyoshi, H., Zhou, L. B., Yamashita, Y., Sakamoto, K., Yoshiki, M., Nagashima, T., Takahashi, M., Kurokawa, J., Takigawa, M., and Imamura, T.: A CCM simulation of the breakup of the Antarctic polar vortex in the years 1980–2004 under the  
15 CCMVal scenarios, *J. Geophys. Res.*, 114, D03103(1–28), doi:10.1029/2007JD009261, 2009.
- Akiyoshi, H., Y. Yamashita, K. Sakamoto, L. B. Zhou, and T. Imamura: Recovery of stratospheric ozone in calculations by the Center for Climate System Research/National Institute for Environmental Studies chemistry–climate model under the CCMVal–REF2 scenario and a no–climate–change run, *J. Geophys. Res.*, 115, D19301(1–22), doi:10.1029/2009JD012683, 2010.
- 20 Akiyoshi, H., Nakamura, T., Miyasaka, T., Shiotani, M., and Suzuki, M.: A nudged chemistry-climate model simulation of chemical constituent distribution at northern high-latitude stratosphere observed by SMILES and MLS during the 2009/2010 stratospheric sudden warming, *J. Geophys. Res. Atmos.*, 121, 1361-1380, doi:10.1002/2015JD023334, 2016.
- Anderson, J. G., Brune, W. H., and Proffitt, M. H.: Ozone destruction by chlorine radicals within the Antarctic vortex: The spatial and temporal evolution of ClO-O<sub>3</sub> anticorrelation based on in situ ER-2 data, *J. Geophys. Res.*, 94, 11,465-11479,  
25 1989.
- Anderson, J., Russell, J. M., III, Solomon, S., and Deaver, L. E.: Halogen Occultation Experiment confirmation of stratospheric chlorine decreases in accordance with the Montreal Protocol, *J. Geophys. Res.*, 105, 4483-4490, doi:10.1029/1999JD901075, 2000.
- Bonne, G. P., Stimpfle, R. M., Cohen, R. C., Voss, P. B., Perkins, K. K., Anderson, J. G., Salawitch, R. J., Elkins, J. W.,  
30 Dutton, G. S., Jucks, K. W., and Toon, G. C.: An examination of the inorganic chlorine budget in the lower stratosphere, *J. Geophys. Res.*, 105, D2, 1957-1971, 2000.

- Butchart, N., and Remsberg, E. E.: The area of the stratospheric polar vortex as a diagnostic for tracer transport on an isentropic surface, *J. Atmos. Sci.*, 43, 1319–1339, 1986.
- Canty, T. P., Salawitch, R. J., and Wilmouth, D. M.: The kinetics of the ClOOCl catalytic cycle, *J. Geophys. Res.*, 121, 13,768–13, 783, doi:10.1002/2016JD025710, 2016.
- 5 Chubachi, S.: Preliminary result of ozone observation at Syowa Station from February 1982 to January 1983, *Mem. Natl Inst. Polar Res., Spec. Issue*, 34, 13-19, 1984.
- Connor, B., Parrish, A., Tsou, J., and McCormick, M.: Error analysis for the ground-based microwave ozone measurements during STOIC, *J. Geophys. Res.*, 100, 9283-9291, 1995.
- de Laat, A. T. J., van Weele, M., and van der A, R. J.: Onset of stratospheric ozone recovery in the Antarctic ozone hole in  
10 assimilated daily total ozone columns, *J. Geophys. Res.*, 122, 11,880-11,899, doi:10.1002/2016JD025723, 2017.
- de Zafra, R. L., Jaramillo, M., Barrett, J., Emmons, L. K., Solomon, P. M., and Parrish, A.: New observations of a large concentration of ClO in the springtime lower stratosphere over Antarctica and its implications for ozone-depleting chemistry, *J. Geophys. Res.*, 94, D9, 11,423-11,428, 1989.
- Dec, D. P., Uppala, S. M., Simmons, A. J., Berrisford, P., Poli, P., Kobayashi, S., Andrae, U., Balsaseda, M. A., Balsamo, G.,  
15 Bauer, P., Bechtold, P., Beljaars, A. C. M., van de Berg, L., Bidlot, J., Bormann, N., Delsol, C., Dragani, R., Fuentes, M., Geer, A. J., Haimberger, L., Healy, S. B., Hersbach, H., Hólm, E. V., Isaksen, I., Kållberg, P., Köhler, M., Matricardi, M., McNally, A. P., Monge-Sanz, B. M., Morcrette, J. -J., Park, B. -K., Peubey, C., de Rosnay, P., Tavolato, C., Thépaut, J. -N., and Vitart, F.: The ERA–Interim reanalysis: configuration and performance of the data assimilation system, *Q. J. R. Meteorol. Soc.*, 137, 553–597, doi:10.1002/qj.828, 2011.
- 20 Douglass, A. R., Schoeberl, M. R., Stolarski, R. S., Waters, J. W., Russell, J. M., III, Roche, A. E., and Massie, S. T.: Interhemispheric differences in springtime production of HCl and ClONO<sub>2</sub> in the polar vortices, *J. Geophys. Res.*, 100, 13,967-13,978, 1995.
- Drdla, K. and Müller, R.: Temperature thresholds for chlorine activation and ozone loss in the polar stratosphere, *Ann. Geophys.*, 30, 1055-1073, doi:10.5194/angeo-30-1055-2012, 2012
- 25 Dufour, G., Nassar, R., Boone, C. D., Skelton, R., Walker, K. A., Bernath, P. F., Rinsland, C. P., Semeniuk, K., Jin, J. J., McConnell, J. C., and Manney, G. L.: Partitioning between the inorganic chlorine reservoirs HCl and ClONO<sub>2</sub> during the Arctic winter 2005 from the ACE-FTS, *Atmos. Chem. Phys.*, 6, 2355-2366, 2006.
- Farman, J. C., Gardiner, B. G., and Shanklin, J. D.: Large losses of total ozone in Antarctica reveal seasonal ClO<sub>x</sub>/NO<sub>x</sub> interaction, *Nature*, 315, 207-210, 1985.
- 30 Farmer, C. B., Toon, G. C., Schaper, P. W., Blavier, J. -F., and Lowes, L. L.: Stratospheric trace gases in the spring 1986 Antarctic atmosphere, *Nature*, 329, 126-130, 1987.
- Fischer, H., and Oelhaf, H.: Remote sensing of vertical profiles of atmospheric trace constituents with MIPAS limb-emission spectrometers, *Appl. Opt.*, 35, 2787-2796, 1996.

- Fischer, H., Birk, M., Blom, C., Carli, B., Carlotti, M., von Clarmann, T., Delbouille, L., Dudhia, A., Ehhalt, D., Endemann, M., Flaud, J. M., Gessner, R., Kleinert, A., Koopmann, R., Langen, J., López-Puertas, M., Mosner, P., Nett, H., Oelhaf, H., Perron, G., Remedios, J., Ridolfi, M., Stiller, G., and Zander, R.: MIPAS: An instrument for atmospheric and climate research, *Atmos., Chem. Phys.*, 8, doi:10.5194/acp-8-2151-2008, 2008.
- 5 Froidevaux, L., et al.: Early validation analyses of atmospheric profiles from EOS MLS on the Aura satellite, *IEEE Trans. Geosci. Remote Sens.*, 44, 1106-1121, 2006.
- Froidevaux, L., Jiang, Y. B., Lambert, A., Livesey, N. J., Read, W. G., Waters, J. W., Browell, E. V., Hair, J. W., Avery, M. A., McGee, T. J., Twigg, L. W., Sumnicht, G. K., Jucks, K. W., Margitan, J. J., Sen, B., Stachnik, R. A., Toon, G. C., Bernath, P. F., Boone, C. D., Walker, K. A., Filipiak, M. J., Harwood, R. S., Fuller, R. A., Manney, G. L., Schwartz, M. J., Daffer, W. H., Drouin, B. J., Cofield, R. E., Cuddy, D. T., Jarnot, R. F., Knosp, B. W., Perun, V. S., Snyder, W. V., Stek, P. C., Thurstans, R. P., and Wagner, P. A.: Validation of Aura Microwave Limb Sounder stratospheric ozone measurements, *J. Geophys. Res.*, 113, D15S20, doi:10.1029/2007JD008771, 2008.
- 10 Gallery, W. O., Kneizys, F. S., and Clough, S. A.: Air mass computer program for atmospheric transmittance/radiance calculation: FSCATM, Environmental Research Paper ERP-828/AFGL-TR-83-0065, Air Force Geophysical Laboratory, Bedford, MA, USA, 1983.
- 15 Goldman, A., Fernald, F. G., Murcray, F. J., Murcray, F. H., and Murcray, D. G.: Spectral least squares quantification of several atmospheric gases from high resolution infrared solar spectra obtained at the South Pole, *J. Quant. Spectrosc. Radiat. Transfer*, 29, 189-204, 1983.
- Goldman, A., Murcray, F. J., Murcray, F. H., and Murcray, D. G.: Quantification of HCl from high resolution infrared solar spectra obtained at the South Pole in December 1986, *Geophys. Res. Lett.*, 14, 622-623, 1987.
- 20 Grooß, J. -U., Pierce, R. B., Crutzen, P. J., Grose, W. L., and Russell III, J. M.: Reformation of chlorine reservoirs in southern hemisphere polar spring, *J. Geophys. Res.*, 102, 13,141-13,152, doi:10.1029/96JD03505, 1997.
- Grooß, J. -U., Brauttsch, K., Pommrich, R., Solomon, S., and Müller, R.: Stratospheric ozone chemistry in the Antarctic: what determines the lowest ozone values reached and their recovery?, *Atmos. Chem. Phys.*, 11, 12,217-12,226, doi:10.5194/acp-11-12217-2011, 2011.
- 25 Grooß, J. -U., Müller, R., Spang, R., Tritscher, I., Wegner, T., Chipperfield, M. P., Feng, W., Kinnison, D. E., and Madronich, S.: On the discrepancy of HCl processing in the core of the wintertime polar vortices, *Atmos. Chem. Phys.*, 18, 8647-8666, doi:10.5194/acp-18-8647-2018, 2018
- Hase, F., Hannigan, J. W., Coley, M. T., Goldman, A., Höpfner, M., Jones, N. B., Rinsland, C. P., Wood, S. W.: Intercomparison of retrieval codes used for the analysis of high-resolution, ground-based FTIR measurements, *J. Quant. Spectrosc. Radiat. Transfer*, 87, 25-52, 2004.
- 30 Hayashida, S., Sugita, T., Ikeda, N., Toda, Y., and Irie, H.: Temporal evolution of ClONO<sub>2</sub> observed with Improved Limb Atmospheric Spectrometer (ILAS) during Arctic late winter and early spring in 1997, *J. Geophys. Res.*, 112, D14311, doi:10.1029/2006JD008108, 2007.

- Höpfner, M., von Clarmann, T., Fischer, H., Glatthor, N., Grabowski, U., Kellmann, S., Kiefer, M., Linden, A., Mengistu Tsidu, G., Milz, M., Steck, T., Stiller, G. P., Wang, D. Y., and Funke, B.: First spaceborne observations of Antarctic stratospheric ClONO<sub>2</sub> recovery: Austral spring 2002, *J. Geophys. Res.*, 109, D11308, doi:10.1029/2004JD004609, 2004.
- 5 Höpfner, M., von Clarmann, T., Fischer, H., Funke, B., Glatthor, N., Grabowski, U., Kellmann, S., Kiefer, M., Linden, A., Milz, M., Steck, T., Stiller, G. P., Bernath, P., Blom, C. E., Blumenstock, Th., Boone, C., Chance, K., Coffey, M. T., Friedl-Vallon, F., Griffith, D., Hannigan, J. W., Hase, F., Jones, N., Jucks, K. W., Keim, C., Kleinert, A., Kouker, W., Liu, G. Y., Mahieu, E., Mellqvist, J., Mikuteit, S., Notholt, J., Oelhaf, H., Piesch, C., Reddman, T., Ruhnke, R., Schneider, M., Strandberg, A., Toon, G., Walker, K. A., Warneke, T., Wetzel, G., Wood, S., and Zander, R.: Validation of MIPAS ClONO<sub>2</sub> measurements, *Atmos. Chem. Phys.*, 7, 257-281, 2007.
- 10 Jaeglé, L., Webster, C. R., May, R. D., Scott, D. C., Stimpfle, R. M., Kohn, D. W., Wennberg, P. O., Hanisco, T. F., Cohen, R. C., Proffitt, M. H., Kelly, K. K., Elkins, J., Baumgardner, D., Dye, J. E., Wilson, J. C., Pueschel, R. F., Chan, K. R., Salawitch, R. J., Tuck, A. F., Hovde, S. J., and Yung, Y. L.: Evolution and stoichiometry of heterogeneous processing in the Antarctic stratosphere, *J. Geophys. Res.*, 102, 13,235-13,253, 1997.
- 15 Ko, M. K. W., Rodriguez, J. M., Sze, N. D., Proffitt, M. H., Starr, W. L., Krueger, A., Browell, E. V., McCormick, M. P.: Implications of AAOE observations for proposed chemical explanations of the seasonal and interannual behavior of Antarctic ozone, *J. Geophys. Res.*, 94, D14, 16,705-16,715, 1989.
- Komhyr, W. D.: Operations handbook – Ozone measurements to 40 km altitude with model 4A-ECC-ozone sondes, NOAA Techn. Memorandum ERL-ARL-149, 1986.
- 20 Kreher, K., Keys, J. G., Johnston, P. V., Platt, U., and Liu, X.: Ground-based measurements of OCIO and HCl in austral spring 1993 at Arrival Heights Antarctica, *Geophys. Res. Lett.*, 23, 1545-1548, 1996.
- Kurokawa, J., Akiyoshi, H., Nagashima, T., Nakane, H., Masunaga, H., Nakajima, T., Takahashi, M.: Effects of atmospheric sphericity on the stratospheric chemistry and dynamics over Antarctica, *J. Geophys. Res.*, 110, D21305, doi:10.1029/2005JD005798, 2005.
- 25 Kuttippurath, J., Goutail, F., Pommereau, J. -P., Lefèvre, F., Roscoe, H. K., Pazmiñno, A., Feng, W., Chipperfield, M. P., and Godin-Beekmann, S.: Estimation of Antarctic ozone loss from ground-based total column measurements, *Atmos. Chem. Phys.*, 10, 6569-6581, 2010.
- Lait, L. R.: An alternative form for potential vorticity, *J. Atmos. Sci.*, 51, 1754-1759, 1994.
- Lee, A. M., Roscoe, H. K., Jones, A. E., Haynes, P. H., Shuckburgh, E. F., Morrey, M. W., and Pumphrey, H. C.: The impact of the mixing properties within the Antarctic stratospheric vortex on ozone loss in spring, *J. Geophys. Res.*, 106, D3, 3203-3211, doi:10.1029/2000JD900398, 2001.
- 30 Lin, S.-J. and Rood, R. B.: Multidimensional flux-form semi-Lagrangian transport schemes, *Mon. Wea. Rev.*, 124, 2046-2070, 1996.
- Livesey, N., Van Snyder, W., Read, W., and Wagner, P.: Retrieval algorithms for the EOS Microwave Limb Sounder (MLS), *Geoscience and Remote Sensing, IEEE Transactions*, 44, 1144-1155, doi:10.1109/TGRS.2006.872327, 2006.

- Livesey, N. J., Read, W. G., Froidevaux, L., Lambert, A., Manney, G. L., Pumphrey, H. C., Santee, M. L., Schwartz, M. J., Wang, S., Cofield, R. E., Cuddy, D. T., Fuller, R. A., Jarnot, R. F., Jiang, J. H., Brian W. Knosp, Stek, P. C., Wagner, P. A., and Wu, D. L.: Version 3.3 and 3.4 Level 2 data quality and description document, Jet Propul. Lab., Tech. Rep. JPL D-33509, Pasadena, CA, USA (Available from <http://mls.jpl.nasa.gov>), 2013.
- 5 Livesey, N. J., Read, W. G., Wagner, P. A., Froidevaux, L., Lambert, A., Manney, G. L., Millán Valle, L. F., Pumphrey, H. C., Santee, M. L., Schwartz, M. J., Wang, S., Fuller, R. A., Jarnot, R. F., Knosp, B. W., Martinez, E., and Lay, R. R.: Version 4.2x Level 2 data quality and description document, Jet Propul. Lab., Tech. Rep. JPL D-33509 Rev. D, Pasadena, CA, USA (Available from <http://mls.jpl.nasa.gov>), 2018.
- Manney, G. L., Santee, M. L., Rex, M., Livesey, N. J., Pitts, M. C., Veefkind, P., Nash, E. R., Wohltmann, I., Lehmann, R.,  
10 Froidevaux, L., Poole, L. R., Schoeberl, M. R., Haffner, D.P., Davies, J., Dorokhov, V., Gernandt, H., Johnson, B., Kivi, R., Kyrö, E., Larsen, N., Levelt, P. F., Makshtas, A., McElroy, C. T., Nakajima, H., Parrondo, M. C., Tarasick, D. W., von der Gathen, P., Walker, K. A., and Zinoviev, N. S.: Unprecedented Arctic ozone loss in 2011, *Nature*, 478, 469-475, doi:10.1038/nature10556, 2011.
- McIntyre, M. E., and Palmer, T. N.: The ‘surf zone’ in the stratosphere, *J. Atmos. Terr. Phys.*, 46, 825–849, 1984.
- 15 Michelsen, H. A., Webster, C. R., Manney, G. L., Scott, D. C., Margitan, J. J., May, R. D., Irion, F. W., Gunson, M. R., Russell III, J. M., and Spivakovskiy, C. M.: Maintenance of high HCl/Cl<sub>y</sub> and NO<sub>x</sub>/NO<sub>y</sub> in the Antarctic vortex: A chemical signature of confinement during spring, *J. Geophys. Res.*, 104, 26,419-26,436, 1999.
- Morgenstern, O., Hegglin, M. I., Rozanov, E., O’Connor, F. M., Abraham, N. L., Akiyoshi, H., Archibald, A. T., Bekki, S.,  
20 Butchart, N., Chipperfield, M. P., Deushi, M., Dhomse, S. S., Garcia, R. R., Hardiman, S. C., Horowitz, L. W., Jöckel, P., Josse, B., Kinnison, D., Lin, M. Y., Mancini, E., Manyin, M. E., Marchand, M., Maréchal, V., Michou, M., Oman, L. D., Pitari, G., Plummer, D. A., Revell, L. E., Saint-Martin, D., Schofield, R., Stenke, A., Stone, K., Sudo, K., Tanaka, T. Y., Tilmes, S., Yamashita, Y., Yoshida, and K., Zeng, G.: Review of the global models used within phase 1 of the Chemistry-Climate Model Initiative (CCMI), *Geosci. Model Dev.*, 10, 639-671, doi:10.5194/gmd-10-639-2017, 2017.
- 25 Müller, R., Peter, T., Crutzen, P. J., Oelhaf, H., Adrian, G. P., v. Clarmann, T., Wegner, A., Schmidt, U., and Lary, D.: Chlorine chemistry and the potential for ozone depletion in the Arctic stratosphere in the winter of 1991/92, *Geophys. Res. Lett.*, 21, 1427-1430, 1994.
- Müller, R., Crutzen, P. J., Groöß, J. -U., Brühl, C., Russell III, J. M., and Tuck, A. F.: Chlorine activation and ozone  
30 depletion in the Arctic vortex: Observations by the Halogen Occultation Experiment on the Upper Atmosphere Research Satellite, *J. Geophys. Res.*, 101, D7, 12,531-12,554, 1996.
- Müller, R., Groöß, J. -U., Zafar, A. M., Robrecht, S., and Lehmann, R.: The maintenance of elevated chlorine levels in the Antarctic lower stratosphere through HCl null cycles, *Atmos. Chem. Phys.*, 18, 2985-2997, doi:10.5194/acp-18-2985-2018, 2018.

- Murcray, F. J., Murcray, F. H., Goldman, A., and Murcray, D. G.: Infrared measurements of several nitrogen species above the South Pole in December 1980 and November-December 1986, *J. Geophys. Res.*, 92, D11, 13,373-13,376, 1987.
- Murcray, F. J., Goldman, A., Blatherwick, R., Matthews, A., and Jones, N. B.: HNO<sub>3</sub> and HCl amounts over McMurdo during the spring of 1987, *J. Geophys. Res.*, 94, D14, 16,615-16,618, 1989.
- 5 Nakajima, H.: Preface to special section on ILAS-II: The Improved Limb Atmospheric Spectrometer II, *J. Geophys. Res.*, 111, D20S90, doi:10.1029/2006JD007412, 2006.
- Nakajima, H., Sugita, T., Yokota, T., Ishigaki, T., Mogi, Y., Araki, N., Waragai, K., Kimura, N., Iwazawa, T., Kuze, A., Tanii, J., Kawasaki, H., Horikawa, M., Togami, T., Uemura, N., Kobayashi, H., and Sasano, Y.: Characteristics and performance of the Improved Limb Atmospheric Spectrometer-II (ILAS-II) on board the ADEOS-II satellite, *J. Geophys. Res.*, 111, D11S01, doi:10.1029/2005JD006334, 2006.
- 10 Nakajima, H., Wohltmann, I., Wegner, T., Takeda, M., Pitts, M. C., Poole, L. R., Lehmann, R., Santee, M. L., and Rex, M.: Polar stratospheric cloud evolution and chlorine activation measured by CALIPSO and MLS, and modeled by ATLAS, *Atmos. Chem. Phys.*, 16, 3311-3325, doi:10.5194/acp-16-3311-2016, 2016.
- Nash, E. R., Newman, P. A., Rosenfield, J. E., and Schoeberl, M. R.: An objective determination of the polar vortex using Ertel's potential vorticity, *J. Geophys. Res.*, 101, 9471-9478, 1996.
- 15 Newman, P. A., Daniel, J. S., Waugh, D. W., and Nash, E. R.: A new formulation of equivalent effective stratospheric chlorine (EESC), *Atmos. Chem. Phys.*, 7, 4537-4552, doi:10.5194/acp-7-4537-2007, 2007.
- Norton, R., and Rinsland, C.: ATMOS data processing and science analysis methods, *Appl. Opt.*, 30, 389-400, 1991.
- Oelhaf, H., v. Clarmann, T., Fischer, H., Friedl-Vallon, F., Fritzsche, C., Linden, A., Piesch, C., Seefeldner, M., and Völker, W.: Stratospheric ClONO<sub>2</sub> and HNO<sub>3</sub> profiles inside the Arctic vortex from MIPAS-B limb emission spectra obtained during EASOE, *Geophys. Res. Lett.*, 21, 1263-1266, doi:10.1029/93GL01303, 1994.
- 20 Parrish, A., Connor, B., Tsou, J., McDermid, I., and Chu, W.: Ground-based microwave monitoring of stratospheric ozone, *J. Geophys. Res.*, 97, 2541-2546, 1992.
- Pitts, M. C., Thomason, L. W., Poole, L. R., and Winker, D. M.: Characterization of Polar Stratospheric Clouds with spaceborne lidar: CALIPSO and the 2006 Antarctic season, *Atmos. Chem. Phys.*, 7, 5207-5228, doi:10.5194/acp-7-5207-2007, 2007.
- 25 Pitts, M. C., Poole, L. R., and Thomason, L. W.: CALIPSO polar stratospheric cloud observations: second-generation detection algorithm and composition discrimination, *Atmos. Chem. Phys.*, 9, 7577-7589, doi:10.5194/acp-9-7577-2009, 2009.
- Pitts, M. C., Poole, L. R., Dörnbrack, A., and Thomason, L. W.: The 2009-2010 Arctic polar stratospheric cloud season: a CALIPSO perspective, *Atmos. Chem. Phys.*, 11, 2161-2177, doi:10.5194/acp-11-2161-2011, 2011.
- 30 Rees, D., Barnett, J. J., and Labitzke, K.: COSPAR International Reference Atmosphere: 1986, Part II, Middle Atmosphere Models, *Adv. Space Res.*, 10, 1-525, 1990.
- Rinsland, C. P., Goldman, A., Murcray, F. J., Murcray, F. H., Blatherwick, R. D., and Murcray, D. G.: Infrared measurements of atmospheric gases above Mauna Loa, Hawaii, in February 1987, *J. Geophys. Res.*, 93, 12,607-12,626, 1988

- Rinsland, C. P., Jones, N. B., Connor, B. J., Logan, J. A., Pougatchev, N. S., Goldman, A., Murcray, F. J., Stephen, T. M., Pine, A. S., Zander, R., Mahieu, E., and Demoulin, P.: Northern and Southern Hemisphere ground-based infrared spectroscopic measurements of tropospheric carbon monoxide and ethane, *J. Geophys. Res.*, 103, 28,197-28,218, 1998.
- Rodgers, C. D.: *Inverse methods for atmospheric sounding: Theory and practice.*, World Scientific, Singapore, 2000.
- 5 Saitoh, N., Hayashida, S., Sugita, T., Nakajima, H., Yokota, T., Hayashi, M., Shiraiishi, K., Kanzawa, H., Ejiri, M. K., Irie, H., Tanaka, T., Terao, Y., Bevilacqua, R. M., Randall, C. E., Thomason, L. W., Taha, G., Kobayashi, H., and Sasano, Y.: Intercomparison of ILAS-II version 1.4 aerosol extinction coefficient at 780 nm with SAGE II, SAGE III, and POAM III, *J. Geophys. Res.*, 111, D11S05, doi:10.1029/2005JD006315, 2006.
- Sander, S. P., Abbatt, J., Barker, J. R., Burkholder, J. B., Friedl, R. R., Golden, D. M., Huie, R. E., Kolb, C. E., Kurylo, M.
- 10 J., Moortgat, G. K., Orkin, V. L. and Wine, P. H.: *Chemical Kinetics and Photochemical Data for Use in Atmospheric Studies*, Evaluation No. 17, JPL Publication 10-6, Jet Propulsion Laboratory, Pasadena, <http://jpldataeval.jpl.nasa.gov/>, 2011.
- Santee, M. L., Manney, G. L., Waters, J. W., and Livesey, N. J.: Variations and climatology of ClO in the polar lower stratosphere from UARS Microwave Limb Sounder measurements, *J. Geophys. Res.*, 108, D15, 4454, doi:10.1029/2002JD003335, 2003.
- 15 Santee, M. L., MacKenzie, I. A., Manney, G. L., Chipperfield, M. P., Bernath, P. F., Walker, K. A., Boone, C. D., Froidevaux, L., Livesey, N. J., and Waters, J. W.: A study of stratospheric chlorine partitioning based on new satellite measurements and modeling, *J. Geophys. Res.*, 113, D12307, doi:10.1029/2007JD009057, 2008.
- Santee, M. L., Manney, G. L., Livesey, N. J., Froidevaux, L., Schwartz, M. J., and Read, W. G.: Trace gas evolution in the
- 20 lowermost stratosphere from Aura Microwave Limb Sounder measurements, *J. Geophys. Res.*, 116, D18306, doi:10.1029/2011JD015590, 2011.
- Schauffler, S. M., Atlas, E. L., Donnelly, S. G., Andrews, A., Montzka, S. A., Elkins, J. W., Hurst, D. F., Romashkin, P. A., Dutton, G. S., and Stroud, V.: Chlorine budget and partitioning during the Stratospheric Aerosol and Gas Experiment (SAGE) III Ozone Loss and Validation Experiment (SOLVE), *J. Geophys. Res.*, 108, 4173, doi:10.1029/2001JD002040,
- 25 2003.
- Schneider, M., Hase, F., Blumenstock, T., Redondas, A., and Cuevas, E.: Quality assessment of O<sub>3</sub> profiles measured by a state-of-the-art ground-based FTIR observing system, *Atmos. Chem. Phys.*, 8, 5579-5588, doi:10.5194/acp-8-5579-2008, 2008.
- Smit, H. G. J. and Straeter, W.: JOSIE-2000, Jülich Ozone Sonde Intercomparison Experiment 2000, The 2000 WMO
- 30 international intercomparison of operating procedures for ECC-ozone sondes at the environmental simulation facility at Jülich, WMO Global Atmosphere Watch report series, No. 158, World Meteorological Organization, Geneva, 2004.
- Solomon, S., Garcia, R. R., Rowland, F. S., and Wuebbles, D. J.: On the depletion of Antarctic ozone, *Nature*, 321, 755-758, 1986.

- Solomon, S., Mount, G. H., Sanders, R. W., and Schmeltekopf, A. L.: Visible spectroscopy at McMurdo Station, Antarctica, 2. Observations of OClO, *J. Geophys. Res.*, 92, 8329-8338, 1987.
- Solomon, S.: Stratospheric ozone depletion: A review of concepts and history, *Rev. Geophys.*, 37, 275-316, doi:10.1029/1999RG900008, 1999
- 5 Solomon, S., Kinnison, D., Bandoro, J., and Garcia, R.: Simulation of polar ozone depletion: An update, *J. Geophys. Res.*, 120, 7958-7974, doi:10.1002/2015JD023365, 2015.
- Solomon, S., Ivy, D. J., Kinnison, D., Mills, M. J., Neely III, R. R., and Schmidt, A.: Emergence of healing in the Antarctic ozone layer, *Science*, doi:10.1126/science.aae0061, 2016.
- SPARC CCMVal: SPARC Report on the Evaluation of Chemistry–Climate Models, V. Eyring, T. G. Shepherd, and D. W. Waugh (Eds.), SPARC Report No.5, WCRP–132, WMO/TD–No.1526, 2010.
- 10 Strahan, S. E., Douglass, A. R., Newman, P. A., and Steenrod, S. D.: Inorganic chlorine variability in the Antarctic vortex and implications for ozone recovery, *J. Geophys. Res. Atmos.*, 119, 14,098-14,109, doi:10.1002/2014JD022295, 2014.
- Sugita, T., Nakajima, H., Yokota, T., Kanzawa, H., Gernandt, H., Herber, A., von der Gathen, P., König-Langlo, G., Sato, K., Dorokhov, V., Yushkov, V. A., Murayama, Y., Yamamori, M., Godin-Beekmann, S., Goutail, F., Roscoe, H. K., Deshler, T., Yela, M., Taalas, P., Kyrö, E., Oltmans, S. J., Johnson, B. J., Allaart, M., Litynska, Z., Klekociuk, A., Andersen, S. B., Braathen, G. O., De Backer, H., Randall, C. E., Bevilacqua, R. M., Taha, G., Thomason, L. W., Irie, H., Ejiri, M. K., Saitoh, N., Tanaka, T., Terao, Y., Kobayashi, H., and Sasano, Y.: Ozone profiles in the high-latitude stratosphere and lower mesosphere measured by the Improved Limb Atmospheric Spectrometer (ILAS)-II: Comparison with other satellite sensors and ozonesondes, *J. Geophys. Res.*, 111, D11S02, doi:10.1029/2005JD006439, 2006.
- 15 20 Tilmes, S., Müller, R., Groöß, J. -U., Nakajima, H., and Sasano, Y., *J. Geophys. Res.*, 111, D24S90, doi:10.1029/2005JD006726, 2006.
- Tomikawa, Y., and Sato, K.: Trapped waves in the edge region of stratospheric polar vortices, *J. Geophys. Res.*, 108, 4047, doi:10.1029/2002JD002579, 2003.
- Tomikawa, Y., Sato, K., Hirasawa, N., Tsutsumi, M., and Nakamura, T.: Balloon-borne observations of lower stratospheric water vapor at Syowa Station, Antarctica in 2013, *Polar Sci.*, 9, 345–353, doi:10.1016/j.polar.2015.08.003, 2015.
- 25 Tuck, A. F., Kelly, K. K., Webster, C. R., Loewenstein, M., Stimpfle, R. M., Proffitt, M. H., and Chan, R. K.: Airborne chemistry and dynamics at the edge of the 1994 Antarctic vortex, *J. Chem. Soc. Faraday Trans.*, 91, 3063-3071, 1995.
- von Clarmann, T. and Johansson, S.: Chlorine nitrate in the atmosphere, *Atmos. Chem. Phys.*, 18, 15,363-15,386, doi:10.5194/acp-18-15363-2018, 2018.
- 30 von Clarmann, T., Fischer, H., Friedl-Vallon, F., Linden, A., Oelhaf, H., Piesch, C., Seefeldner, M., and Völker, W.: Retrieval of stratospheric O<sub>3</sub>, HNO<sub>3</sub>, and ClONO<sub>2</sub> profiles from 1992 MIPAS-B limb emission spectra: method, results and error analysis, *J. Geophys. Res.*, 98, 20,495-20,506, 1993.
- von Clarmann, T., Glatthor, N., Grabowski, U., Höpfner, M., Kellmann, S., Kiefer, M., Linden, A., Tsidu, G. M., Milz, M., Steck, T., Stiller, G. P., Wand, D. Y., and Fischer, H.: Retrieval of temperature and tangent altitude pointing from limb

- emission spectra recorded from space by the Michelson Interferometer for Passive Atmospheric Sounding (MIPAS), *J. Geophys. Res.*, 108, 4736, doi:10.1029/2003JD003602, 2003.
- Waters, J. W., et al.: The Earth Observing System Microwave Limb Sounder (EOS MLS) on the Aura satellite, *IEEE Trans. Geosci. Remote Sens.*, 44, 1075-1092, 2006.
- 5 Wegner, T., Grooß, J. -U., vonHobe, M., Strohm, F., Sumińska-Ebersoldt, O., Volk, C. M., Hösen, E., Mitev, V., Shur, G., and Müller, R.: Heterogeneous chlorine activation on stratospheric aerosols and clouds in the Arctic polar vortex, *Atmos. Chem. Phys.*, 12, 11,095-11,106, doi:10.5194/acp-12-11095-2012, 2012.
- Winker, D. M., McGill, M., and Hunt, W. H.: Initial performance assessment of CALIOP, *Geophys. Res. Lett.*, 34, L19803, doi:10.1029/2007GL30135, 2007.
- 10 WMO: Scientific Assessment of Ozone Depletion: 2006, Global Ozone Research and Monitoring Project—Report No. 50, 572 pp., Geneva, Switzerland, 2007.
- WMO: Scientific Assessment of Ozone Depletion: 2010, Global Ozone Research and Monitoring Project—Report No. 52, 516 pp., Geneva, Switzerland, 2011.
- WMO: Scientific Assessment of Ozone Depletion: 2014, Global Ozone Research and Monitoring Project—Report No. 55, 15 416 pp., Geneva, Switzerland, 2014.
- WMO: Scientific Assessment of Ozone Depletion: 2018, Global Ozone Research and Monitoring Project—Report No. 58, 590 pp., Geneva, Switzerland, 2019.
- Wood, S. W., Bodeker, G. E., Boyd, I. S., Jones, N. B., Connor, B. J., Johnston, P. V., Matthews, W. A., Nichol, S. E., Murcray, F. J., Nakajima, H., and Sasano, Y.: Validation of version 5.20 ILAS HNO<sub>3</sub>, CH<sub>4</sub>, N<sub>2</sub>O, O<sub>3</sub>, and NO<sub>2</sub> using ground-based 20 measurements at Arrival Heights and Kiruna, *J. Geophys. Res.*, 107, 8208, doi:10.1029/2001JD000581, 2002.
- Wood, S. W., Batchelor, R. L., Goldman, A., Rinsland, C. P., Connor, B. J., Murcray, F. J., Stephen, T. M., and Heuff, D. N.: Ground-based nitric acid measurements at Arrival Heights, Antarctica, using solar and lunar Fourier transform infrared observations, *J. Geophys. Res.*, 109, D18307, doi:10.1029/2004JD004665, 2004.
- Yang, E.-S., Cunnold, D. M., Newchurch, M. J., Salawitch, R. J., McCormick, M. P., Russell III, J. M., Zawodny, J. M., and 25 Oltmans, S. J.: First stage of Antarctic ozone recovery, *J. Geophys. Res.*, 113, D20308, doi:10.1029/2007JD009675, 2008.
- Ziemke, J. R., Chandra, S., Labow, G. J., Bhartia, P. K., Froidevaux, L., and Witte, J. C.: A global climatology of tropospheric and stratospheric ozone derived from Aura OMI and MLS measurements, *Atmos. Chem. Phys.*, 11, 9237-9251, doi:10.5194/acp-11-9237-2011, 2011.

## Tables

Table 1. Retrieval parameters of SFIT2

Species	O <sub>3</sub>	HNO <sub>3</sub>	HCl
<b>Spectroscopy</b>	HITRAN 2008	HITRAN 2008	HITRAN 2008
<b>Pressure and temperature profile</b>	Daily sonde (0-30 km)	Daily sonde (0-30 km)	Daily sonde (0-30 km)
	CIRA 86 (30-100 km)	CIRA 86 (30-100 km)	CIRA 86 (30-100 km)
<b>A priori profiles</b>	Monthly averaged by ozonesonde (0-30 km) & ILAS-II (30-100 km)	Monthly averaged by ILAS-II	Monthly averaged by HALOE
<b>Microwindows (cm<sup>-1</sup>)</b>	1002.578 – 1003.500	867.000 – 869.591	2727.730 – 2727.830
	1003.900 – 1004.400	872.800 – 874.000	2775.700 – 2775.800
	1004.578 – 1005.000		2925.800 – 2926.000
<b>Retrieved interfering species</b>	O <sub>3</sub> (668), O <sub>3</sub> (686), CO <sub>2</sub> , H <sub>2</sub> O	H <sub>2</sub> O, OCS, NH <sub>3</sub> , CO <sub>2</sub> , C <sub>2</sub> H <sub>6</sub>	CO <sub>2</sub> , H <sub>2</sub> O, O <sub>3</sub> , NO <sub>2</sub>
<b>Typical retrieval error (%) for 15-25 km</b>	5	15	17
<b>Typical vertical resolution (km)</b>	<del>57</del>	<del>75</del>	6
<b>Mean degrees of freedom (DOFS)</b>	4.9	2.8	2.3

**Table 2. Summary of validation results of FTIR profiles compared with ozonesonde and Aura/MLS measurements, and possible Aura/MLS biases from literatures**

	Number of coincidences	Root mean squares of official errors* (%) at 18-22 km	D (%) at 18-22 km	Min/Max (%) at 18-22 km	Range of mean absolute differences for 15-25 km (ppmv/ppbv)	Literature values
<b>O<sub>3</sub> (sonde)</b>	14	7.1	+6.1	-10.4/+19.2	-0.02~+0.40	
<b>O<sub>3</sub> (MLS)</b>	33	9.4	-5.5	-16.3/+4.5	-0.13~+0.16	Aura/MLS is +8% higher than ACE-FTS at 70°S (Froidevoux et al., 2008)
<b>HNO<sub>3</sub></b>	47	19.2	+13.2	+0.2/+21.9	-0.56~+0.57	Aura/MLS no bias with errors (0.6 ppbv) (Livesey et al., 2011)
<b>HCl</b>	50	39.5	-9.7	-14.6/-3.0	-0.20~+0.09	Aura/MLS > HALOE by 10-15%, precision 0.2-0.6 ppbv (Livesey et al., 2013)

\*Root mean squares of official absolute and relative errors given by each data set.

**Table A1. FTIR observation dates at Syowa Station in 2007 and 2011**

<b>Month</b>	Dates (2007)	Dates (2011)	Number of days inside the polar vortex (2007/2011)	Number of days in the boundary region of the polar vortex (2007/2011)	Number of days outside the polar vortex (2007/2011)	Number of measurement days (2007/2011)
<b>March</b>	25		0 / 0	0 / 0	1 / 0	1 / 0
<b>April</b>	1, 3, 4, 5, 8, 24, 26, 28		0 / 0	0 / 0	8 / 0	8 / 0
<b>May</b>	8, 9, 10, 13, 14, 15, 20, 21, 22		7 / 0	0 / 0	2 / 0	9 / 0
<b>June</b>			0 / 0	0 / 0	0 / 0	0 / 0
<b>July</b>	29, 30		0 / 0	2 / 0	0 / 0	2 / 0
<b>August</b>	1, 8, 9, 10, 24, 25, 26, 28, 29		8 / 0	1 / 0	0 / 0	9 / 0
<b>September</b>	1, 4, 5, 6, 7, 8, 16, 18, 23, 26, 27, 30	25, 29, 30	12 / 3	0 / 0	0 / 0	12 / 3
<b>October</b>	6, 10, 11, 14, 19, 20, 25, 26, 27	1, 3, 4, 8, 11, 22, 23, 24, 26	9 / 9	0 / 0	0 / 0	9 / 9
<b>November</b>	2, 3, 5, 6, 7, 8, 9, 10, 11, 16, 17, 18, 19, 21, 27, 29, 30	1, 2, 3, 9, 11, 16, 19	12 / 7	1 / 0	4 / 0	17 / 7
<b>December</b>	4, 7, 8, 9, 13, 15, 16, 17, 20, 22, 29		8 / 0	0 / 0	3 / 0	11 / 0
<b>Total</b>			56 / 19	4 / 0	18 / 0	78 / 19

**Table A2. Chemical reactions in the MIROC3.2 Chemistry-Climate Model**

<b><u>(1) Photolysis reactions</u></b>	<b><u>Reaction coefficients (reference)</u></b>
<u><math>O_2 + hv \rightarrow O(1D) + O</math></u>	<u>JPL-2010</u>
<u><math>O_2 + hv \rightarrow 2O</math></u>	<u>JPL-2010</u>
<u><math>O_3 + hv \rightarrow O(1D) + O_2</math></u>	<u>JPL-2010</u>
<u><math>O_3 + hv \rightarrow O + O_2</math></u>	<u>JPL-2010</u>
<u><math>H_2O + hv \rightarrow OH + H</math></u>	<u>JPL-2010</u>
<u><math>CH_3OOH + hv \rightarrow CH_3O + OH</math></u>	<u>JPL-2010</u>
<u><math>CH_2O + hv \rightarrow CHO + H</math></u>	<u>JPL-2010</u>
<u><math>CH_2O + hv \rightarrow CO + H_2</math></u>	<u>JPL-2010</u>
<u><math>H_2O_2 + hv \rightarrow 2OH</math></u>	<u>JPL-2010</u>
<u><math>N_2O + hv \rightarrow N_2 + O(1D)</math></u>	<u>JPL-2010</u>
<u><math>NO + hv \rightarrow N + O</math></u>	<u>JPL-2010</u>
<u><math>NO_3 + hv \rightarrow NO_2 + O</math></u>	<u>JPL-2010</u>
<u><math>NO_3 + hv \rightarrow NO + O_2</math></u>	<u>JPL-2010</u>
<u><math>HNO_3 + hv \rightarrow OH + NO_2</math></u>	<u>JPL-2010</u>
<u><math>HNO_4 + hv \rightarrow OH + NO_3</math></u>	<u>JPL-2010</u>
<u><math>HNO_4 + hv \rightarrow HO_2 + NO_2</math></u>	<u>JPL-2010</u>
<u><math>N_2O_5 + hv \rightarrow NO_2 + NO_3</math></u>	<u>JPL-2010</u>
<u><math>HCl + hv \rightarrow H + Cl</math></u>	<u>JPL-2010</u>
<u><math>HOCl + hv \rightarrow OH + Cl</math></u>	<u>JPL-2010</u>
<u><math>ClONO_2 + hv \rightarrow Cl + NO_3</math></u>	<u>JPL-2010</u>
<u><math>ClONO_2 + hv \rightarrow O + ClONO</math></u>	<u>JPL-2010</u>
<u><math>Cl_2O_2 + hv \rightarrow ClOO + Cl</math></u>	<u>JPL-2010</u>
<u><math>OCIO + hv \rightarrow O + ClO</math></u>	<u>JPL-2010</u>
<u><math>Cl_2 + hv \rightarrow 2Cl</math></u>	<u>JPL-2010</u>
<u><math>BrONO_2 + hv \rightarrow BrO + NO_2</math></u>	<u>JPL-2010</u>
<u><math>BrONO_2 + hv \rightarrow Br + NO_3</math></u>	<u>JPL-2010</u>
<u><math>BrCl + hv \rightarrow Br + Cl</math></u>	<u>JPL-2010</u>
<u><math>HOBr + hv \rightarrow Br + OH</math></u>	<u>JPL-2010</u>
<u><math>BrO + hv \rightarrow Br + O</math></u>	<u>JPL-2010</u>
<u><math>HBr + hv \rightarrow Br + H</math></u>	<u>JPL-2010</u>
<u><math>Br_2 + hv \rightarrow 2Br</math></u>	<u>JPL-2010</u>
<u><math>CCl_4 + hv \rightarrow 4Cl + \text{products}</math></u>	<u>JPL-2010</u>
<u><math>CH_3CCl_3 + hv \rightarrow 3Cl + \text{products}</math></u>	<u>JPL-2010</u>
<u><math>CH_3Cl + hv \rightarrow Cl + \text{products}</math></u>	<u>JPL-2010</u>
<u><math>CFCl_3(\text{CFC-11}) + hv \rightarrow 3Cl + \text{products}</math></u>	<u>JPL-2010</u>
<u><math>CF_2Cl_2(\text{CFC-12}) + hv \rightarrow 2Cl + \text{products}</math></u>	<u>JPL-2010</u>
<u><math>CClF_2CCl_2F(\text{CFC-113}) + hv \rightarrow 3Cl + \text{products}</math></u>	<u>JPL-2010</u>
<u><math>CHClF_2(\text{HCFC-22}) + hv \rightarrow Cl + \text{products}</math></u>	<u>JPL-2010</u>
<u><math>CHBr_3 + hv \rightarrow 3Br + \text{products}</math></u>	<u>JPL-2010</u>
<u><math>CH_3Br + hv \rightarrow Br + \text{products}</math></u>	<u>JPL-2010</u>
<u><math>CF_2ClBr(\text{Halon-1211}) + hv \rightarrow Br + Cl + \text{products}</math></u>	<u>JPL-2010</u>
<u><math>CF_3Br(\text{Halon-1301}) + hv \rightarrow Br + \text{products}</math></u>	<u>JPL-2010</u>
<b><u>(2) Gas phase reactions</u></b>	<b><u>Reaction coefficients (reference)</u></b>

<u>O + O + M → O<sub>2</sub> + M</u>	<u>Brasseur and Solomon (1986)</u>
<u>O + O<sub>2</sub> + M → O<sub>3</sub> + M</u>	<u>see JPL-2010</u>
<u>O + O<sub>3</sub> → O<sub>2</sub> + O<sub>2</sub></u>	<u>8.0×10<sup>-12</sup> exp[-2060/T]</u>
<u>O(1D) + N<sub>2</sub> → O + N<sub>2</sub></u>	<u>2.15×10<sup>-11</sup> exp[110/T]</u>
<u>O(1D) + O<sub>2</sub> → O + O<sub>2</sub></u>	<u>3.3×10<sup>-11</sup> exp[55/T]</u>
<u>H<sub>2</sub>O + O(1D) → 2OH</u>	<u>1.63×10<sup>-10</sup> exp[60/T]</u>
<u>H<sub>2</sub> + O(1D) → H + OH</u>	<u>1.2×10<sup>-10</sup></u>
<u>CH<sub>4</sub> + O(1D) → CH<sub>3</sub> + OH</u>	<u>1.75×10<sup>-10</sup></u>
<u>CH<sub>4</sub> + OH → CH<sub>3</sub> + H<sub>2</sub>O</u>	<u>see JPL-2010</u>
<u>CH<sub>3</sub> + O<sub>2</sub> + M → CH<sub>3</sub>O<sub>2</sub> + M</u>	<u>see JPL-2010</u>
<u>CH<sub>3</sub> + O → CH<sub>2</sub>O + H</u>	<u>1.1×10<sup>-10</sup></u>
<u>CH<sub>3</sub>O<sub>2</sub> + CH<sub>3</sub>O<sub>2</sub> → products</u>	<u>9.5×10<sup>-14</sup> exp[390/T]</u>
<u>CH<sub>3</sub>O<sub>2</sub> + HO<sub>2</sub> → CH<sub>3</sub>OOH + O<sub>2</sub></u>	<u>4.1×10<sup>-13</sup> exp[750/T]</u>
<u>OH + CH<sub>3</sub>OOH → CH<sub>3</sub>O<sub>2</sub> + H<sub>2</sub>O</u>	<u>3.8×10<sup>-12</sup> exp[200/T]</u>
<u>CH<sub>3</sub>O<sub>2</sub> + NO → CH<sub>3</sub>O + NO<sub>2</sub></u>	<u>2.8×10<sup>-12</sup> exp[300/T]</u>
<u>CH<sub>3</sub>O + O<sub>2</sub> → CH<sub>2</sub>O + HO<sub>2</sub></u>	<u>3.9×10<sup>-14</sup> exp[-900/T]</u>
<u>CH<sub>2</sub>O + OH → CHO + H<sub>2</sub>O</u>	<u>5.5×10<sup>-12</sup> exp[125/T]</u>
<u>CH<sub>2</sub>O + O → products (CHO + OH, H + HCO<sub>2</sub>)</u>	<u>3.4×10<sup>-11</sup> exp[-1600/T]</u>
<u>CHO + O<sub>2</sub> → CO + HO<sub>2</sub></u>	<u>5.2×10<sup>-12</sup></u>
<u>CO + OH → H + CO<sub>2</sub></u>	<u>see JPL-2010</u>
<u>OH + HO<sub>2</sub> → H<sub>2</sub>O + O<sub>2</sub></u>	<u>4.8×10<sup>-11</sup> exp[250/T]</u>
<u>H + HO<sub>2</sub> → products</u>	<u>8.05×10<sup>-11</sup></u>
<u>H + HO<sub>2</sub> → H<sub>2</sub>O + O</u>	<u>1.6×10<sup>-12</sup></u>
<u>O<sub>3</sub> + OH → HO<sub>2</sub> + O<sub>2</sub></u>	<u>1.7×10<sup>-12</sup> exp[-940/T]</u>
<u>O + OH → H + O<sub>2</sub></u>	<u>1.8×10<sup>-11</sup> exp[180/T]</u>
<u>H + O<sub>3</sub> → OH + O<sub>2</sub></u>	<u>1.4×10<sup>-10</sup> exp[-470/T]</u>
<u>H + O<sub>2</sub> + M → HO<sub>2</sub> + M</u>	<u>see JPL-2010</u>
<u>HO<sub>2</sub> + O → OH + O<sub>2</sub></u>	<u>3.0×10<sup>-11</sup> exp[200/T]</u>
<u>HO<sub>2</sub> + O<sub>3</sub> → OH + 2O<sub>2</sub></u>	<u>1.0×10<sup>-14</sup> exp[-490/T]</u>
<u>2HO<sub>2</sub> → H<sub>2</sub>O<sub>2</sub> + O<sub>2</sub></u>	<u>see JPL-2010</u>
<u>H<sub>2</sub>O<sub>2</sub> + OH → H<sub>2</sub>O + HO<sub>2</sub></u>	<u>1.8×10<sup>-12</sup></u>
<u>OH + OH → H<sub>2</sub>O + O</u>	<u>1.8×10<sup>-12</sup></u>
<u>H<sub>2</sub> + OH → H<sub>2</sub>O + H</u>	<u>2.8×10<sup>-12</sup> exp[-1800/T]</u>
<u>N<sub>2</sub>O + O(1D) → 2NO</u>	<u>7.25×10<sup>-11</sup> exp[20/T]</u>
<u>N<sub>2</sub>O + O(1D) → N<sub>2</sub> + O<sub>2</sub></u>	<u>4.63×10<sup>-11</sup> exp[20/T]</u>
<u>N + NO → N<sub>2</sub> + O</u>	<u>2.1×10<sup>-11</sup> exp[100/T]</u>
<u>N + O<sub>2</sub> → NO + O</u>	<u>1.5×10<sup>-11</sup> exp[-3600/T]</u>
<u>N + O<sub>3</sub> → NO + O<sub>2</sub></u>	<u>1.0×10<sup>-16</sup></u>
<u>NO + HO<sub>2</sub> → NO<sub>2</sub> + OH</u>	<u>3.3×10<sup>-12</sup> exp[270/T]</u>
<u>NO + O<sub>3</sub> → NO<sub>2</sub> + O<sub>2</sub></u>	<u>3.0×10<sup>-12</sup> exp[-1500/T]</u>
<u>NO<sub>2</sub> + O → NO + O<sub>2</sub></u>	<u>5.1×10<sup>-12</sup> exp[210/T]</u>
<u>NO<sub>2</sub> + O<sub>3</sub> → NO<sub>3</sub> + O<sub>2</sub></u>	<u>1.2×10<sup>-13</sup> exp[-2450/T]</u>
<u>OH + NO<sub>2</sub> + M → HNO<sub>3</sub> + M</u>	<u>see JPL-2010</u>
<u>HNO<sub>3</sub> + OH → NO<sub>3</sub> + H<sub>2</sub>O</u>	<u>see JPL-2010</u>
<u>HO<sub>2</sub> + NO<sub>2</sub> + M → HNO<sub>4</sub> + M</u>	<u>see JPL-2010</u>
<u>HO<sub>2</sub> + NO<sub>2</sub> ⇌ HNO<sub>4</sub></u>	<u>2.1×10<sup>-27</sup> exp[10900/T] (equilibrium constant)</u>
<u>HNO<sub>4</sub> + OH → H<sub>2</sub>O + NO<sub>2</sub></u>	<u>1.3×10<sup>-12</sup> exp[380/T]</u>

<u>NO<sub>3</sub> + NO<sub>2</sub> + M → N<sub>2</sub>O<sub>5</sub> + M</u>	<u>see JPL-2010</u>
<u>NO<sub>3</sub> + NO<sub>2</sub> → N<sub>2</sub>O<sub>5</sub></u>	<u>2.7×10<sup>-27</sup> exp[11000/T]</u>
<u>Cl + O<sub>3</sub> → ClO + O<sub>2</sub></u>	<u>2.3×10<sup>-11</sup> exp[-200/T]</u>
<u>ClO + O → Cl + O<sub>2</sub></u>	<u>2.8×10<sup>-11</sup> exp[85/T]</u>
<u>ClO + NO → Cl + NO<sub>2</sub></u>	<u>6.4×10<sup>-12</sup> exp[290/T]</u>
<u>Cl + CH<sub>4</sub> → CH<sub>3</sub> + HCl</u>	<u>7.3×10<sup>-12</sup> exp[-1280/T]</u>
<u>Cl + HO<sub>2</sub> → O<sub>2</sub> + HCl</u>	<u>1.4×10<sup>-11</sup> exp[270/T]</u>
<u>HCl + OH → H<sub>2</sub>O + Cl</u>	<u>1.8×10<sup>-12</sup> exp[-250/T]</u>
<u>HO<sub>2</sub> + ClO → HOCl + O<sub>2</sub></u>	<u>2.6×10<sup>-12</sup> exp[290/T]</u>
<u>HOCl + OH → H<sub>2</sub>O + ClO</u>	<u>3.0×10<sup>-12</sup> exp[-500/T]</u>
<u>ClO + NO<sub>2</sub> + M → ClONO<sub>2</sub> + M</u>	<u>see JPL-2010</u>
<u>ClONO<sub>2</sub> + O → products</u>	<u>3.6×10<sup>-12</sup> exp[-840/T]</u>
<u>ClO + ClO + M → Cl<sub>2</sub>O<sub>2</sub> + M</u>	<u>see JPL-2010</u>
<u>ClO + ClO ⇌ Cl<sub>2</sub>O<sub>2</sub></u>	<u>1.72×10<sup>-27</sup> exp[8649/T] (equilibrium constant)</u>
<u>Cl + O<sub>2</sub> + M → ClOO + M</u>	<u>see JPL-2010</u>
<u>Cl + O<sub>2</sub> ⇌ ClOO</u>	<u>6.6×10<sup>-25</sup> exp[2502/T] (equilibrium constant)</u>
<u>ClO + O<sub>3</sub> → OCIO + O<sub>2</sub></u>	<u>1.0×10<sup>-12</sup> exp[-4117/T]</u>
<u>OCIO + Cl → ClO + ClO</u>	<u>3.4×10<sup>-11</sup> exp[160/T]</u>
<u>OCIO + OH → HOCl + O<sub>2</sub></u>	<u>1.4×10<sup>-12</sup> exp[600/T]</u>
<u>OCIO + NO → ClO + NO<sub>2</sub></u>	<u>2.5×10<sup>-12</sup> exp[-600/T]</u>
<u>OCIO + O → ClO + O<sub>2</sub></u>	<u>2.4×10<sup>-12</sup> exp[-960/T]</u>
<u>Cl + H<sub>2</sub> → H + HCl</u>	<u>3.05×10<sup>-11</sup> exp[-2270/T]</u>
<u>Cl + H<sub>2</sub>O<sub>2</sub> → HCl + HO<sub>2</sub></u>	<u>1.1×10<sup>-11</sup> exp[-980/T]</u>
<u>Cl + CH<sub>2</sub>O → CHO + HCl</u>	<u>8.1×10<sup>-11</sup> exp[-30/T]</u>
<u>HCl + O → OH + Cl</u>	<u>1.0×10<sup>-11</sup> exp[-3300/T]</u>
<u>Cl + HO<sub>2</sub> → Cl<sub>2</sub> + OH</u>	<u>3.6×10<sup>-11</sup> exp[-375/T]</u>
<u>Cl + HOCl → products (Cl<sub>2</sub> + OH, HCl + ClO)</u>	<u>3.4×10<sup>-12</sup> exp[-130/T]</u>
<u>HOCl + O → OH + ClO</u>	<u>1.7×10<sup>-13</sup></u>
<u>ClO + ClO → Cl<sub>2</sub> + O<sub>2</sub></u>	<u>1.0×10<sup>-12</sup> exp[-1590/T]</u>
<u>ClO + ClO → OCIO + Cl</u>	<u>3.5×10<sup>-13</sup> exp[-1370/T]</u>
<u>ClO + ClO → ClOO + Cl</u>	<u>3.0×10<sup>-11</sup> exp[-2450/T]</u>
<u>ClO + OH → Cl + HO<sub>2</sub></u>	<u>7.4×10<sup>-12</sup> exp[270/T]</u>
<u>ClO + OH → HCl + O<sub>2</sub></u>	<u>6.0×10<sup>-13</sup> exp[230/T]</u>
<u>CH<sub>2</sub>O + Cl → HCl + CHO</u>	<u>8.1×10<sup>-11</sup> exp[-30/T]</u>
<u>CH<sub>3</sub>O<sub>2</sub> + ClO → products (ClOO + CH<sub>3</sub>O, CH<sub>3</sub>OCl + O<sub>2</sub>)</u>	<u>3.3×10<sup>-12</sup> exp[-115/T]</u>
<u>Cl + NO<sub>2</sub> + M → ClNO<sub>2</sub> + M</u>	<u>see JPL-2010</u>
<u>OH + ClNO<sub>2</sub> → HOCl + NO<sub>2</sub></u>	<u>2.4×10<sup>-12</sup> exp[-1250/T]</u>
<u>CH<sub>3</sub>CCl<sub>3</sub> + OH → 3Cl + products</u>	<u>1.64×10<sup>-12</sup> exp[-1520/T]</u>
<u>CH<sub>3</sub>CCl<sub>3</sub> + Cl → CH<sub>2</sub>CCl<sub>3</sub> + HCl</u>	<u>3.23×10<sup>-12</sup> exp[-1770/T]</u>
<u>CH<sub>3</sub>Cl + OH → Cl + products</u>	<u>2.4×10<sup>-12</sup> exp[-1250/T]</u>
<u>CH<sub>3</sub>Cl + Cl → CH<sub>2</sub>Cl + HCl</u>	<u>2.17×10<sup>-11</sup> exp[-1130/T]</u>
<u>CCl<sub>4</sub> + O(1D) → products</u>	<u>3.3×10<sup>-10</sup></u>
<u>CFCl<sub>3</sub> + O(1D) → products</u>	<u>2.3×10<sup>-10</sup></u>
<u>CF<sub>2</sub>Cl<sub>2</sub> + O(1D) → products</u>	<u>1.4×10<sup>-10</sup></u>
<u>CClF<sub>2</sub>CCl<sub>2</sub>F + O(1D) → products</u>	<u>2.0×10<sup>-10</sup></u>
<u>CHClF<sub>2</sub> + O(1D) → products</u>	<u>1.0×10<sup>-10</sup></u>
<u>Br + O<sub>3</sub> → BrO + O<sub>2</sub></u>	<u>1.6×10<sup>-11</sup> exp[-780/T]</u>

<u>Br + HO<sub>2</sub> → HBr + O<sub>2</sub></u>	<u>4.8×10<sup>-12</sup> exp[-310/T]</u>
<u>Br + H<sub>2</sub>O<sub>2</sub> → HBr + HO<sub>2</sub></u>	<u>1.0×10<sup>-11</sup> exp[-3000/T]</u>
<u>Br + OCIO → BrO + ClO</u>	<u>2.6×10<sup>-11</sup> exp[-1300/T]</u>
<u>Br + CH<sub>2</sub>O → HBr + CHO</u>	<u>1.7×10<sup>-11</sup> exp[-800/T]</u>
<u>BrO + O → Br + O<sub>2</sub></u>	<u>1.9×10<sup>-11</sup> exp[230/T]</u>
<u>BrO + OH → Br + HO<sub>2</sub></u>	<u>1.666×10<sup>-11</sup> exp[250/T]</u>
<u>BrO + OH → HBr + O<sub>2</sub></u>	<u>3.4×10<sup>-13</sup> exp[250/T]</u>
<u>BrO + HO<sub>2</sub> → HOBr + O<sub>2</sub></u>	<u>4.5×10<sup>-12</sup> exp[460/T]</u>
<u>BrO + NO → Br + NO<sub>2</sub></u>	<u>8.8×10<sup>-12</sup> exp[260/T]</u>
<u>BrO + NO<sub>2</sub> + M → BrONO<sub>2</sub> + M</u>	<u>see JPL-2010</u>
<u>BrO + ClO → Br + OCIO</u>	<u>9.5×10<sup>-13</sup> exp[550/T]</u>
<u>BrO + ClO → Br + ClOO</u>	<u>2.3×10<sup>-12</sup> exp[260/T]</u>
<u>BrO + ClO → BrCl + O<sub>2</sub></u>	<u>4.1×10<sup>-13</sup> exp[290/T]</u>
<u>HBr + O(1D) → products (Br + OH, HBr + O, H + BrO)</u>	<u>1.5×10<sup>-10</sup></u>
<u>HBr + O → OH + Br</u>	<u>5.8×10<sup>-12</sup> exp[-1500/T]</u>
<u>HBr + OH → Br + H<sub>2</sub>O</u>	<u>5.5×10<sup>-12</sup> exp[200/T]</u>
<u>BrO + BrO → 2Br + O<sub>2</sub></u>	<u>2.4×10<sup>-12</sup> exp[40/T]</u>
<u>BrO + BrO → Br<sub>2</sub> + O<sub>2</sub></u>	<u>2.8×10<sup>-14</sup> exp[860/T]</u>
<u>BrO + O<sub>3</sub> → Br + 2O<sub>2</sub></u>	<u>1.0×10<sup>-12</sup> exp[-3225/T]</u>
<u>BrONO<sub>2</sub> + O → BrO + NO<sub>3</sub></u>	<u>1.9×10<sup>-11</sup> exp[215/T]</u>
<u>CHBr<sub>3</sub> + O(1D) → products</u>	<u>6.6×10<sup>-10</sup></u>
<u>CHBr<sub>3</sub> + OH → 3Br + products</u>	<u>1.35×10<sup>-12</sup> exp[-600/T]</u>
<u>CHBr<sub>3</sub> + Cl → CBr<sub>3</sub> + HCl</u>	<u>4.85×10<sup>-12</sup> exp[-850/T]</u>
<u>CH<sub>3</sub>Br + O(1D) → products</u>	<u>1.8×10<sup>-10</sup></u>
<u>CH<sub>3</sub>Br + OH → Br + products</u>	<u>2.35×10<sup>-12</sup> exp[-1300/T]</u>
<u>CH<sub>3</sub>Br + Cl → CH<sub>2</sub>Br + HCl</u>	<u>1.4×10<sup>-11</sup> exp[-1030/T]</u>
<u>CH<sub>2</sub>Br<sub>2</sub> + O(1D) → Br + products</u>	<u>2.7×10<sup>-10</sup></u>
<u>CH<sub>2</sub>Br<sub>2</sub> + OH → CHBr<sub>2</sub> + H<sub>2</sub>O</u>	<u>2.0×10<sup>-12</sup> exp[-840/T]</u>
<u>CH<sub>2</sub>Br<sub>2</sub> + Cl → CHBr<sub>2</sub> + HCl</u>	<u>6.3×10<sup>-12</sup> exp[-800/T]</u>
<u>CF<sub>2</sub>ClBr + O(1D) → products</u>	<u>1.5×10<sup>-10</sup></u>
<u>CF<sub>3</sub>Br + O(1D) → products</u>	<u>1.0×10<sup>-10</sup></u>

### (3) Heterogeneous reactions

### Reaction coefficients (reference)

<u>N<sub>2</sub>O<sub>5</sub> + H<sub>2</sub>O → 2HNO<sub>3</sub></u>	<u>see JPL-2010 and Akiyoshi (2007)</u>
<u>ClONO<sub>2</sub> + H<sub>2</sub>O → HOCl + HNO<sub>3</sub></u>	<u>see JPL-2010 and Akiyoshi (2007)</u>
<u>ClONO<sub>2</sub> + HCl → Cl<sub>2</sub> + HNO<sub>3</sub></u>	<u>see JPL-2010 and Akiyoshi (2007)</u>
<u>HOCl + HCl → Cl<sub>2</sub> + H<sub>2</sub>O</u>	<u>see JPL-2010 and Akiyoshi (2007)</u>
<u>BrONO<sub>2</sub> + H<sub>2</sub>O → HOBr + HNO<sub>3</sub></u>	<u>see JPL-2010 and Akiyoshi (2007)</u>
<u>HOBr + HCl → BrCl + H<sub>2</sub>O</u>	<u>see JPL-2010 and Akiyoshi (2007)</u>
<u>BrONO<sub>2</sub> + HCl → BrCl + HNO<sub>3</sub></u>	<u>see JPL-2010 and Akiyoshi (2007)</u>
<u>ClONO<sub>2</sub> + HBr → BrCl + HNO<sub>3</sub></u>	<u>see JPL-2010 and Akiyoshi (2007)</u>
<u>BrONO<sub>2</sub> + HBr → Br<sub>2</sub> + HNO<sub>3</sub></u>	<u>see JPL-2010 and Akiyoshi (2007)</u>
<u>HOCl + HBr → BrCl + H<sub>2</sub>O</u>	<u>see JPL-2010 and Akiyoshi (2007)</u>
<u>HOBr + HBr → Br<sub>2</sub> + H<sub>2</sub>O</u>	<u>see JPL-2010 and Akiyoshi (2007)</u>
<u>N<sub>2</sub>O<sub>5</sub> + HBr → BrNO<sub>2</sub> + HNO<sub>3</sub></u>	<u>see JPL-2010 and Akiyoshi (2007)</u>
<u>N<sub>2</sub>O<sub>5</sub> + HCl → ClONO<sub>2</sub> + HNO<sub>3</sub></u>	<u>see JPL-2010 and Akiyoshi (2007)</u>

Total:

42 photolysis reactions  
140 gas phase reactions  
13 heterogeneous reactions

5

## Figures

Figure 1. Averaging kernel functions of the SFIT2 retrievals for (a) O<sub>3</sub>, (b) HNO<sub>3</sub>, and (c) HCl.

- 5 Figure 2. (a) Mean absolute and (b) mean relative differences of O<sub>3</sub> profiles retrieved from FTIR measurements minus those from ozonesonde measurements. (c) Mean absolute and (d) mean relative differences of O<sub>3</sub> profiles retrieved from FTIR measurements minus those from Aura/MLS measurements. (e) Mean absolute and (f) mean relative differences of HNO<sub>3</sub> profiles retrieved from FTIR measurements minus those from Aura/MLS measurements. (g) Mean absolute and (h) mean relative differences of HCl profiles retrieved from FTIR measurements minus those from Aura/MLS measurements.
- 10 Horizontal bars indicate the root mean squares of differences at each altitude. Horizontal dashed bars indicate the altitude range of our focus (15-25 km).

- Figure 3. Time series of (a) daytime hour, temperatures at 18 km in (b) 2007 and (c) 2011, and at 22 km in (d) 2007 and (e) 2011 over Syowa Station using ERA-Interim data. Approximate saturation temperatures for nitric acid trihydrate  $PSC(T_{NAT})$  and ice  $PSC(T_{ICE})$  calculated by assuming 6 ppbv HNO<sub>3</sub> and 4.5 ppmv H<sub>2</sub>O are also plotted in the figures by dotted lines.
- 15 Dates when PSCs were observed over Syowa Station are indicated by asterisks on the bottom of the figures.

- Figure 4. Time series of (a) HCl, ClONO<sub>2</sub>, ClO, Cl<sub>y</sub>\*, (b) O<sub>3</sub>, and HNO<sub>3</sub> mixing ratios at 18 km in 2007 over Syowa Station. O<sub>3</sub>(FTIR), HCl(FTIR), and HNO<sub>3</sub>(FTIR) were measured by FTIR at Syowa Station, while HCl(MLS), ClO(MLS), and
- 20 HNO<sub>3</sub>(MLS) were measured by Aura/MLS. O<sub>3</sub>(sonde) was measured by ozonesonde. ClONO<sub>2</sub> was measured by Envisat/MIPAS. Cl<sub>y</sub>\* is calculated from Aura/MLS N<sub>2</sub>O value. See text in detail. The unit of O<sub>3</sub> is ppmv and the other gases are ppbv. The dark shaded area, the light shaded area, and the white area indicate the days when Syowa Station was located outside, in the boundary region, and inside the polar vortex, respectively.

- 25 Figure 5. Same as Figure 4 but in 2011.

Figure 6. Same as Figure 4 but at 22 km.

Figure 7. Same as Figure 5 but at 22 km.

30

Figure 8. Time series of the ratios of HCl (dark blue or light blue), ClONO<sub>2</sub> (yellow), and ClO (red) to total chlorine (Cl<sub>y</sub>\*) over Syowa Station at 18 km in (a) 2007 and in (b) 2011. Light blue shows either ClONO<sub>2</sub> or ClO data was missing on that day, while dark blue shows all three data were available on that day. Shaded areas are the same as Figure 4.

Figure 9. Same as Figure 8 but at 22 km.

Figure 10. Scatter plot between ClO (Aura/MLS) and ClONO<sub>2</sub> (Envisat/MIPAS) mixing ratios between August 8 and September 17 (day 220 – 260) at 18 km and 22 km in 2007 and 2011. Crosses, triangles, and squares represent the data when Syowa Station was located inside the polar vortex, the boundary region, and outside the polar vortex, respectively. Solid lines are regression lines obtained by RMA regression. Color represents the equivalent latitude over Syowa Station on that day. Circles with crosses represent the days which are shown in Figures 13 and 14.

Figure 11. Daily time series of measured and modeled minor species over Syowa Station at 18 km. Black diamonds are data by FTIR, red squares are by Aura/MLS and Envisat/MIPAS, blue triangles are data by MIROC3.2 CCM. (a) is for ClO, (b) is for HCl, (c) is for ClONO<sub>2</sub>, (d) is for Cly, and (e) is for O<sub>3</sub> in 2007. (f) is for ClO, (g) is for HCl, (h) is for ClONO<sub>2</sub>, (i) is for Cly, and (j) is for O<sub>3</sub> in 2011.

Figure 12. Same as Figure 11 but for 22 km.

Figure 13. Polar southern hemispheric plots for ERA-Interim temperature, simulated mixing ratios of O<sub>3</sub>, NO<sub>2</sub>, HNO<sub>3</sub>, ClO, HCl, and ClONO<sub>2</sub> by a MIROC3.2 chemistry-climate model (CCM) at 50 hPa for June 24 (day 175), September 2 (day 245), September 6 (day 249), and October 6 (day 279), 2007. Polar vortex (outer) edges defined as the method described in Appendix B at 450 K was plotted by white circle in each panel. The location of Syowa Station was shown by white star in each panel.

Figure 14. Same as Figure 13 but for July 5 (day 186), August 19 (day 231), August 21 (day 233), and October 9 (day 282), 2011. Polar vortex edges on July 5 plotted by dotted white circles indicates that the inner vortex edge was defined on this day.

Figure 15. Three-hourly zonal-mean time series of MIROC3.2 CCM outputs for (a) ClO+2\*Cl<sub>2</sub>O<sub>2</sub>+2\*Cl<sub>2</sub>, (b) Cl<sub>2</sub>O<sub>2</sub>, (c) Cl<sub>2</sub>, (d) ClO, (e) HOCl, (f) HCl, and (g) ClONO<sub>2</sub> during day number 120–300 at 50 hPa in 2007.

Figure A1. Time-equivalent latitude sections of MPV (contours) and its gradient with respect to EL (colors) at (a) 450 K and (b) 560 K isentropic PT surfaces in 2007. Black dots represent the inner and outer edge(s) of the polar vortex. Red dots represent the EL of Syowa Station on each day.

Figure A2. Same as Figure A1 but for the year in 2011.

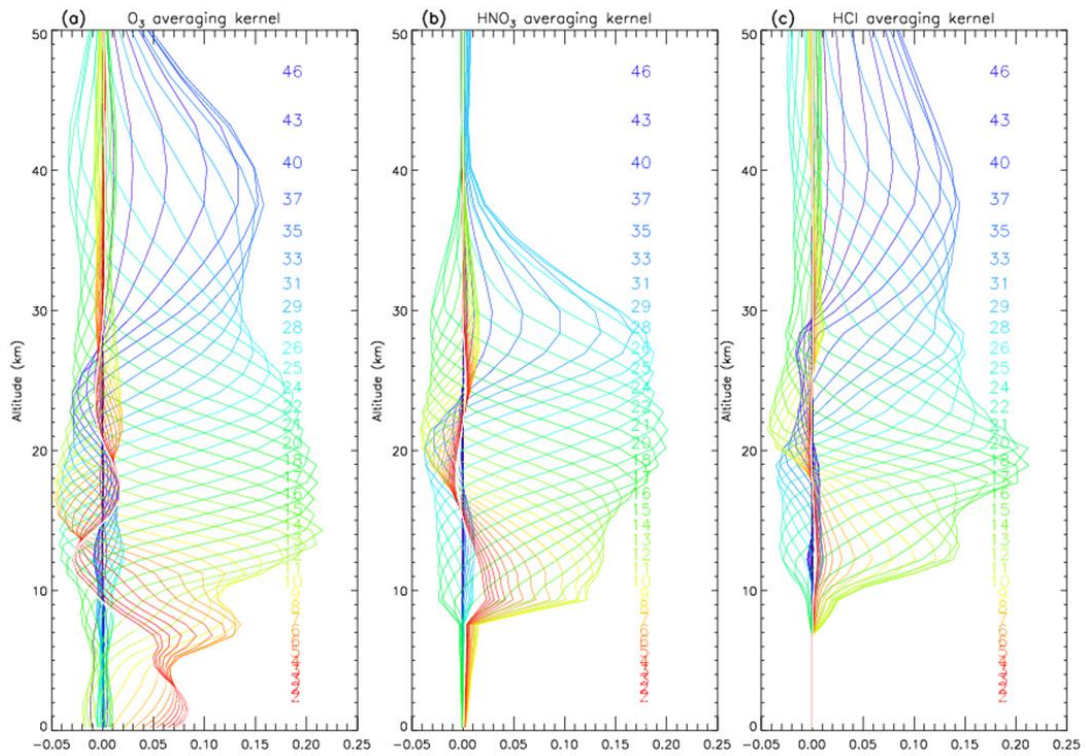


Figure 1. Averaging kernel functions of the SFIT2 retrievals for (a) O<sub>3</sub>, (b) HNO<sub>3</sub>, and (c) HCl.

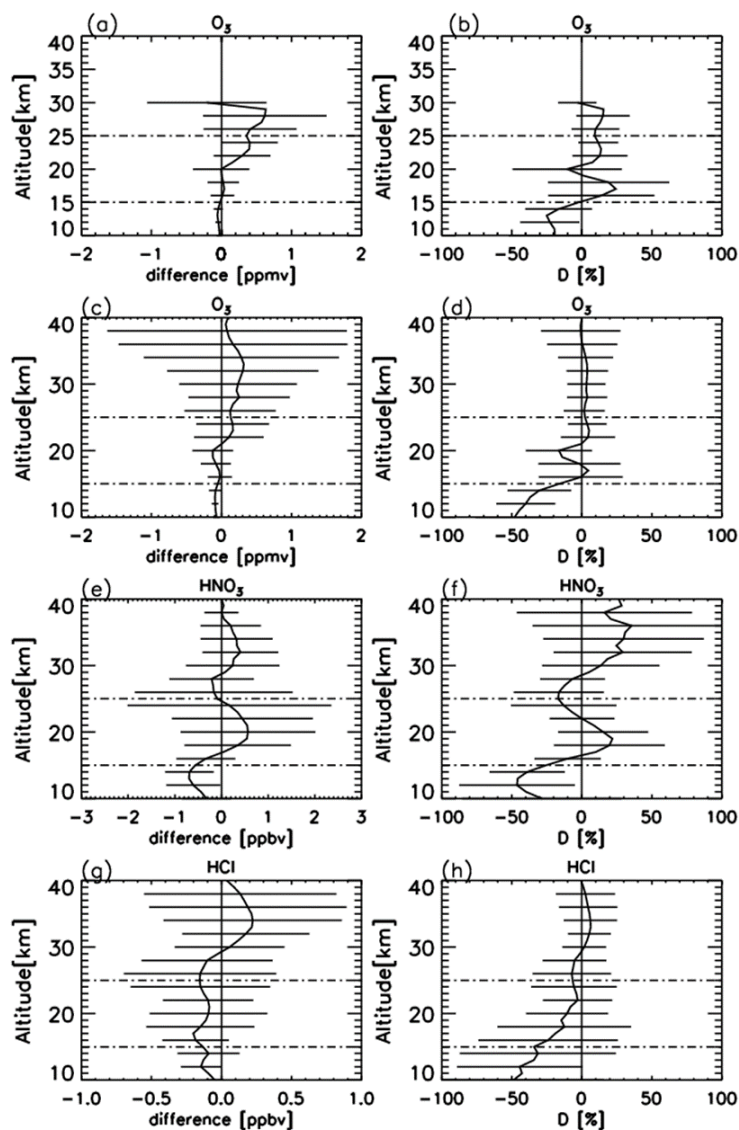


Figure 2. (a) Mean absolute and (b) mean relative differences of O<sub>3</sub> profiles retrieved from FTIR measurements minus those from ozonesonde measurements. (c) Mean absolute and (d) mean relative differences of O<sub>3</sub> profiles retrieved from FTIR measurements minus those from Aura/MLS measurements. (e) Mean absolute and (f) mean relative differences of HNO<sub>3</sub> profiles retrieved from FTIR measurements minus those from Aura/MLS measurements. (g) Mean absolute and (h) mean relative differences of HCl profiles retrieved from FTIR measurements minus those from Aura/MLS measurements. Horizontal bars indicate the root mean squares of differences at each altitude. Horizontal dashed bars indicate the altitude range of our focus (15-25 km).

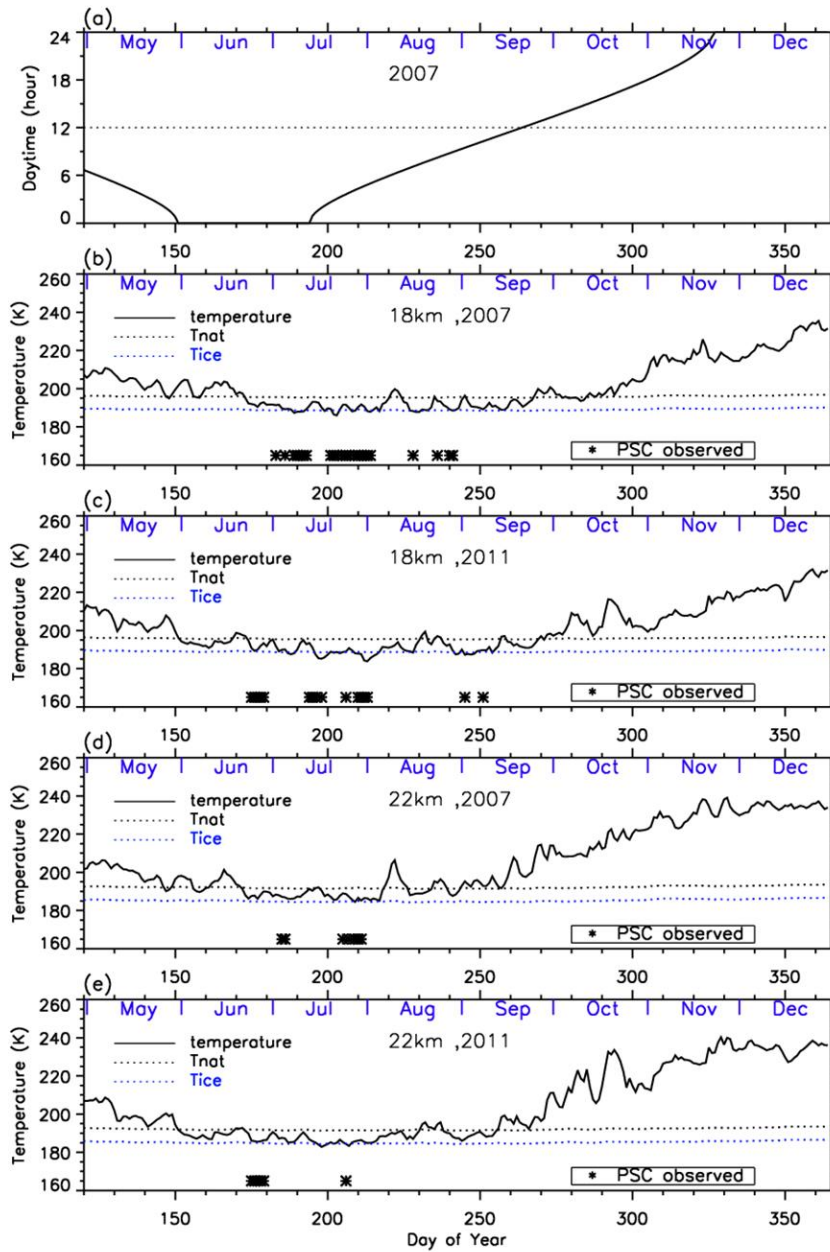


Figure 3. Time series of (a) daytime hour, temperatures at 18 km in (b) 2007 and (c) 2011, and at 22 km in (d) 2007 and (e) 2011 over Syowa Station using ERA-Interim data. Approximate saturation temperatures for nitric acid trihydrate ( $T_{\text{NAT}}$ ) and ice ( $T_{\text{ICE}}$ ) calculated by assuming 6 ppbv  $\text{HNO}_3$  and 4.5 ppmv  $\text{H}_2\text{O}$  are also plotted in the figures by dotted lines. Dates when PSCs were observed over Syowa Station are indicated by asterisks on the bottom of the figures.

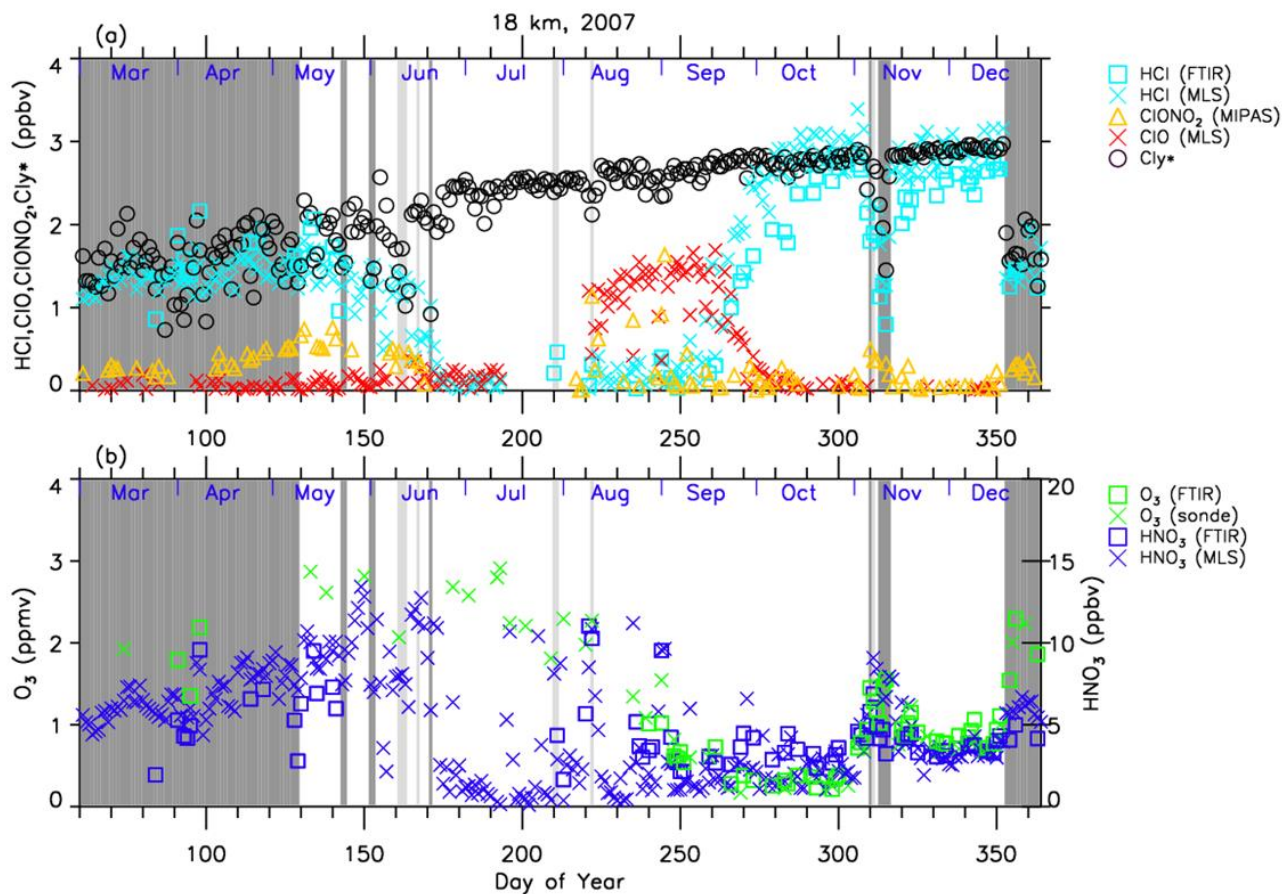


Figure 4. Time series of (a) HCl, ClONO<sub>2</sub>, ClO, Cl<sub>y</sub>\*, (b) O<sub>3</sub>, and HNO<sub>3</sub> mixing ratios at 18 km in 2007 over Syowa Station. O<sub>3</sub>(FTIR), HCl(FTIR), and HNO<sub>3</sub>(FTIR) were measured by FTIR at Syowa Station, while HCl(MLS), ClO(MLS), and HNO<sub>3</sub>(MLS) were measured by Aura/MLS. O<sub>3</sub>(sonde) was measured by ozonesonde. ClONO<sub>2</sub> was measured by 5 Envisat/MIPAS. Cl<sub>y</sub>\* is calculated from Aura/MLS N<sub>2</sub>O value. See text in detail. The unit of O<sub>3</sub> is ppmv and the other gases are ppbv. The dark shaded area, the light shaded area, and the white area indicate the days when Syowa Station was located outside, in the boundary region, and inside the polar vortex, respectively.

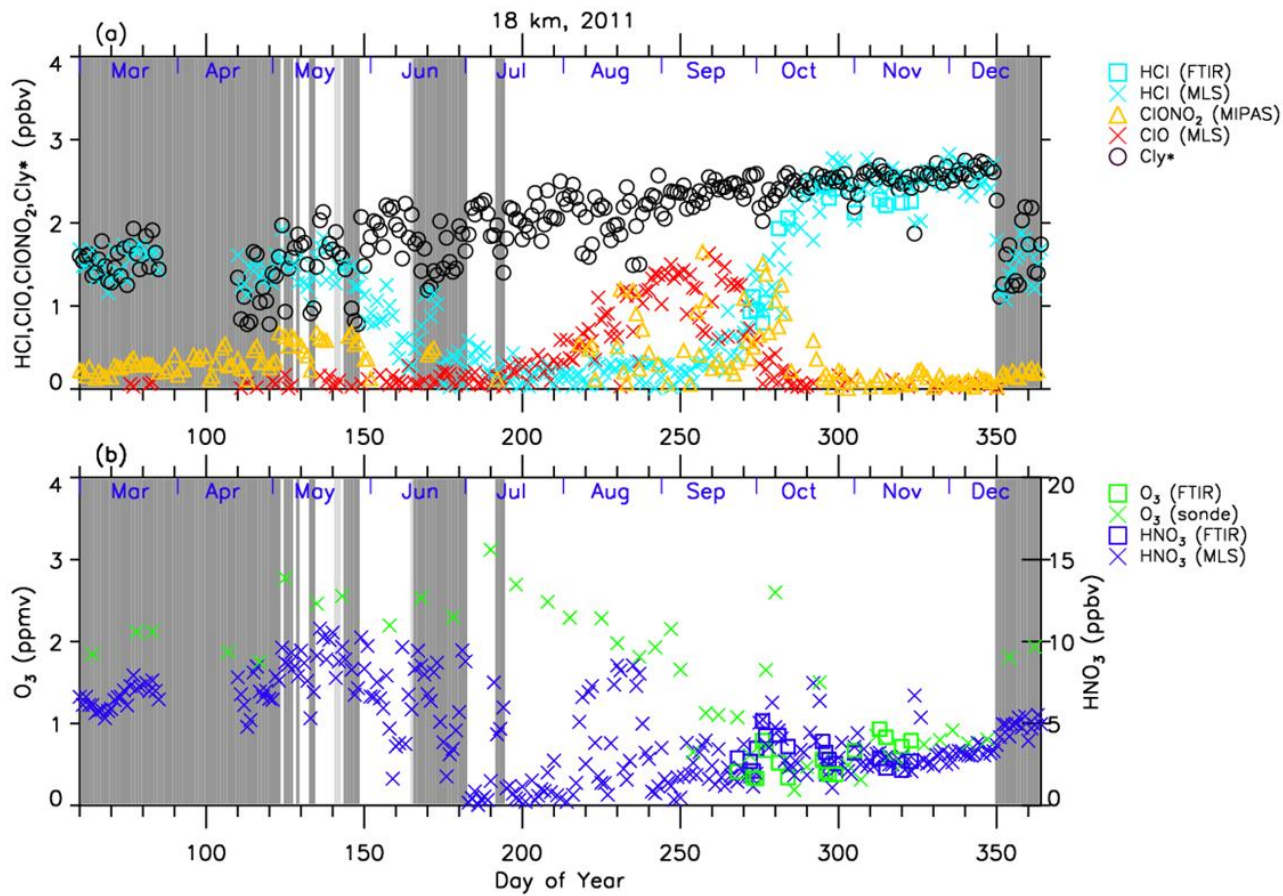


Figure 5. Same as Figure 4 but in 2011.

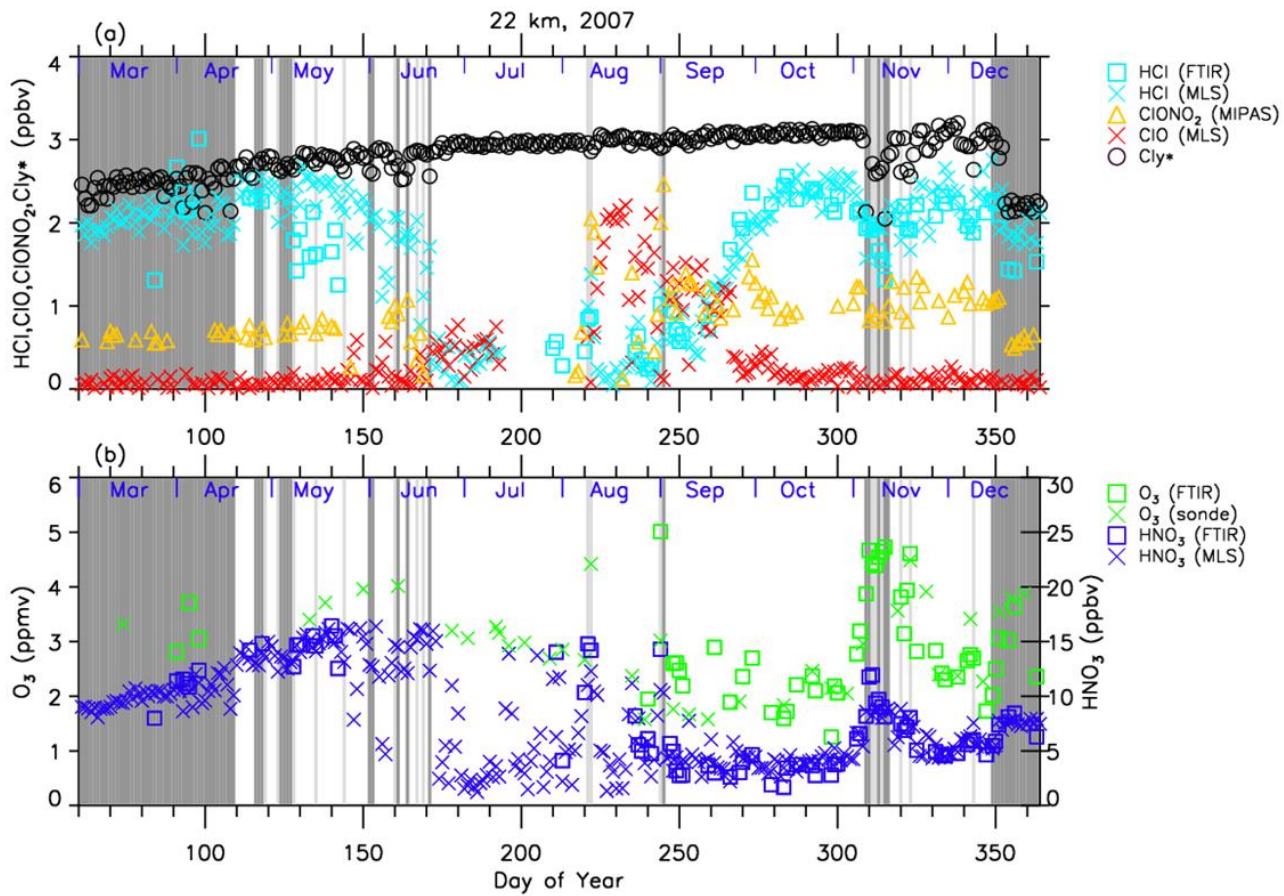


Figure 6. Same as Figure 4 but at 22 km.

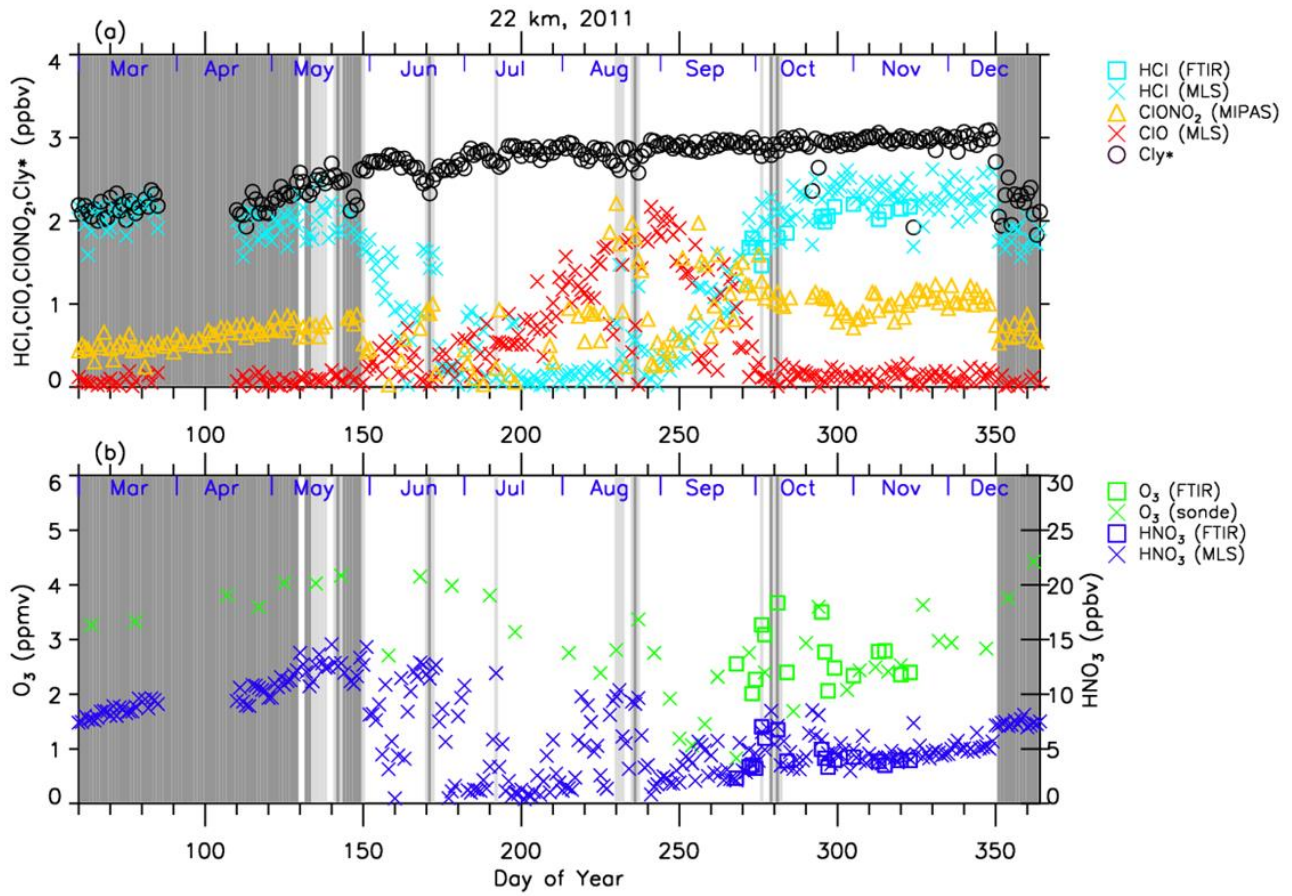


Figure 7. Same as Figure 5 but at 22 km.

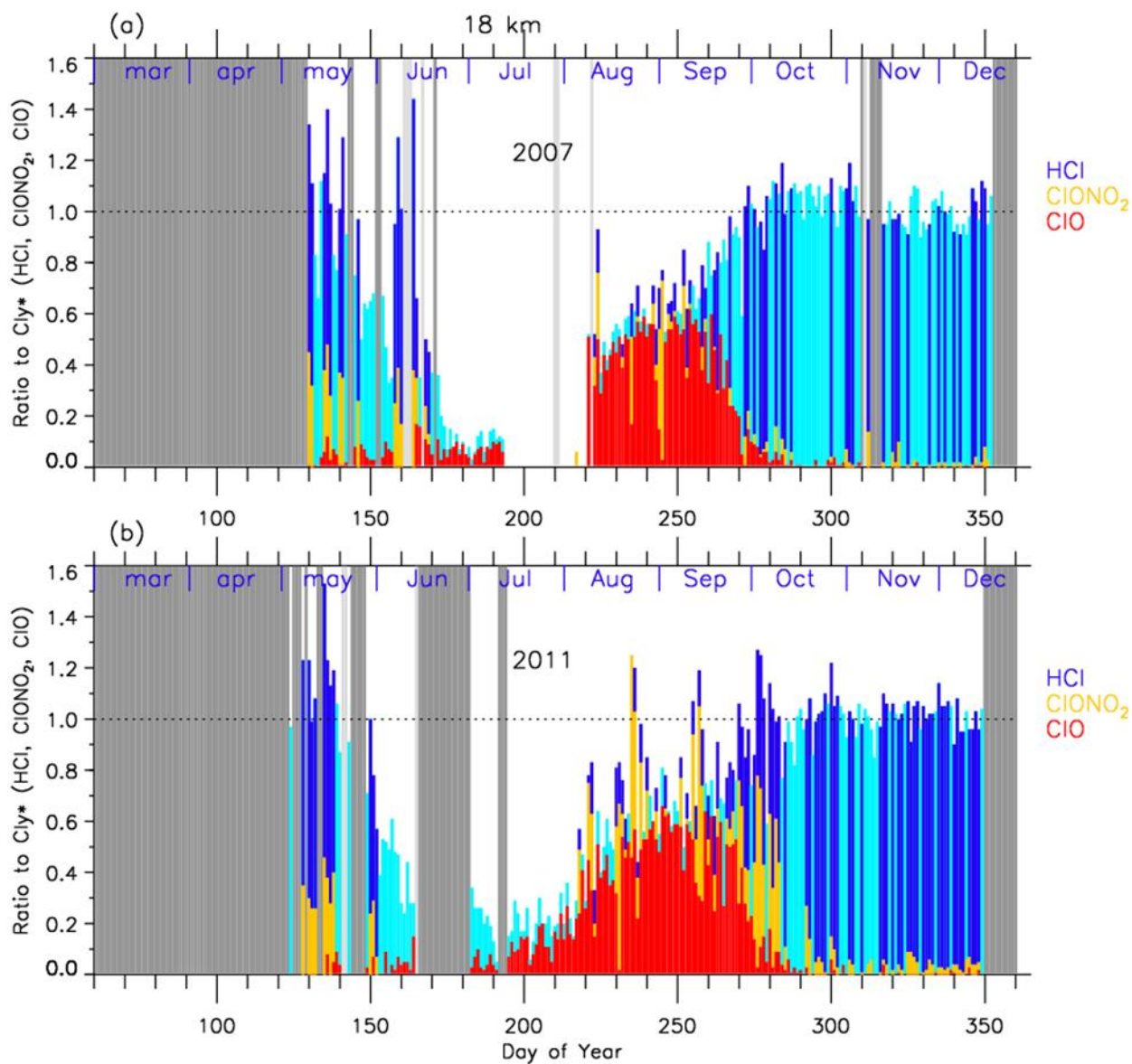
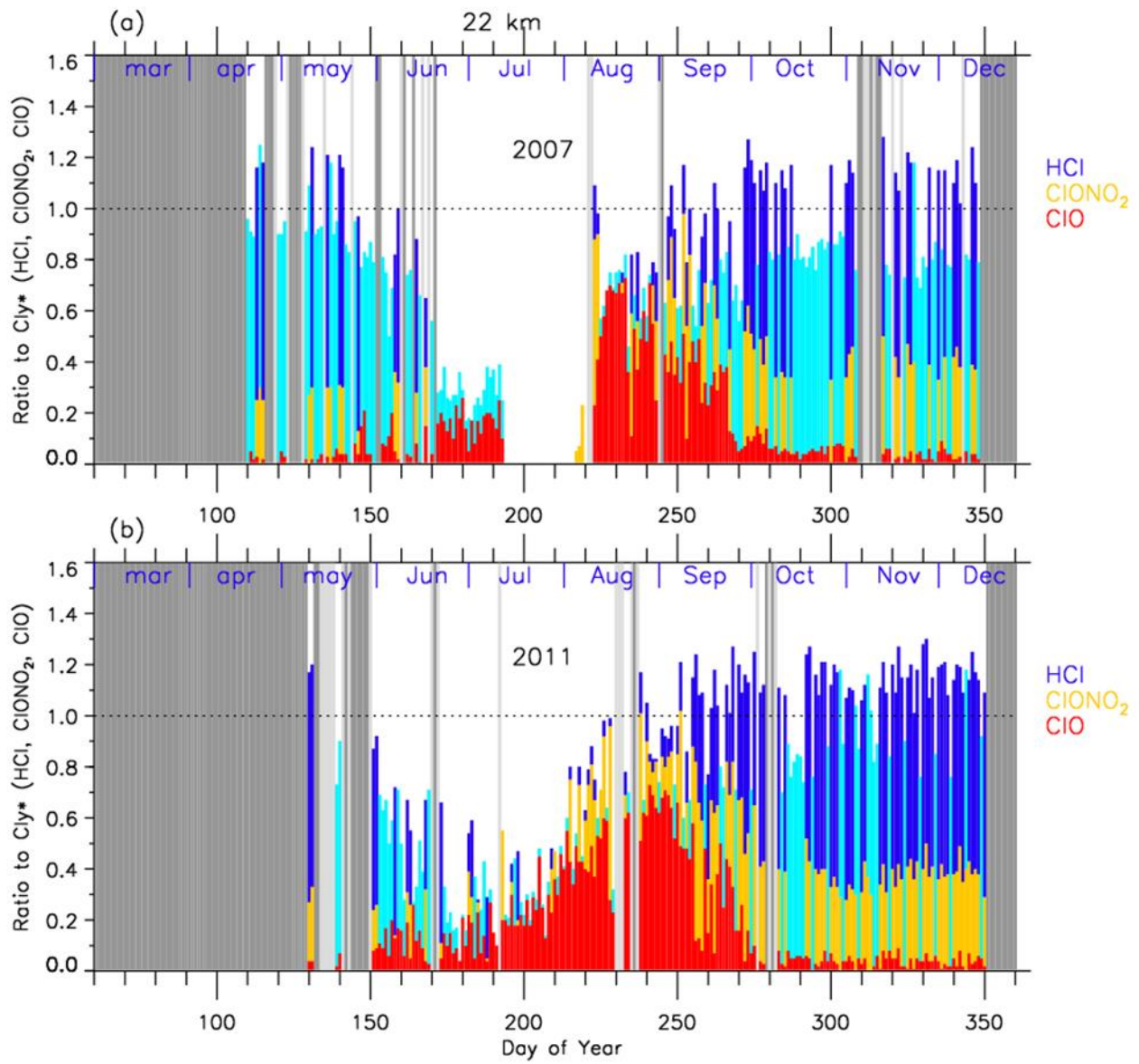


Figure 8. Time series of the ratios of HCl (dark blue or light blue),  $ClONO_2$  (yellow), and ClO (red) to total chlorine ( $Cl_y^*$ ) over Syowa Station at 18 km in (a) 2007 and in (b) 2011. Light blue shows either  $ClONO_2$  or ClO data was missing on that day, while dark blue shows all three data were available on that day. Shaded areas are the same as Figure 4.



30 Figure 9. Same as Figure 8 but at 22 km.

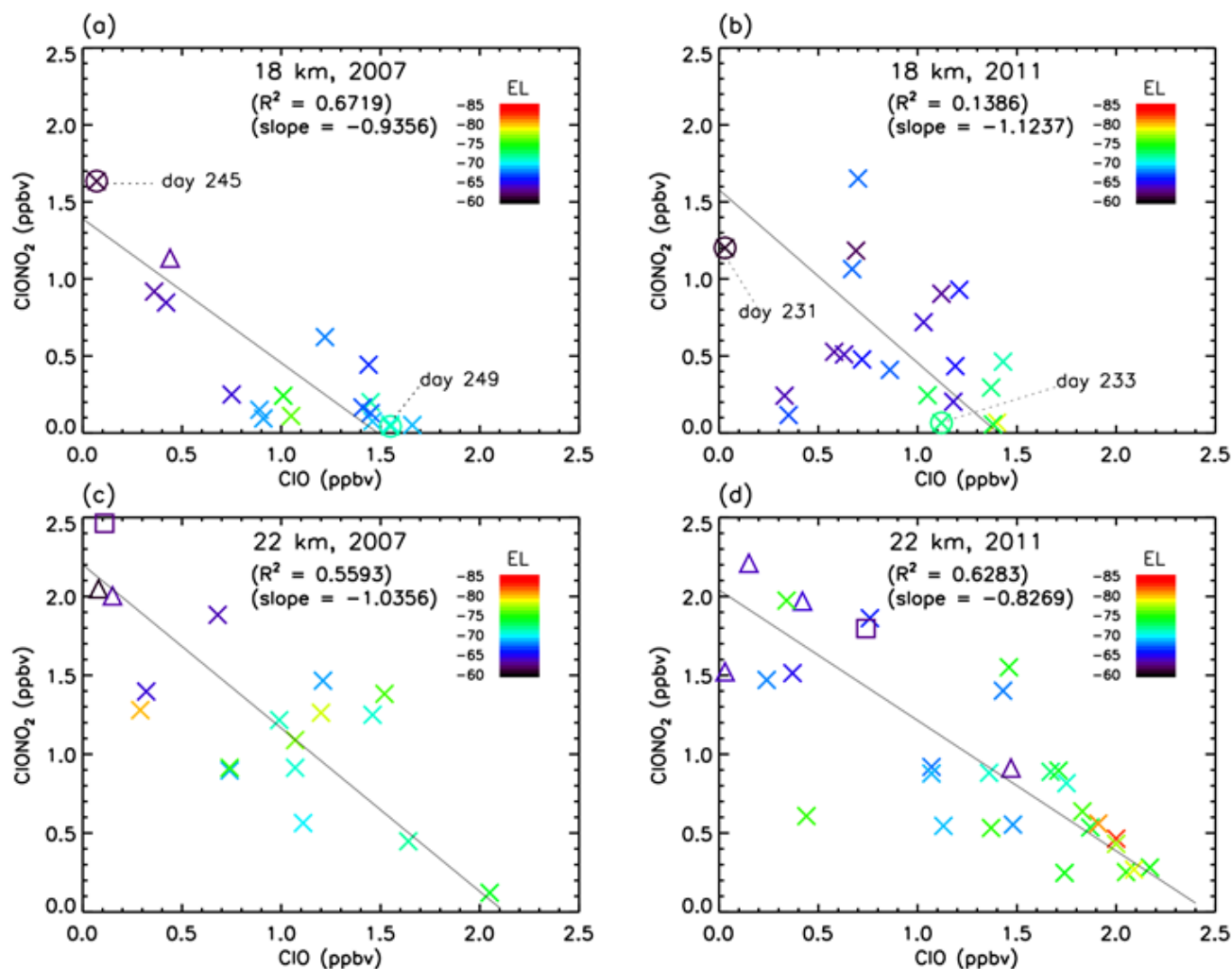


Figure 10. Scatter plot between CIO (Aura/MLS) and ClONO<sub>2</sub> (Envisat/MIPAS) mixing ratios between August 8 and September 17 (day 220 – 260) at 18 km and 22 km in 2007 and 2011. Crosses, triangles, and squares represent the data when Syowa Station was located inside the polar vortex, the boundary region, and outside the polar vortex, respectively. Solid lines are regression lines obtained by RMA regression. Color represents the equivalent latitude over Syowa Station on that day.

30 Circles with crosses represent the days which are shown in Figures 13 and 14.

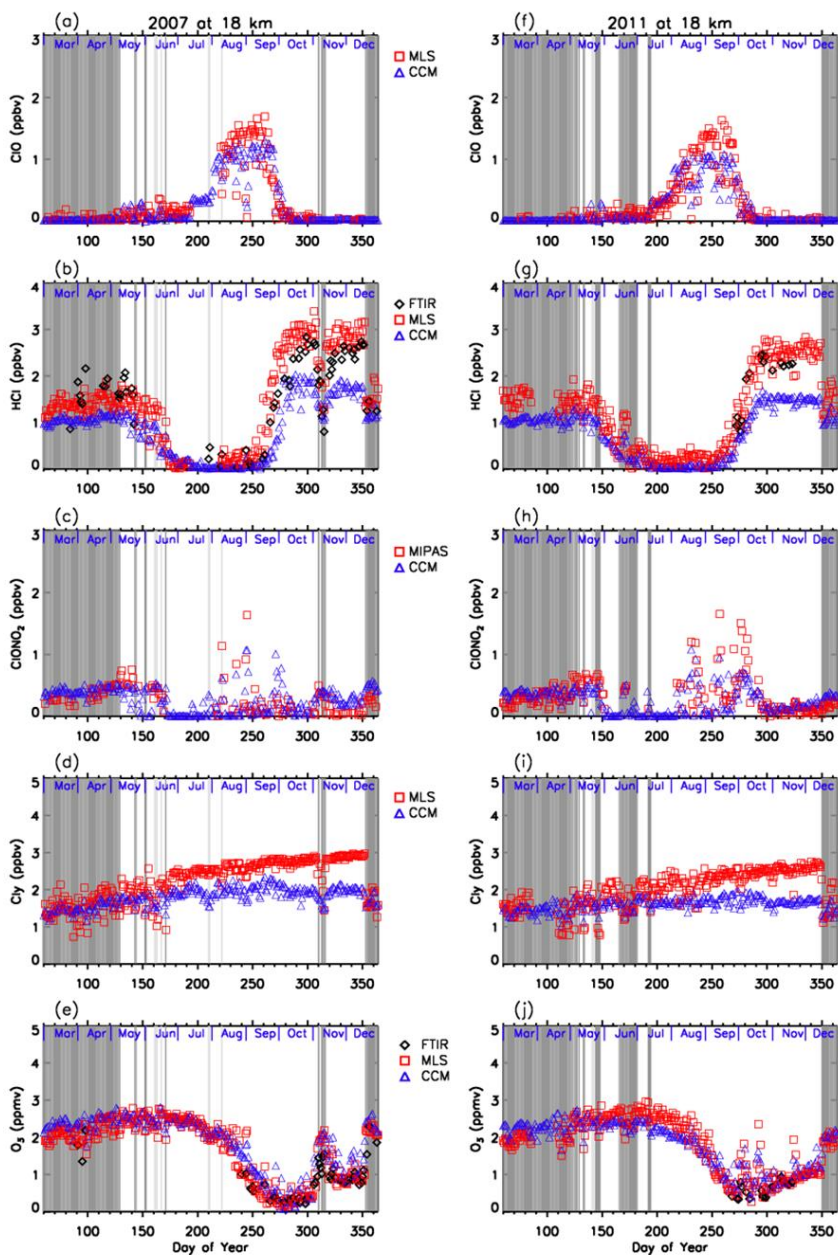


Figure 11. Daily time series of measured and modeled minor species over Syowa Station at 18 km. Black diamonds are data by FTIR, red squares are by Aura/MLS and Envisat/MIPAS, blue triangles are data by MIROC3.2 CCM. (a) is for ClO, (b) is for HCl, (c) is for ClONO<sub>2</sub>, (d) is for Cly, and (e) is for O<sub>3</sub> in 2007. (f) is for ClO, (g) is for HCl, (h) is for ClONO<sub>2</sub>, (i) is for Cly, and (j) is for O<sub>3</sub> in 2011.

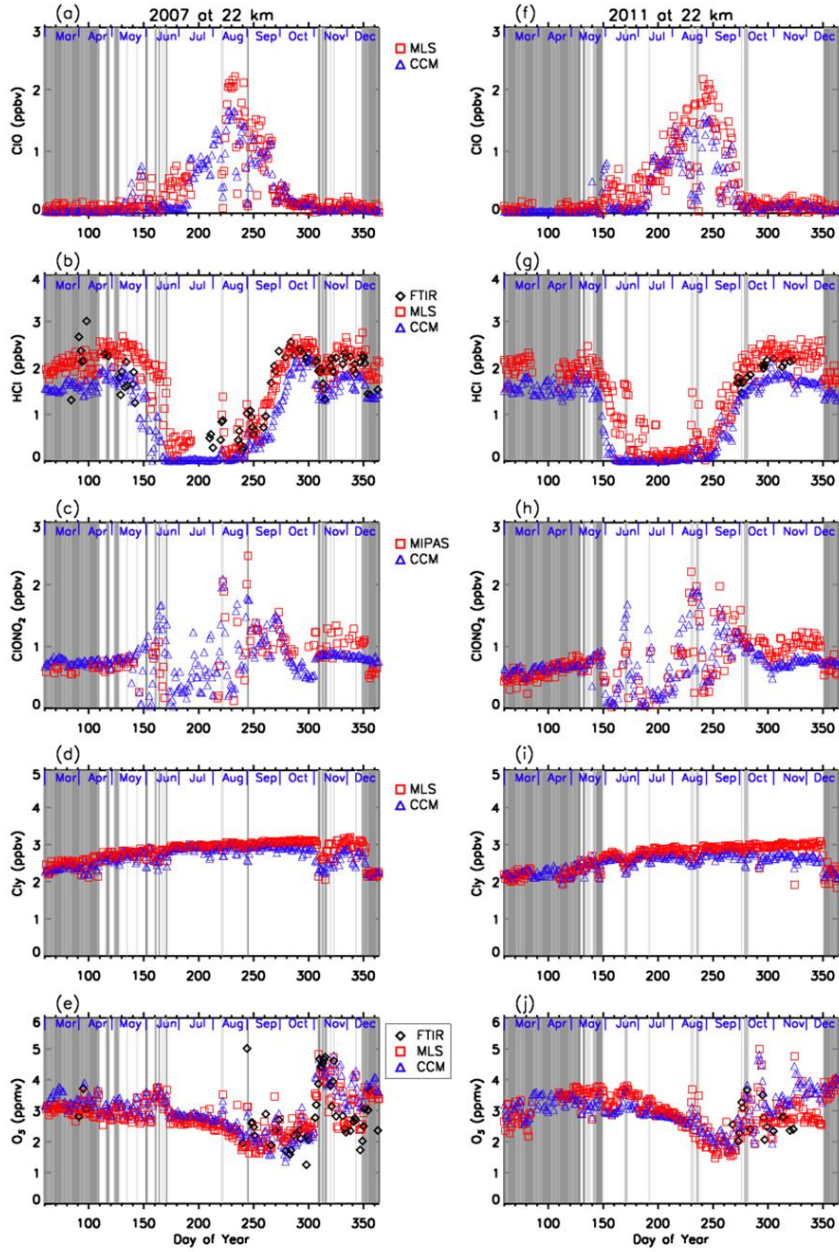


Figure 12. Same as Figure 11 but for 22 km.

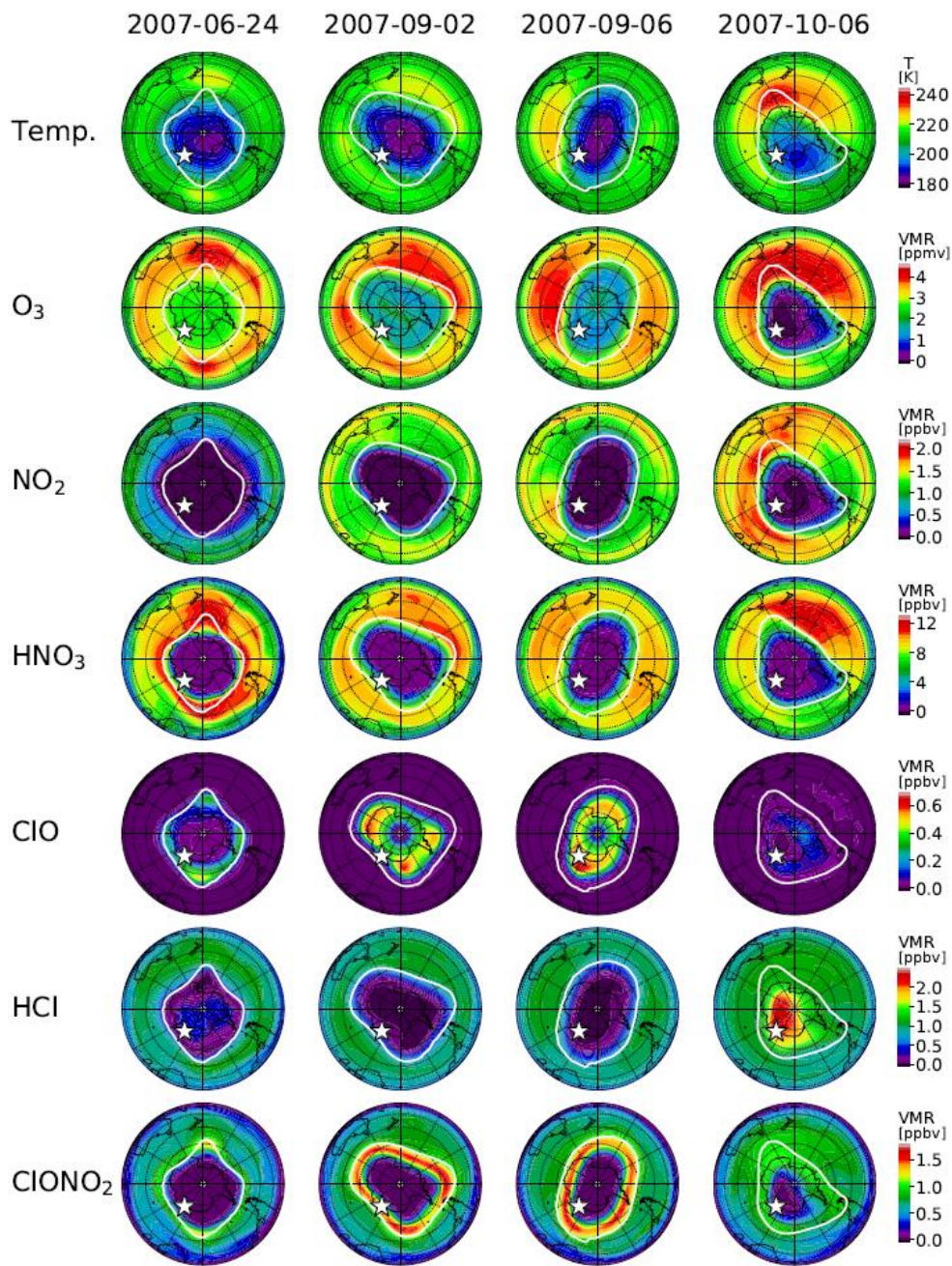


Figure 13. Polar southern hemispheric plots for temperature from the model nudged toward the ERA-Interim data, simulated mixing ratios of  $O_3$ ,  $NO_2$ ,  $HNO_3$ ,  $ClO$ ,  $HCl$ , and  $ClONO_2$  by a MIROC3.2 chemistry-climate model (CCM) at 50 hPa for June 24 (day 175), September 2 (day 245), September 6 (day 249), and October 6 (day 279), 2007. Polar vortex (outer) edge defined by the method described in Appendix B at 450 K was plotted by white circle in each panel. The location of Syowa Station was shown by white star in each panel.

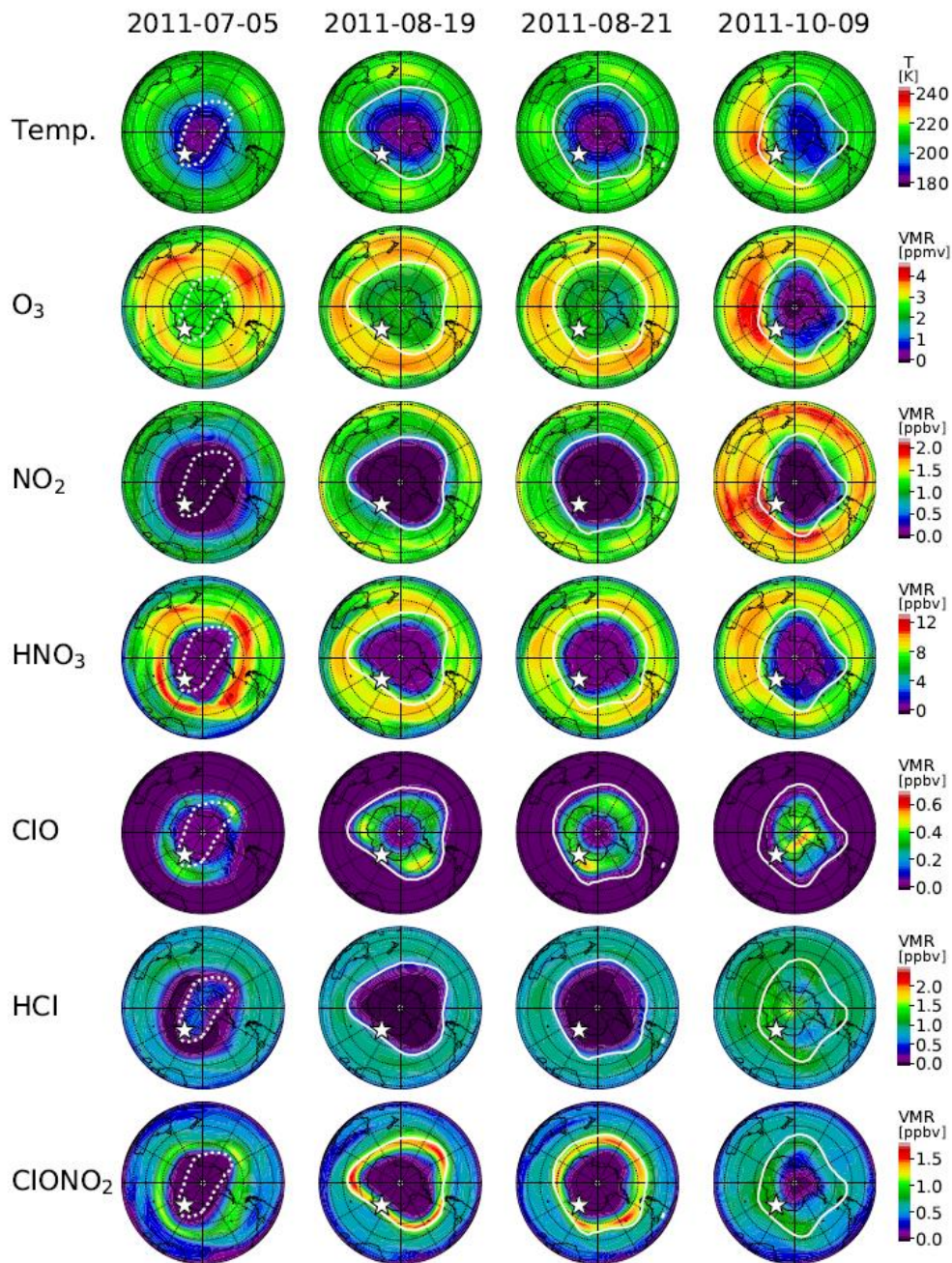


Figure 14. Same as Figure 13 but for July 5 (day 186), August 19 (day 231), August 21 (day 233), and October 9 (day 282), 2011. Polar vortex edge on July 5 plotted by dotted while circle indicates that the inner vortex edge was defined on this day.

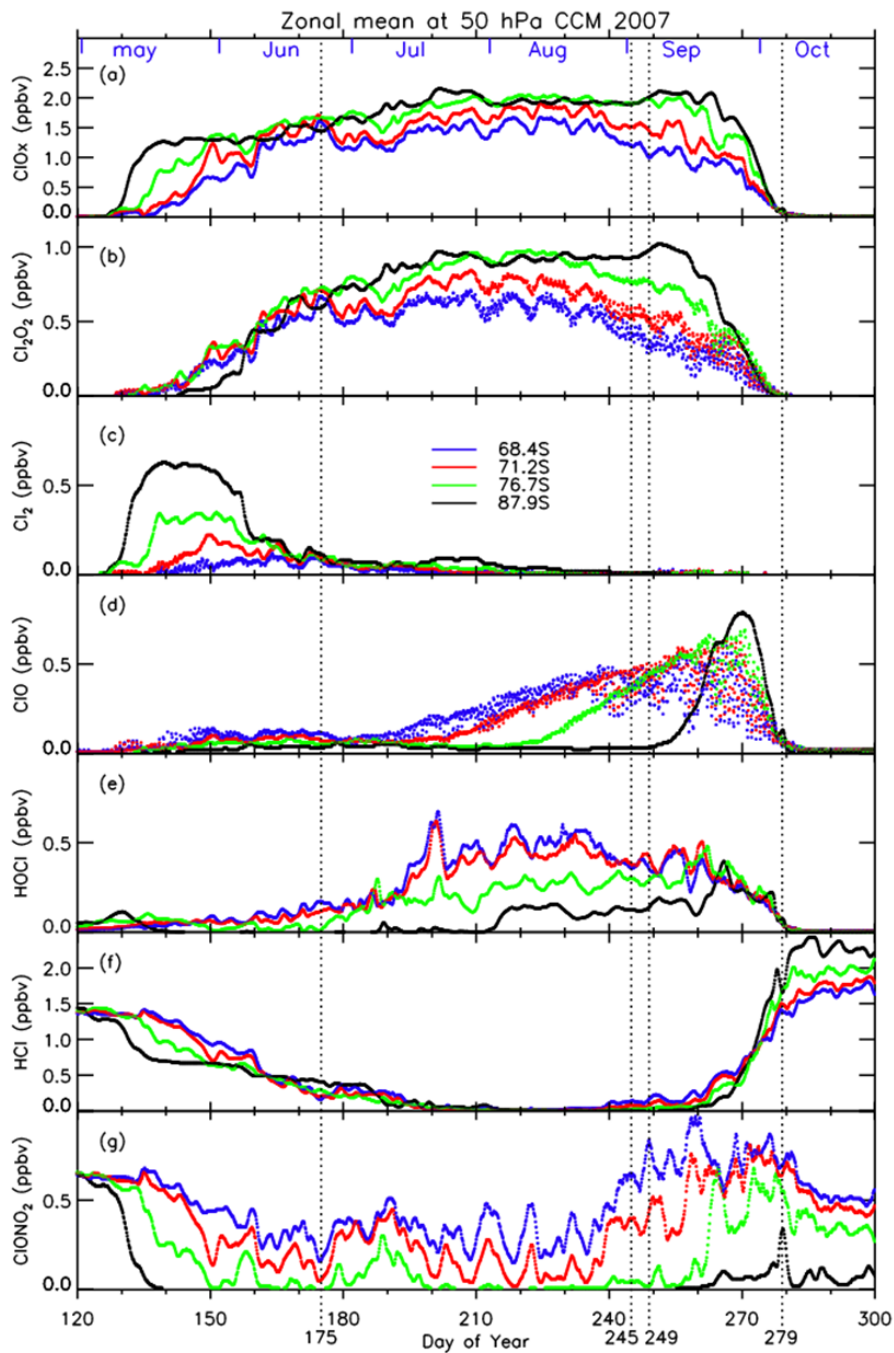


Figure 15. Three-hourly zonal-mean time series of MIROC3.2 CCM outputs for (a)  $\text{ClO} + 2 \times \text{Cl}_2\text{O}_2 + 2 \times \text{Cl}_2$ , (b)  $\text{Cl}_2\text{O}_2$ , (c)  $\text{Cl}_2$ , (d)  $\text{ClO}$ , (e)  $\text{HOCl}$ , (f)  $\text{HCl}$ , and (g)  $\text{ClONO}_2$  during day number 120–300 at 50 hPa in 2007.

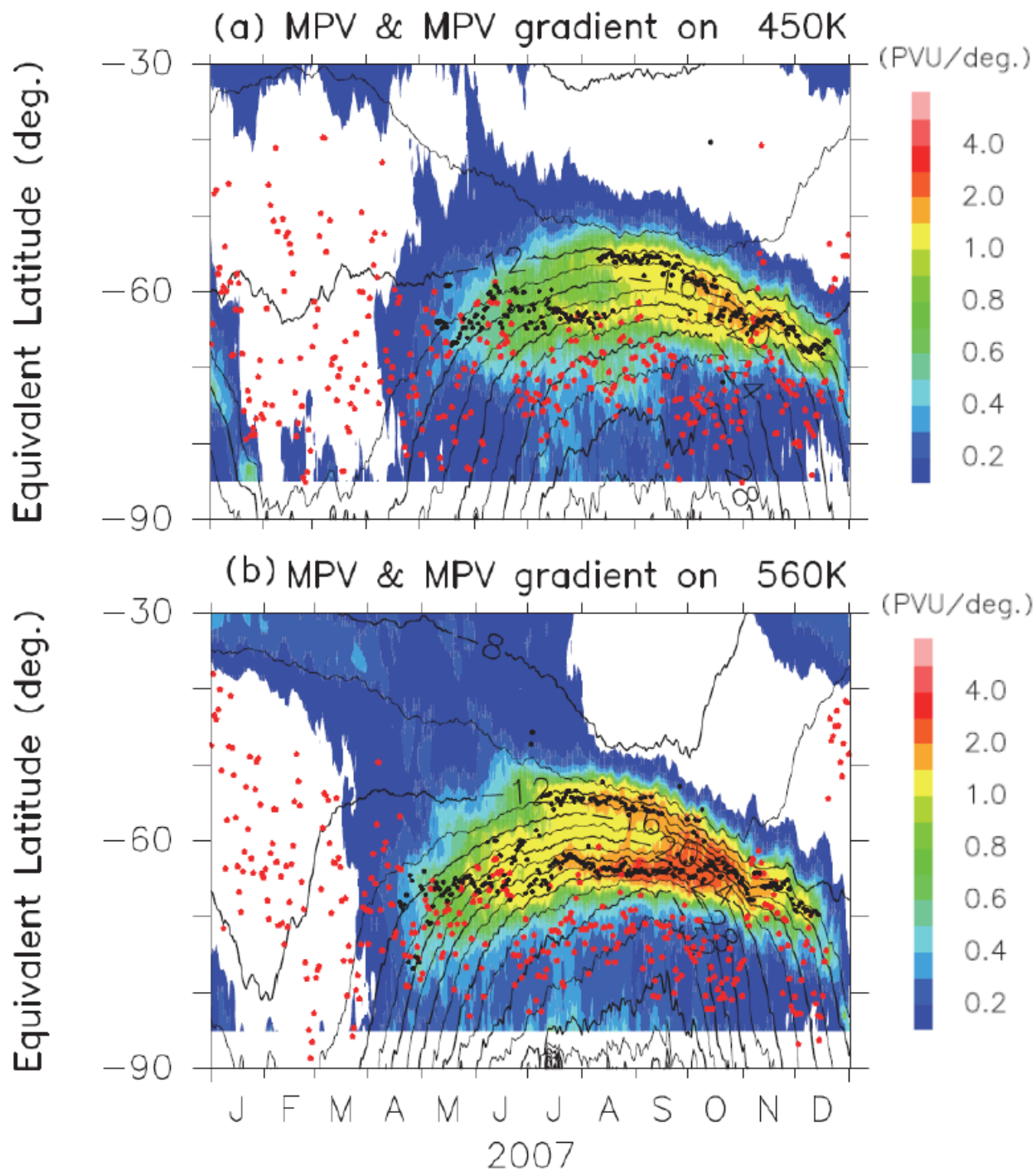


Figure A1. Time-equivalent latitude sections of MPV (contours) and its gradient with respect to EL (colors) at (a) 450 K and (b) 560 K isentropic PT surfaces in 2007. Black dots represent the inner and outer edge(s) of the polar vortex. Red dots represent the EL of Syowa Station on each day.

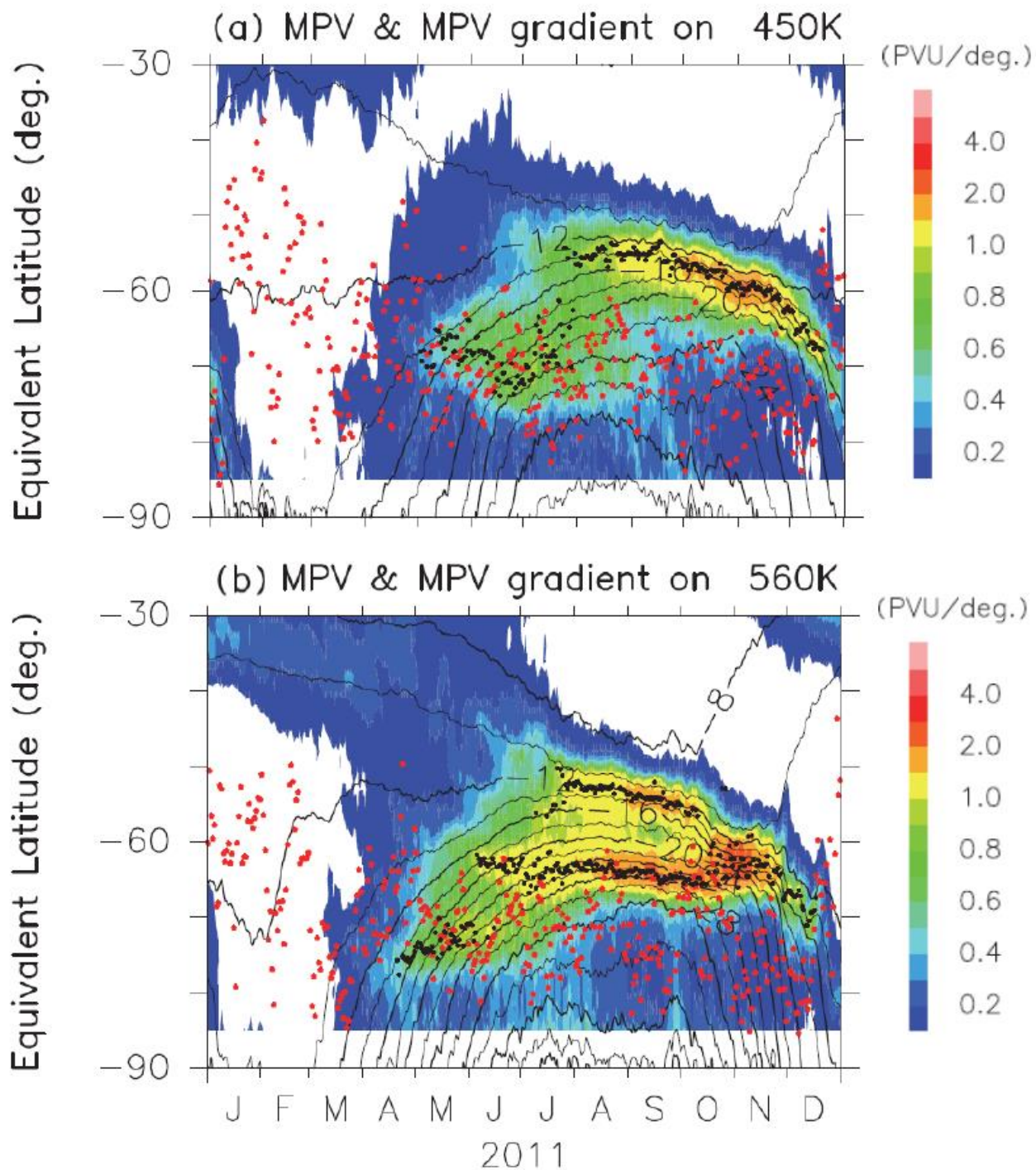


Figure A2. Same as Figure A1 but for the year in 2011.